TÉCNICO LISBOA

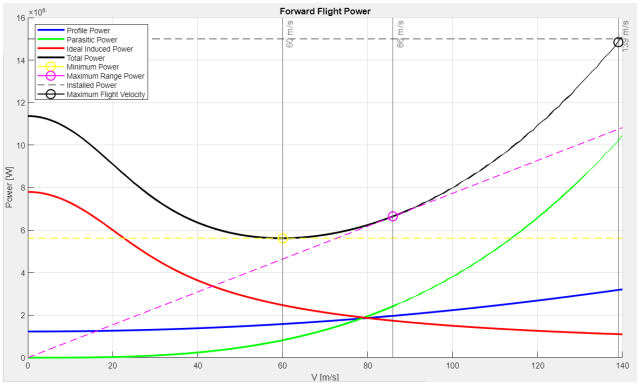

Conceptual Design and Performance Analysis Tool for Rotorcraft Systems

Tomás Figueiredo Ventura Pimentel Fontes

Thesis to obtain the Master of Science Degree in

Aerospace Engineering

Supervisor: Prof. Filipe Szolnoky Ramos Pinto Cunha

Examination Committee

Chairperson: Prof. Fernando José Parracho Lau
Supervisor: Prof. Filipe Szolnoky Ramos Pinto Cunha
Member of the Committee: Prof. João Manuel Melo de Sousa

July 2020

Acknowledgments

I would like to thank professor Filipe Szolnoky Cunha for the oportunity to work with him in such a project, and for all the guidance and availability throughout the whole work.

A special thank you to my friend Tomás Bernardo Bastos with whom I discussed a lot of ideas which helped to improve the software presented here.

Resumo

A disponibilidade de uma ferramenta grátis e *open source* para o *design* e avaliação de desempenho de aeronaves com asas rotativas é escassa, este trabalho pretende providenciar uma solução a alunos de engenharia, engenheiros de aeronaves e qualquer pessoa interessada no *design* de aeronaves uma ferramenta desse tipo.

A ferramenta aplica a teoria do Momento Linear e a teoria de Elementos de Pá para fazer a análise do desempenho do rotor e apresenta os resultados de uma forma clara e simples (em gráficos de potência em função da velocidade de avanço, de gráficos com a distribuição das diversas variáveis calculadas ao longo do disco do rotor e ainda como resultados numéricos directos explicitamente identificados).

Uma pequena base de dados com alguns perfis aerodinâmicos (e respectivas características de desempenho) está incluída na ferramenta.

A validação dos resultados obtidos na ferramenta é feita e apresentada de modo a assegurar ao utilizador a fiabilidade das análises feitas.

Palavras chave: Teoria do momento linear, Teoria de Elementos de Pá, desempenho da aeronave, projecto preliminar, equilíbrio da aeronave, espaço de projecto.

Abstract

The availability of a free open source toll for the design and performance evaluation of rotary wing aircrafts is scarce, this work intends to provide a solution for engineering students, aircraft engineers or anyone interested in aircraft design with such a tool.

The tool applies the Momentum theory and the Blade Element theory to do the analysis of the rotor performance and presents the results in a clear and simple way (power against airspeed plots, rotor disk distribution plots of the calculated variables, as well as numerical results explicitly identified).

A small data base with airfoils (and their aerodynamic performances) is included in the tool.

The tool's results validation is done and presented to assure the user of the reliability of the analyses done.

Keywords: Momentum Theory, Blade Element Theory, aircraft performance, preliminary design, aircraft trimming, design space.

Contents

List of Figures

List of Tables

List of Symbols

Greek symbols

- α - Angle of attack [°]
- α^{TTP} - Rotor disk inclination [°]
- β - Blade coning angle [°]
- γ - Lock number
- Δy - Blade section width $[m]$
- ϵ - convergence criteria
- θ - Blade section pitch angle [°]
- θ_0 - collective pitch [°]
- θ_c - longitudinal cyclic pitch [°]
- θ_s - lateral cyclic pitch [°]
- λ - Inflow ratio
- λ_0 - induced inflow at the center of the rotor
- λ_c - Climb ratio
- λ_d - Descent ratio
- μ - Advance ratio
- ν_β - Nondimensional flapping frequency
- ρ - Specific mass $[kg/m^3]$
- ρ_{fuel} - Fuel specific mass $[kg/m^3]$
- σ - Rotor solidity
- τ - Blade taper ratio
- ϕ - Inflow velocity angle [°]
- χ - Wake skew angle [°]
- Ψ - Azimuth angle [°]
- Ω - Rotor angular velocity $[rad/s]$

Roman symbols

- A - Rotor disk area $[m^2]$
- a_{heli} - Tail rotor arm $[m]$
- A_{ov} - Overlapping area $[m^2]$
- B - Tip loss factor
- c - Rotor blade chord $[m]$
- C_d - Drag coefficient
- C_{d_0} - Drag coefficient at zero-lift angle of attack
- C_l - Lift coefficient
- C_{l_α} - Lift coefficient derivative with respect to the angle of attack
- C_P - Power coefficiente
- C_Q - Torque coefficient

- C_T - Thrust coefficient
- D - Aerodynamic drag $[N]$
- d - Rotor shaft distance in tandem configuration $[m]$
- $d*$ - incremental of property *
- DL - Disk Loading $[N/m^2]$
- $\overrightarrow{dS}$ - Unit normal area vector
- E - Energy $[J]$
- e - Energy density $[Wh/kg]$
- End_h - Hover endurance $[minutes]$
- $\overrightarrow{F}$ - Force $[N]$
- F - Prandtl's correction factor
- f - equivalent wetted area $[m^2]$
- F_{CF} - Centrifugal force $[N]$
- FM - Figure of Merit
- h - flight altitude $[m]$
- h_{heli} - Helicopter height $[m]$
- I - Moment of inertia $[kg/m^2]$
- k - induced power correction factor
- k_{int} - interference factor
- k_{ov} - overlapping factor
- k_s - empirical factor to account for the severity of the wake contraction
- k_x - inflow longitudinal slope
- k_y - inflow lateral slope
- L - Aerodynamic lift $[N]$
- l_{heli} - Helicopter length $[m]$
- $\dot{m}$ - mass flow rate $[kg/s]$
- M - Mach number
- $m_{batteries}$ - Aircraft batteries mass $[kg]$
- M_{CF} - Centrifugal moment
- M_{dd} - Two dimensional divergence Mach number
- m_{crew} - Crew and passengers mass $[kg]$
- m_E - Aircraft empty mass $[kg]$
- m_f - Drone airframe mass $[kg]$
- m_F - Aircraft fuel mass $[kg]$
- m_{gross} - Aircraft gross mass $[kg]$
- m_{motors} - Aircraft motors mass $[kg]$
- $m_{payload}$ - Aircraft payload $[kg]$
- m_r - Rotor mass $[kg]$
- m_{total} - Aircraft total mass $[kg]$

- m_{useful} - Aircraft useful mass $[kg]$
- $M_{\Omega R}$ - Hover tip Mach number
- m' - area overlap factor
- N_b - Number of rotor blades
- N_{pass} - Number of passengers
- P - Power $[W]$
- p - Pressure $[Pa]$
- PL - Power Loading $[N/W]$
- Q - Torque $[Nm]$
- r - nondimensional radial position
- R - Rotor radius $[m]$
- R_e - Effective radius $[m]$
- r_0 - root cut out
- S - Slipstream boundary surface $[m^2]$
- s - Vertical distance between a given plane and the rotor disk plane $[m]$
- S_{ref} - reference area $[m^2]$
- SFC - Specific fuel consumption $[kg\,W^{-1}\,s^{-1}]$
- T - Rotor thrust $[N]$
- t - time $[s]$
- ttt_{heli} - Helicopter tip to tip length $[m]$
- U - Total flight velocity $[m/s]$
- U_P - Perpendicular inflow velocity $[m/s]$
- U_R - Radial inflow velocity $[m/s]$
- U_T - Transverse inflow velocity $[m/s]$
- V - Velocity $[m/s]$
- v - Inflow velocity $[m/s]$
- V_c - Climb velocity $[m/s]$
- V_f - Drone airframe volume $[m^3]$
- V_{mp} - Velocity for minimum power $[m/s]$
- V_s - Velocity along the streamtube centerline $[m/s]$
- V_{tip} - Blade tip velocity $[m/s]$
- V_∞ - Flight velocity $[m/s]$
- w - Flow velocity in the far wake plane $[m/s]$
- W - Aircraft weight $[N]$
- W_F - Weight of fuel burned $[kg]$
- w_{heli} - Helicopter width $[m]$
- y - radial position $[m]$

Subscripts

- ∞ - Far wake plane
- 0 - Far upstream plane
- 1 - Section just above the rotor disk
- 2 - Section just below the rotor disk
- f - Front rotor
- h - Hover
- i - Induced
- l - Lower rotor
- r - Rear rotor
- $root$ - Blade root
- tip - Blade tip
- TR - Tail rotor
- u - Upper rotor
- x - x direction
- z - z direction

List of Acronyms

- BET - Blade Element Theory
- MT - Momentum Theory
- MTOW - Maximum Take Off Weight
- SFC - Specific Fuel Consumption
- TTP - Tip Path Plane

1 Introduction

1.1 Motivation and goals

Many software tools for conceptual and preliminary rotorcraft design have been developed throughout the last 40 to 50 years, but a free and open source tool is still not easy to come across. The work developed in this thesis aims to provide such a tool for anyone interested in rotary wing aircrafts' design, these might be Aerospace Engineering students, aircraft designers that want to quickly access some design characteristic, or simply someone who whishes to learn about rotary wing aircrafts and try out different configurations. The simple and direct nature of the MatLab tool will allow the user to easily make design modifications and calculate their impact on the aircraft performance as to verify theoretical concepts, empirical models or any other performance related aspect of the rotorcraft.

1.2 Topic Overview

A helicopter is an aircraft that uses rotary wing systems (rotors) to produce lift, thrust and control forces. This generation of force does not require forward velocity, so the aircraft can lift vertically and hover. Motion can be induced by tilting the rotor, depending on the direction of this action the helicopter can move forwards or backwards, left or right. The wide range of flight movements even at low speeds give the helicopter characteristics like no other aircraft making it suitable for all kinds of operation.

Versatility doesn't come without a cost, for this kind of aircraft can have very different flight conditions, each having specific requirements, making it delicate (or near impossible) to have an optimal performance for all the different design points (hovering, cruise flight, maximum speed flight, climb). Rotorcraft design is a multidisciplinary problem that includes fields as aerodynamics, aeroelasticity, thermodynamics, structures and materials, flight dynamics and controls.

There are three typical configurations for a helicopter, the conventional one (with a main rotor for useful thrust, and a tail rotor for anti torque and yaw control, see Figure 1.1 (a)), the co-axial (with two counter rotating rotors with a common shaft see Figure 1.1 (b)), and the tandem (with two separate counter rotating rotors that may be side by side or longitudinally aligned see Figure 1.1 (c)). In the work developed here the software user will be able to design the aircraft in any of these three configuration and to compare their performance.

(a) Conventional

(b) Co-axial

(c) Tandem

Figure 1.1: Different helicopter configurations ((a) and (b) are courtesy of Prof. Filipe Cunha, and (c) is a royalty free image

(a) Octacopter - Agras MG-1P (b) Quadcopter

Figure 1.2: Multi-rotor drones (royalty free images)

1.3 State of the art

A lot of rotorcraft design tools have been developed throughout the years to evaluate flight performance (considering rotor and fuselage aerodynamics, structural and weight analysis, and control and stability), environmental impact (fuel consumption, noise, and exhaust gas emissions) and aircraft manufacturing, maintenance and operational costs. Some of these tools are commercial and are used by aircrafts manufacturers others are developed in university programs for research purposes and academic use.

Projects of Instituto Superior Técnico

Previous to this work several tools were already developed in other Masters' thesis. The tools based their calculations on both Momentum theory (MT) and on Blade Element theory (BET). Roman Vasyliovych Rutsky, see [1], developed a tool for the preliminary design of a conventional helicopter, Anatol Conjocari, see [2], expanded the tool to other helicopters configurations (co-axial and tandem), and Miguel Ponte, see [3], further developed the complexity of the tool introducing the possibility of a more detailed rotor blade design (airfoil change along the blade, as well as chord and twist distributions).

RAPID/RaTE

Developed by the Israel Institute of Technology this is a software package for rotorcraft preliminary design analysis, it models general configurations (conventional helicopters and tilt-rotors) based on existing aircrafts by extracting common features, or "design trends", which are then used in the first sizing stage of the helicopter design, later it performs trim response, mission, vibration, and stability analysis as well as flight mechanics and aeroelastic simulations, see [4].

CAMRAD - II

Comprehensive analytical model for the aerodynamics and dynamics of rotorcrafts. The analysis calculates rotor performance, loads and noise, helicopter vibration and gust response, flight dynamics and handling, aeroelastic stability. Structural, inertial and aerodynamic models are combined to comprise the analysis required for the design, testing and evaluation of the aircraft. Different rotor hub designs and rotorcraft configurations are supported by this tool, articulated, hingeless, gimballed, and teetering rotors, can be used in typical two rotor configurations, conventional, coaxial, tandem, side by side or tilt rotors. The trim analyses include the six degrees of freedom that represent the complete motion of the helicopter. The rotor aerodynamic analysis is based on BET, too a complete description see [5].

HOPLITE

This is a design tool developed to investigate the effects of rotor morphing on engine emissions and fuel burn. Low-fidelity models are used for quick force and power calculations. HOPLITE has a modular architecture and performs single-point analyses for four main aircraft systems, main rotor, fuselage, tail rotor, and engine, these are encompassed in the "Analysis Modules" which are controlled by the "Control Modules" that are the direct contact between the user and the software. The main rotor is modelled using BET as to account for the geometrical changes in the blade, see [6].

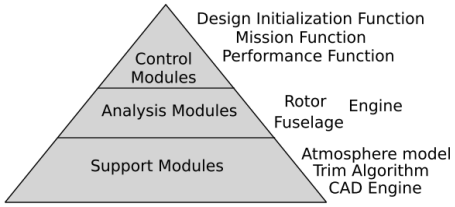

Figure 1.3: Architecture levels of HOPLITE, see [6]

RIDE project

This project aimed to provide a basis for a multidisciplinary (geometry, aerodynamics, structures, mass and engine statistics) tool for preliminary rotorcraft design with a strong focus on the assessment of the selected configuration, see [7]. The analyses are made using HOST (Helicopter Overall Simulation Tool), see [8].

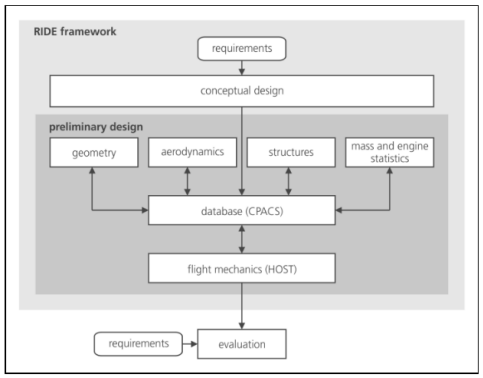

Figure 1.4: RIDE workflow and modules interaction, see [7]

HOST

This is a performance analysis tool that does trim calculations, simulations in the time domain, and linear equivalent system calculations (used to verify handling qualities and stability of the helicopter), see [8].

2 Theoretical background

A helicopter is an aircraft that generates its aerodynamics forces through the spinning blades in the rotors. The understanding of these aerodynamic problems has been done using different approaches such as analytical theories, numerical modeling, and experimentation. Two main theories have been developed to evaluate the helicopter rotor's performance, the momentum theory, and the blade element theory. Each of these theories will be described in detail in this chapter following the content presented in [9].

2.1 Momentum theory

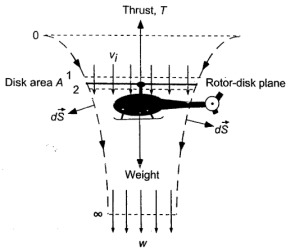

Figure 2.1: Flow model for momentum theory in hovering flight ([9], pg. 61)

The generic approach of this problem (as is shown in Figure 2.1) assumes that the flow is one-dimensional, quasi-steady, incompressible and inviscid, and although it does not take into account the complex vortical wake structure associated with the rotor aerodynamics or the actual details of the flow environment (local flow around the rotor blade), it allows for a first-order prediction of the thrust generated and power required for a given flight condition. The physical principles considered in this theory can be used as a starting point for more elaborate analyses of the rotor aerodynamics. The thrust created by the action of the air on the blades is supported by the rotor disk, as a result an equal but opposite reaction exists of the rotor on the air thus inducing velocity to the rotor wake.

Applying basic conservation laws of fluid mechanics to the control volume of Figure 2.1 (such as conservation of mass, equation 2.1, momentum, equation 2.2 and energy, equation 2.3) to the rotor flow, as a whole, estimations of the performance can be made, this simple approach became known as the Rankine-Froude momentum theory.

$$\int\int_S \rho \overrightarrow{V}.\overrightarrow{dS} = 0 \tag{2.1}$$

Where ρ is the specific mass, $\overrightarrow{V}$ the flow velocity, and $\overrightarrow{dS}$ the unit vector normal to the control volume surface S.

$$\int\int_S p\overrightarrow{dS} + \int\int_S (\rho \overrightarrow{V} \cdot \overrightarrow{dS})\overrightarrow{V} = \overrightarrow{F} \tag{2.2}$$

Where p is the pressure and $\overrightarrow{F}$ the resultant force.

$$\int\int_S \frac{1}{2}(p\overrightarrow{V} \cdot \overrightarrow{dS})|\overrightarrow{V}|^2 = E \tag{2.3}$$

Where E is the work done on the fluid by the rotor.

2.1.1 Hover flight

In this flight condition the aircraft has zero velocity (longitudinal, lateral and vertical), this means that the flow field is azimuthially axisymmetric.

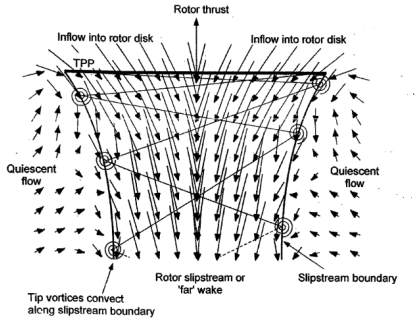

Figure 2.2: Velocity field near a rotor in hover ([9], pg. 59)

As can be seen in figure 2.2 the velocity is increased, without jumps, as it goes through the rotor disk plane, the same does not apply to the pressure, as thrust is produced by the rotor, there must be a jump (discontinuity) in pressure. A wake boundary is clearly defined, with the flow outside this boundary being relatively undisturbed, and the flow inside being accelerated downwards as the wake contracts.

Considering an unconstrained flow, the net pressure force on the control volume is zero. Therefore the net force, $\overrightarrow{F}$, is equal to the rate of change of fluid momentum across the surface, S.

Hovering rotor

Applying these general equations to the hovering rotor problem several results can be derived. From the assumption of quasi-steady flow:

$$\dot{m} = \int\int_{\infty} \rho \overrightarrow{V} \cdot \overrightarrow{dS} = \int\int_{2} \rho \overrightarrow{V} \cdot \overrightarrow{dS} \tag{2.4}$$

Where $\dot{m}$ is the mass flow rate.

And the 1-D assumption leads to:

$$\dot{m} = \rho A_{\infty} w = \rho A_2 v_2 = \rho A v_i \tag{2.5}$$

Where $A = A_2$ is the rotor disk area, A_{∞} the wake area, v the inflow velocity at the rotor disk, and w the inflow velocity at the fully developed wake.

The conservation of momentum relates the thrust , $\overrightarrow{T}$, and the rate of change of fluid momentum. The thrust is equal and opposite to the force $\overrightarrow{F}$ on the fluid:

$$-\overrightarrow{F} = \overrightarrow{T} = \int\int_{\infty} (\rho \overrightarrow{V} \cdot \overrightarrow{dS}) \overrightarrow{V} - \int\int_{0} (\rho \overrightarrow{V} \cdot \overrightarrow{dS}) \overrightarrow{V} \tag{2.6}$$

The far upstream is considered to be a region of undisturbed flow so the second term of equation 2.6 is zero, additionally as we are assuming a 1-D approximation the velocity $\overrightarrow{V}$ can be simply represented by its scalar value V, and the rotor thrust is given by:

$$T = \int\int_{\infty} (\rho \overrightarrow{V} \cdot \overrightarrow{dS}) V = \dot{m} w \tag{2.7}$$

From the principle of conservation of energy the work done per unit time on the rotor is, Tv_i:

$$E = T v_i = \int\int_{\infty} \frac{1}{2} (\rho \overrightarrow{V} \cdot \overrightarrow{dS}) V^2 - \int\int_{0} \frac{1}{2} (\rho \overrightarrow{V} \cdot \overrightarrow{dS}) V^2 \tag{2.8}$$

The second term is zero because the velocity on the far upstream plane is zero, thus resulting:

$$T v_i = \int\int_{\infty} \frac{1}{2} (\rho \overrightarrow{V} \cdot \overrightarrow{dS}) V^2 = \frac{1}{2} \dot{m} w^2 \tag{2.9}$$

From the equations 2.6 and 2.9 it is clear that:

$$v_i = \frac{1}{2} w \tag{2.10}$$

This gives a simple relation between the induced velocity in the rotor plane, v_i, and the wake velocity, w, in the vena contracta.

Induced Velocity and Rotor Power

Considering the equations 2.5, 2.7 and 2.10 the rotor thrust, T, and induced velocity, v_i, can be related:

$$T = \dot{m}w = \dot{m}2v_i = 2\rho A v_i v_i = 2\rho A v_i^2 \tag{2.11}$$

Rearranging to solve for the induced volecity:

$$v_h \equiv v_i = \sqrt{\frac{T}{2\rho A}} \tag{2.12}$$

The ratio T/A is known as Disk Loading, DL measured in Newtons per square meter, and is an important parameter in the helicopter analysis. Note that v_h is used to represent the induced velocity for the hover condition. The power P is given by:

$$P = Tv_i = T\sqrt{\frac{T}{2\rho A}} = \sqrt{\frac{T^3}{2\rho A}} \tag{2.13}$$

From this equation another parameter can be defined, the power loading, PL measured in Newtons per Watt, which is given by:

$$\frac{P}{T} = \sqrt{\frac{T}{2\rho A}} = v_i = (PL)^{-1} \tag{2.14}$$

2.1.2 Nondimensional coefficients

Induced inflow ratio:

$$\lambda_i = \frac{v_i}{\Omega R} \tag{2.15}$$

Where Ω is the blade angular velocity, and R is the rotor radius.
The thrust C_T, torque C_Q, and power C_P coefficients are:

$$C_T = \frac{T}{\rho A V_{tip}^2} = \frac{T}{\rho A \Omega^2 R^2} \tag{2.16}$$

Where V_{tip} is the blade tip velocity.

$$C_Q = \frac{Q}{\rho A V_{tip}^2 R} = \frac{Q}{\rho A \Omega^2 R^3} \tag{2.17}$$

Where Q is the rotor torque.

$$C_P = \frac{P}{\rho A V_{tip}^3} = \frac{P}{\rho A \Omega^3 R^3} \tag{2.18}$$

Considering the results from the equations 2.12, 2.15, and 2.16 the following expression can be defined:

$$\lambda_i = \frac{v_i}{\Omega R} = \frac{1}{\Omega R}\sqrt{\frac{T}{2\rho A}} = \sqrt{\frac{T}{2\rho A(\Omega R)^2}} = \sqrt{\frac{C_T}{2}} \tag{2.19}$$

Based on momentum theory:

$$C_P = \frac{Tv_i}{\rho A \Omega^3 R^3} = \left(\frac{T}{\rho A \Omega^2 R^2}\right)\left(\frac{v_i}{\Omega R}\right) = C_T \lambda_i = \frac{C_T^{3/2}}{\sqrt{2}} \tag{2.20}$$

This is calculated based on the uniform inflow assumption, not considering viscous losses, thus being called the *ideal power* coefficient.

2.1.3 Nonideal effects on Rotor Performance

Following chapter 2.7 from [9] it is known that the momentum theory underpredicts the actual power required, although the trend $C_P \propto C_T^{3/2}$ is essentially correct, the difference in the results is due to the neglect of a series of physical effects such as nonuniform inflow, tip losses, wake swirl, less than ideal wake contraction, finite number of blades, tip vortices interaction, and so on. This implies that a correction can be done using an empirical modification to the momentum theory result:

$$C_{P_i} = \frac{kC_T^{3/2}}{\sqrt{2}} \tag{2.21}$$

Where k is called induced power correction factor, and can be derived from flight and wind tunnel tests.

The result given in equation 2.21 only represents the induced power coefficient, for a proper estimate of the total rotor power another component needs to be taken into account, the power that the rotor blades require to keep rotating despite of the aerodynamic drag, the profile power:

$$P_0 = \Omega N_b \int_0^R D y dy \tag{2.22}$$

Where N_b is the number of rotor blades, y is the spanwise coordinate along the blade and the drag force, D, can be expressed as:

$$D = \frac{1}{2}\rho V^2 c C_d = \frac{1}{2}\rho(\Omega y)^2 c C_d \tag{2.23}$$

This result assumes a constant profile drag coefficient, $C_d = C_{d_0}$, and a rectangular blade, constant chord, c, now the profile power can be calculated (by integration along the blade) as:

$$P_0 = \frac{1}{8}\rho N_b \Omega^3 c C_{d_0} R^4 \tag{2.24}$$

Converting to a profile power coefficient leads to:

$$C_{P_0} = \frac{P_0}{\rho A(\Omega R)^3} = \frac{1}{8}\left(\frac{N_b c R}{A}\right) C_{d_0} = \frac{1}{8}\sigma C_{d_0} \tag{2.25}$$

With σ being the rotor solidity which is defined as the ratio between the rotor blades area and the total rotor area. So now the rotor power coefficient can be expressed as:

$$C_P = C_{P_i} + C_{P_0} = \frac{kC_T^{3/2}}{\sqrt{2}} + \frac{\sigma C_{d_0}}{8} \tag{2.26}$$

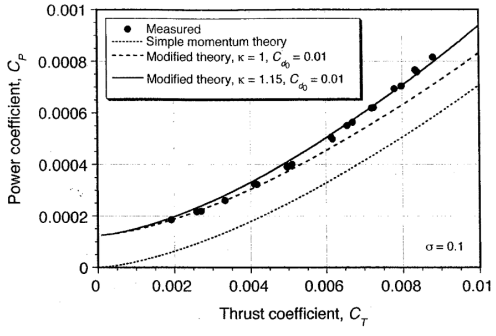

Figure 2.3: Momentum theory power predictions comparison ([9], pg. 68)

2.1.4 Figure of Merit

The definition of an efficiency factor for a helicopter is not simple given the multitude of parameters involved. The power loading is one measure of rotor efficiency and is to be made as large as possible in order to reduce the power requirements of the rotorcraft for a given thrust, however the PL is a dimensional quantity making it not viable to compare very different rotors. The idea of figure of merit, FM,

was adopted to fill this void in nondimensional evaluation of the helicopter efficiency, it was introduced in its present form by Richard H. Prewitt in the 1940s, see [9]. The figure of merit is the ratio of the ideal power of a rotor and the actual power required to hover.

$$FM = \frac{P_{ideal}}{P_{measured}} = \frac{\frac{C_T^{3/2}}{\sqrt{2}}}{\frac{kC_T^{3/2}}{\sqrt{2}} + \frac{\sigma C_{d_0}}{8}} \tag{2.27}$$

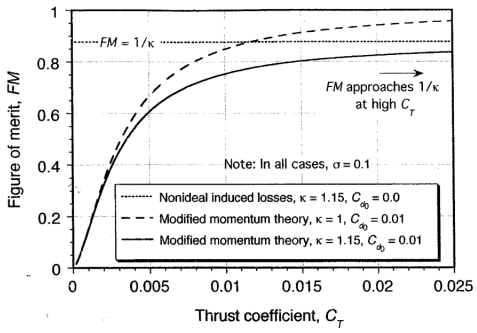

Figure 2.4: Figure of merit variation with thrust coefficient for different assumptions ([9], pg. 72)

2.1.5 Induced Tip Loss

At the tip of each blade a trailed vortex is formed which produces a high local inflow and reduces the lift capability over that region, this phenomenon is known as tip loss.

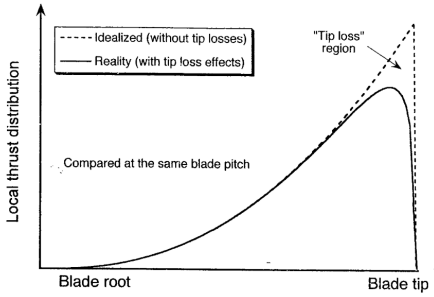

Figure 2.5: Tip loss effect ([9], pg. 75)

In the preliminary rotor design phase a simple tip loss factor, B, can be used to estimate the effect of the tip vortices where the product, $B \times R$, corresponds to the effective rotor radius. Prandtl, see [9], showed that when accounting for the tip losses the effective radius can be given by:

$$\frac{R_e}{R} \approx 1 - \left(\frac{1.386}{N_b}\right) \frac{\lambda_i}{\sqrt{1+\lambda_i^2}} \tag{2.28}$$

Gessow & Meyers (1952), see [10], propose the empirical relation based on the blade geometry:

$$B = 1 - \frac{c}{2R} \tag{2.29}$$

This result is not general as to deal with blades that are not rectangular and so Sissingh (1939), see [11], suggested the following adaptation:

$$B = 1 - \frac{c_0(1+0.7\tau)}{1.5R} \tag{2.30}$$

Where c_o is the blade root chord, and τ is the blade taper ratio.

2.1.6 Axial flight

The difference in axial flight when compared to the hover condition is that a vertical velocity V_c exists and will register alterations to the conservation equations (2.1, 2.2, and 2.3).

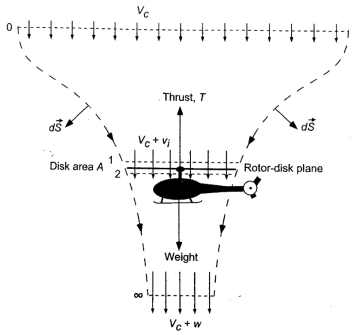

Figure 2.6: Flow model for momentum theory in axial flight ([9], pg. 82)

Applying the conservation of mass equation to the control volume in Figure 2.6:

$$\dot{m} = \int\int_{\infty} \rho \overrightarrow{V} \cdot d\overrightarrow{S} = \int\int_{2} \rho \overrightarrow{V} \cdot d\overrightarrow{S} = \rho A_{\infty}(V_c + w) = \rho A(V_c + v_i) \tag{2.31}$$

Applying the conservation of momentum:

$$T = \int\int_{\infty} \rho(\overrightarrow{V} \cdot d\overrightarrow{S})V - \int\int_{0} \rho(\overrightarrow{V} \cdot d\overrightarrow{S})V = \dot{m}(V_c + w) - \dot{m}V_c = \dot{m}w \tag{2.32}$$

The work done by the climbing rotor is now given by:

$$\begin{aligned} T(V_c + v_i) = \int\int_{\infty} \frac{1}{2}\rho(\overrightarrow{V} \cdot d\overrightarrow{S})V^2 - \int\int_{0} \frac{1}{2}\rho(\overrightarrow{V} \cdot d\overrightarrow{S})V^2 = \\ \frac{1}{2}\dot{m}(V_c + w)^2 - \frac{1}{2}\dot{m}V_c^2 = \frac{1}{2}\dot{m}w(2V_c + w) \end{aligned} \tag{2.33}$$

Where V_c is the climb velocity.
Taking the results of the equations 2.31 and 2.32:

$$T = \dot{m}w = \rho A(V_c + v_i)w = 2\rho A(V_c + v_i)v_i \tag{2.34}$$

Now also considering the result of the equation 2.12:

$$\frac{T}{2\rho A} = v_h^2 = (V_c + v_i)v_i \tag{2.35}$$

Dividing by v_h^2:

$$\left(\frac{v_i}{v_h}\right)^2 + \frac{V_c}{v_h}\left(\frac{v_i}{v_h}\right) - 1 = 0 \tag{2.36}$$

This is a quadratic equation in v_i/v_h which has the solutions:

$$\frac{v_i}{v_h} = -\left(\frac{V_c}{2v_h}\right) \pm \sqrt{\left(\frac{V_c}{2v_h}\right)^2 + 1} \tag{2.37}$$

One of these solution is negative, this violates the assumed model so the only solution that can be considered in this case is:

$$\frac{v_i}{v_h} = -\left(\frac{V_c}{2v_h}\right) + \sqrt{\left(\frac{V_c}{2v_h}\right)^2 + 1} \tag{2.38}$$

2.1.7 Axial Descent

In the case that the climb velocity is negative the model used in section 2.1.6 cannot be used because the slipstream will be above the rotor disk, this will happen whenever the axial velocity, $|V_c|$, is more than twice the value of v_h.

For the case where $-2v_h \leq V_c \leq 0$ a complicated recirculating flow pattern may exist at the rotor and the slipstream can be either above or below the rotor, this case will be discussed separately.

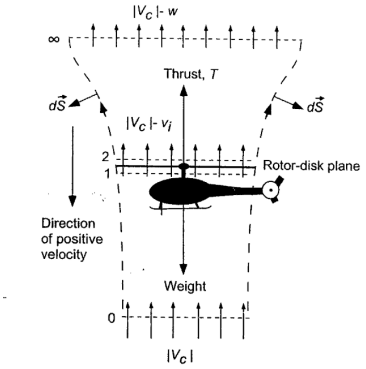

Figure 2.7: Flow model for momentum theory in axial flight (descent) ([9], pg. 85)

Applying the conservation of mass to the control volume in Figure 2.7:

$$\dot{m} = \int\int_{\infty} \rho \overrightarrow{V} \cdot d\overrightarrow{S} = \int\int_{2} \rho \overrightarrow{V} \cdot d\overrightarrow{S} = \rho A_{\infty}(V_c + w) = \rho A(V_c + v_i) \tag{2.39}$$

Applying the conservation of momentum:

$$T = \left[\int\int_{\infty} \rho(\overrightarrow{V} \cdot d\overrightarrow{S})V - \int\int_{0} \rho(\overrightarrow{V} \cdot d\overrightarrow{S})V\right] = (-\dot{m})(V_c + w) - (-\dot{m})V_c = -\dot{m}w \tag{2.40}$$

The sign convention dictates that the velocity is positive in the downward direction, considering this it can be noted that the thrust, T, is positive in equation 2.40.

The work done by the descending rotor is now given by:

$$\begin{aligned} T(V_c + v_i) = \int\int_{0} \frac{1}{2}\rho(\overrightarrow{V} \cdot d\overrightarrow{S})V^2 - \int\int_{\infty} \frac{1}{2}\rho(\overrightarrow{V} \cdot d\overrightarrow{S})V^2 = \\ \frac{1}{2}\dot{m}V_c^2 - \frac{1}{2}\dot{m}(V_c + w)^2 = -\frac{1}{2}\dot{m}w(2V_c + w) \end{aligned} \tag{2.41}$$

The result of equation 2.41 is negative, meaning that the rotor is extracting power from the airstream, this condition is known as *windmill state*.

Combining equations 2.40 and 2.41 it follows again that $w = 2v_i$ and so it can be derived that:

$$T = -\dot{m}w = -\rho A(V_c + v_i)w = -2\rho A(V_c + v_i)v_i \tag{2.42}$$

Now relating with the hover induced velocity, v_h:

$$\frac{T}{2\rho A} = v_h^2 = -(V_c + v_i)v_i = -V_c v_i - v_i^2 \tag{2.43}$$

Dividing by v_h^2:

$$\left(\frac{v_i}{v_h}\right)^2 + \frac{V_c}{v_h}\left(\frac{v_i}{v_h}\right) + 1 = 0 \tag{2.44}$$

This is a quadratic equation in v_i/v_h which has two solutions, however one of these violates the assumed model as it produces values of $v_i/v_h > 1$, thus the only valid solution is:

$$\frac{v_i}{v_h} = -\left(\frac{V_c}{2v_h}\right) - \sqrt{\left(\frac{V_c}{2v_h}\right)^2 - 1} \tag{2.45}$$

2.1.8 Vortex Ring state

In the region $-2 \leq V_c/v_h \leq 0$ a slipstream that is well defined ceases to exist thus rendering the momentum theory invalid. However, using empirical methods an approximate velocity curve can still be defined.

In descending flight the iterations between the tip vortices and other blades is accentuated, the flow becomes unsteady and the average induced velocity is difficult to measure directly, instead it is obtained from the measurement of the rotor power and thrust. This working state is known as *Vortex Ring state*.

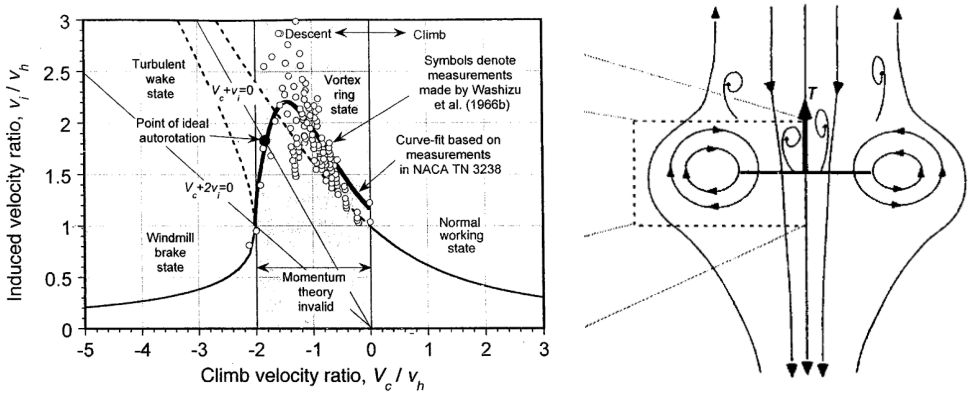

(a) Induced velocity variation ([9], pg. 84)

(b) Flow model ([9], pg. 89)

Figure 2.8: Vortex Ring state

$$P_{measure} = T(V_c + \overline{v_i}) + P_0 \tag{2.46}$$

Where $\overline{v_i}$ is the average induced velocity over the rotor disk.

Therefore to estimate the average induced velocity not only the rotor power needs to be measure but also the profile power P_0. As stated in equation 2.25, $C_{P_0} = \frac{1}{8}\sigma C_{d_0}$, so knowing the rotor solidity and knowing the mean drag coefficient of the blades this portion of the power can be calculated.

Given the flow conditions and approximations made in this process, the results have a scattered nature, as can be seen in Figure 2.8 (a). As the induced velocity curve can not be analytically predicted in the range $-2 \leq V_c/v_h \leq 0$ the experimental results required a fitted approximation for v_i at a given rate of descent V_c.

A continuous approximation valid for the full range of the vortex ring state is presented, see [9]:

$$\frac{v_i}{v_h} = k + k_1\left(\frac{V_c}{v_h}\right) + k_2\left(\frac{V_c}{v_h}\right)^2 + k_3\left(\frac{V_c}{v_h}\right)^3 + k_4\left(\frac{V_c}{v_h}\right)^4 \tag{2.47}$$

Where k is the induced power factor in hover, $k_1 = -1.125$, $k_2 = -1.372$, $k_3 = -1.718$, and $k_4 = -0.655$.

2.1.9 Forward flight

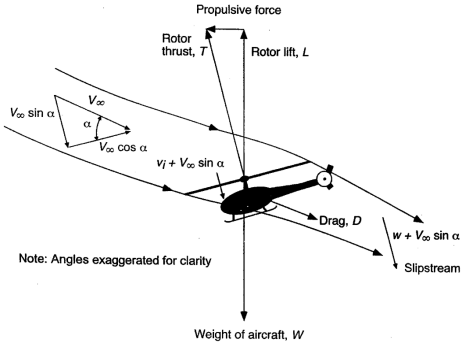

Figure 2.9: Flow model for momentum theory in forward flight ([9], pg. 93)

In the forward flight case the total velocity has a component that is parallel to the rotor plane. Helicopter rotors are required to produce the total force of the aircraft, this means that to overcome the aerodynamic drag originated by the forward velocity the rotor needs to be tilted forward, see Figure 2.9, in these conditions the flow axisymmetry is lost.

The mass flow rate through the disk is:

$$\dot{m} = \rho A U \tag{2.48}$$

With U being:

$$U = \sqrt{(V_\infty cos\alpha^{TTP})^2 + (V_\infty sin\alpha^{TTP} + v_i)^2} = \sqrt{V_\infty^2 + 2V_\infty v_i sin\alpha^{TTP} + v_i} \tag{2.49}$$

Where α^{TTP} is the rotor disk inclination.

Applying the momentum conservation equation to the direction perpendicular to the rotor disk:

$$T = \dot{m}(w + V_\infty sin\alpha^{TTP}) - \dot{m}V_\infty sin\alpha^{TTP} = \dot{m}w \tag{2.50}$$

And applying the energy conservation equation to the same plane:

$$P = T(v_i + V_\infty sin\alpha^{TTP}) = \frac{1}{2}\dot{m}(V_\infty sin\alpha^{TTP} + w)^2 - \frac{1}{2}V_\infty^2 sin^2\alpha^{TTP} = \frac{1}{2}\dot{m}(2V_\infty w sin\alpha^{TTP} + w^2) \tag{2.51}$$

Note: In here only the induced power is being considered, in further sections a more global analysis will be done to account for the total rotor power in forward flight.

Combining equations 2.50 and 2.51 we arrive once again at $w = 2v_i$, and therefore:

$$T = 2\dot{m}v_i = 2\rho A U v_i = 2\rho A v_i \sqrt{V_\infty^2 + 2V_\infty v_i sin\alpha^{TTP} + v_i^2} \tag{2.52}$$

2.1.10 Induced Velocity in Forward Flight

Recalling the equation 2.12 where $v_h^2 = T/2\rho A$ and combining this result with the one from equation 2.52 we obtain:

$$v_i = \frac{v_h^2}{\sqrt{(V_\infty cos\alpha^{TTP})^2 + (V_\infty sin\alpha^{TTP} + v_i)^2}} \tag{2.53}$$

The concept of *tip speed ratio*, or *advance ratio*, μ, can now be introduced and it is defined as the ratio between the blade tip speed and the velocity parallel to the rotor disk:

$$\mu = \frac{V_\infty cos\alpha^{TTP}}{\Omega R} \tag{2.54}$$

The general function for the inflow ratio:

$$\lambda = \frac{V_\infty sin\alpha^{TTP} + v_i}{\Omega R} = \mu\, tan\alpha^{TTP} + \lambda_i \tag{2.55}$$

Taking into account equation 2.19 where $\lambda_h = \sqrt{C_T/2}$, and the concepts of *advance ratio* and *inflow ratio* equation 2.53 can be written as:

$$\lambda_i = \frac{\lambda_h^2}{\sqrt{\mu^2 + \lambda^2}} = \frac{C_T}{2\sqrt{\mu^2 + \lambda^2}} \tag{2.56}$$

Combining equations 2.55 and 2.56 we can obtain the final equation for the inflow ratio λ:

$$\lambda = \mu\, tan\alpha^{TTP} + \frac{C_T}{2\sqrt{\mu^2 + \lambda^2}} \tag{2.57}$$

Analytical solutions can be found for this equation but usually a numerical procedure is used to solve it.

2.1.11 Co-axial Rotor Systems

A co-axial rotor system consists in a contrarotating rotor arrangement that has the advantage of a reduced net size of the system, furthermore the need for a tail rotor for anti-torque purposes ceases to exist, this allows all of the power to be used to produce useful thrust. This doesn't come without a cost, given the configuration, the strong interaction between rotor wakes has an impact on the total performance resulting in a loss of aerodynamic efficiency.

As in chapter 2.15.1 from [9] the analysis starts by assuming that the rotors are sufficiently close together (the lifting area is the same) and the the thrust is equal between them, rendering $W = 2T$.

The induced velocity of the system will be:

$$(v_i)_e = \sqrt{\frac{2T}{2\rho A}} \tag{2.58}$$

The induced power:

$$(P_i)_e = 2T(v_i)_e = \frac{(2T)^{3/2}}{\sqrt{2\rho A}} \tag{2.59}$$

However if the rotors are treated separately:

$$P_i = \frac{2(T)^{3/2}}{\sqrt{2\rho A}} \tag{2.60}$$

Comparing the two results we arrive at the following:

$$k_{int} = \frac{(P_i)_e}{P_i} = \frac{(2T)^{3/2}}{\sqrt{2\rho A}} / \frac{2(T)^{3/2}}{\sqrt{2\rho A}} = \frac{2^{3/2}}{2} = \sqrt{2} \tag{2.61}$$

Where k_{int} is the interference induced power factor.

This assumption shows that the induced power in a coaxial rotor system will be approximately 41% greater than the induced power of two separate rotors producing the same thrust. This result is over pessimistic when compared to experimental tests, the main reason for this inaccuracy is related to the actual finite spacing between the rotors which is a major factor when calculating the interference factor.

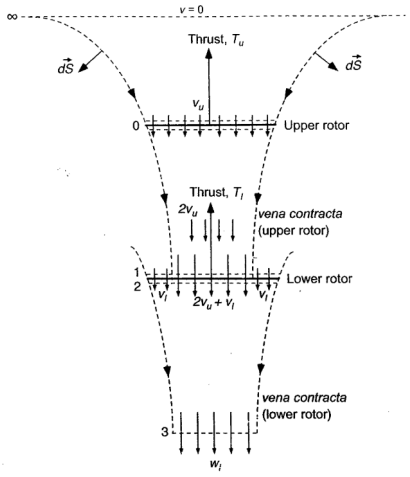

Figure 2.10: Flow model for momentum theory in hovering flight for a coaxial configuration ([9], pg. 102)

Taking the same approach as in all section of this chapter and assuming a rotor spacing such as the lower rotor, denoted with the subscript l, is in the fully developed wake of the upper rotor, denoted with the subscript u, see Figure 2.10, and that the top rotor's performance is not influenced:

$$v_u = \sqrt{\frac{T}{2\rho A}} = v_h \tag{2.62}$$

The vena contracta of the upper rotor is shedded into an area of $A/2$ with a velcity of $2v_u = w_l$ on the lower rotor, so in this central zone the inflow velocity is of $2v_u + v_l$ whereas in the outer region the inflow velocity is v_l.

Applying the mass conservation to the lower rotor:

$$\dot{m} = \rho\frac{A}{2}(2v_u + v_l) + \rho\left(\frac{A}{2}\right)v_l = \rho A(v_u + v_l) \tag{2.63}$$

Applying the momentum conservation to the plane of the fully developed wake of the system to calculate the lower rotor thrust:

$$T_l = \rho A(v_u + v_l)w_l - 2\rho A v_u^2 \tag{2.64}$$

The power required is:

$$P_l = T_l(v_u + v_l) \tag{2.65}$$

Which is equal to the gain in kinetic energy by the slipstream:

$$T_l(v_u + v_l) = \frac{1}{2}\rho A(v_u + v_l)w_l^2 - \frac{1}{2}\rho\left(\frac{A}{2}\right)(2v_u)(2v_u)^2 = \frac{1}{2}\rho A(v_u + v_l)w_l^2 - 2\rho A v_u^3 \tag{2.66}$$

If it is assumed that $T_u = T_l = T = 2\rho A v_u^3$ then:

$$T_l = T = \frac{1}{2}\rho A(v_u + v_l)w_l \tag{2.67}$$

Applying this result to equation 2.66:

$$T(2v_u + v_l) = \frac{1}{2}\rho A(v_u + v_l)w_l^2 \tag{2.68}$$

Combining the last two equations (2.67 and 2.68) it arises that $w_l = 2v_u + v_l$, using this and $T = 2\rho A v_u^3$ in equation 2.67:

$$4\rho A v_u^2 = \rho A(v_u + v_l)w_l = \rho A(v_u + v_l)(2v_u + v_l) \tag{2.69}$$

Rearranging as a quadratic and solving for v_l the result is:

$$v_l = \left(\frac{-3 + \sqrt{17}}{2}\right)v_u \approx 0.5616 v_u \tag{2.70}$$

Finally taking the upper rotor power $P_u = Tv_u$ and the lower rotor power $P_l = T(v_u + v_l) \approx 1.5616 Tv_u$ the total power is given by $P \approx 2.5616 Tv_u \approx 2.5616 Tv_h$. Resulting in an interference factor of:

$$k_{int} = \frac{(P_i)_{coaxial}}{2P_i} \approx \frac{2.5616 Tv_h}{2Tv_h} = 1.2808 \tag{2.71}$$

Which is significantly smaller than what was obtained in equation 2.61 and closer to values obtained experimentally, $k_{int} = 1.16$.

After having established the estimation of the induced power we can now write the expression for the total power for the coaxial rotor system:

$$P = \frac{k_{int}k2(T)^{3/2}}{\sqrt{4\rho A}} + \rho A(\Omega R)^3\left(\frac{2\sigma C_{d_0}}{8}\right) \tag{2.72}$$

2.1.12 Tandem Rotor Systems

The tandem rotor configuration consists of a pair of rotors, typically geometrically identical, that overlap to some extent but not like coaxial rotors which are concentric. This system has no need for a tail rotor as an anti torque device as the two rotors will be controlled as to produce a null net torque.

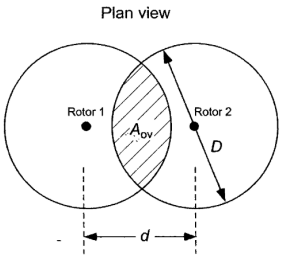

Figure 2.11: Tandem configuration overview ([9], pg. 107)

The analysis of this system from the MT perspective is usually based on the idea of overlapping areas, see chapter 2.15.2 from [9]. Assuming that the rotors have no vertical spacing, let $A_{ov} = m'A$ so we can define it as:

$$m' = \frac{A_{ov}}{A} = \frac{2}{\pi}\left[\theta - \frac{d}{D}sin\theta\right], \quad \text{where} \quad \theta = cos^{-1}\left(\frac{d}{D}\right) \tag{2.73}$$

Where d is the distance between the two rotor shafts and D the rotor diameter.

We can now breakdown the power consumed in each of the areas represented in figure 2.11:

$$P_1 = \frac{(1-m')T_1^{3/2}}{\sqrt{2\rho A}}, \qquad P_2 = \frac{(1-m')T_2^{3/2}}{\sqrt{2\rho A}}, \qquad P_{ov} = \frac{m'(T_1+T_2)^{3/2}}{\sqrt{2\rho A}} \tag{2.74}$$

The total power is given by $P_{i_{tot}} = P_1 + P_2 + P_{ov}$ and the ideal power if we consider two isolated rotors ($m' = 0$) is $P_i = \frac{T_1^{3/2}+T_2^{3/2}}{\sqrt{2\rho A}}$, so now we can define the overlapping factor, k_{ov} as:

$$k_{ov} = \frac{P_{i_{tot}}}{P_i} = \frac{(1-m')T_1^{3/2} + (1-m')T_2^{3/2} + m'(T_1+T_2)^{3/2}}{T_1^{3/2} + T_2^{3/2}} \tag{2.75}$$

And the induced power required to hover can now be expressed as:

$$P_i = k_{ov}kT\sqrt{\frac{T}{4\rho A}} \tag{2.76}$$

Where T is the total thrust produced by the system.

If both rotors are assumed to generate the same amount of thrust an approximation for the overlapping factor can be used:

$$k_{ov} \approx \left[\sqrt{2} - \frac{\sqrt{2}}{2}\left(\frac{d}{D}\right) + \left(1 - \frac{\sqrt{2}}{2}\right)\left(\frac{d}{D}\right)^2\right] \tag{2.77}$$

It is easily shown that if $d \to 0$, $m' \to 1$, then $k_{ov} \to \sqrt{2}$ which is the result for the coaxial case, and if $d \to D$, $m' \to 0$, then $k_{ov} \to 1$ as the rotors are now isolated from each other.

Finally we can express the total power as:

$$P = \frac{k_{ov}k(T)^{3/2}}{\sqrt{4\rho A}} + \rho A(\Omega R)^3\left(\frac{2\sigma C_{d_0}}{8}\right) \tag{2.78}$$

2.1.13 Rotor Wake modelling

In the case of non conventional configurations for the helicopter there might be a strong interaction between rotors. The wake from the top rotor (in the coaxial case) or the front rotor (in the tandem case) will be shedded onto the lower/rear rotor and have an impact on it's performance. It becomes essential to evaluate the rotor wake and measure its influence.

The wake can be modelled as a streamtube, following [12]. MT doesn't have the ability of providing a detailed solution but a trustworthy velocity, V_s, along the streamtube centerline can be defined:

$$V_s = V_c + v_i + v_i\, tanh\left(s\frac{k_s}{h}\right) \tag{2.79}$$

Where s is the vertical spacing between a given plane and the rotor disk plane, h is the extent of the streamtube (above and below the rotor), and k_s is a factor to account for the severity of the wake contraction.

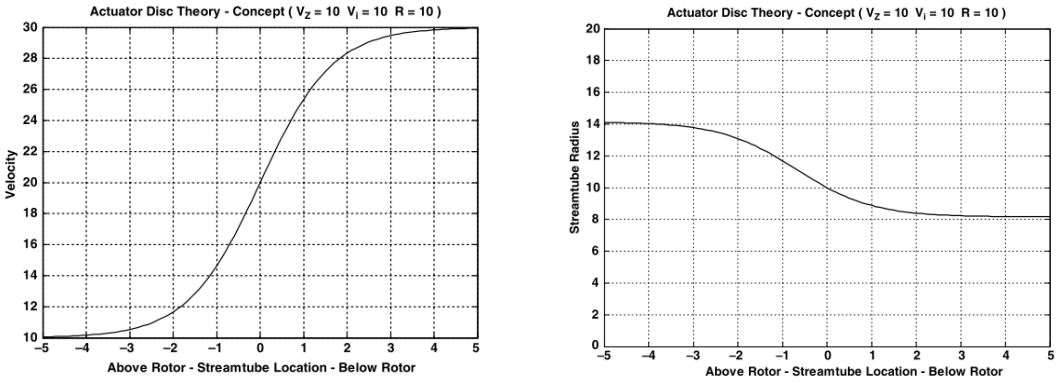

(a) Axial velocity ([12], pg. 35)

(b) Streamtube radius ([12], pg. 36)

Figure 2.12: Variations along the streamtube centerline

In [12] the values for k/h are not defined so using the results obtained in [13] it will be assumed in this work that $k/h = 0.593$.

2.2 Blade Element theory

Rotor aerodynamics analysis has its foundation on blade element theory (BET) as is allows to calculate radial and azimuthal distributions of the aerodynamic loads over the rotor disk. The base assumption of this theory is that each blade section acts as a 2D airfoil to produce forces. Some factors may be applied to account for three dimensional effects (tip losses for example). The rotor performance is calculated integrating the airloads of each section along the blade and averaging the results over a complete revolution. This theory, unlike the momentum theory, can be used as a basis to design the rotor blade in terms of twist and chord distribution, as well as in terms of the airfoil, or airfoils, to be used.

In this analysis the aerodynamic forces are assumed to be produced solely by the velocity and angle of attack normal to the leading edge, the radial component of the velocity is ignored in terms of lift contribution in accordance with the principle of independence [14].

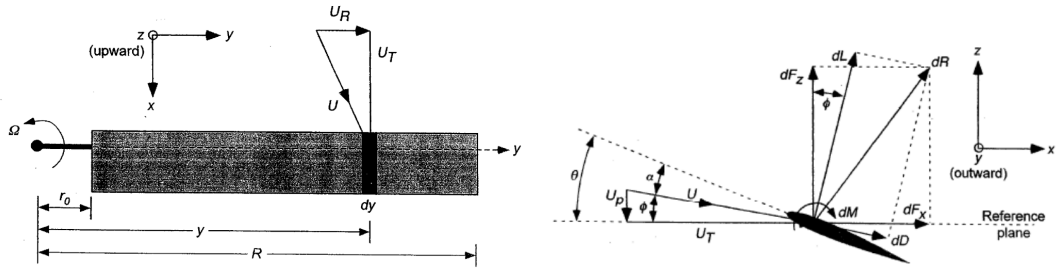

(a) Blade top view

(b) Blade element

Figure 2.13: Incident velocities and aerodynamic environment in a blade element ([9], pg. 116)

2.2.1 Hover and axial flight

From the figure 2.19 we can note that the vertical component of the velocity (perpendicular to the rotor plane) is given by $U_P = V_c + v_i$, the transverse component (in plane and perpendicular to the blade's leading edge) is $U_T = \Omega y$.

The total velocity, U, is given by:

$$U = \sqrt{(V_c + v_i)^2 + (\Omega y)^2} = \sqrt{U_P^2 + U_T^2} \tag{2.80}$$

The relative inflow angle:

$$\phi = tan^{-1}\left(\frac{U_P}{U_T}\right) \tag{2.81}$$

Considering the pitch angle, θ, of the blade element, the angle of attack, α, is given by:

$$\alpha = \theta - \phi \tag{2.82}$$

The resultant incremental aerodynamic forces, lift dL and drag dD, per unit span are:

$$dL = \frac{1}{2}\rho U^2 c C_l dy, \quad \text{and} \quad dD = \frac{1}{2}\rho U^2 c C_d dy \tag{2.83}$$

Where c is the blade chord, C_l the airfoil lift coefficient, C_d the airfoil drag coefficient, and y is the spanwise coordinate.

The forces aligned with the perpendicular (z) and parallel (x) directions (in relation with the rotor plane) can be expressed:

$$dF_z = dLcos\phi - dDsin\phi, \quad \text{and} \quad dF_x = dLsin\phi + dDcos\phi \tag{2.84}$$

And consequently the thrust, torque and power contributions are:

$$dT = N_b dF_z, \quad dQ = N_b dF_x y \quad \text{and} \quad dP = N_b dF_x \Omega y \tag{2.85}$$

To get the total values of the aerodynamic forces the quantities in equation 2.83 need to be integrated along the blade, this process might may need computational methods because of the non linearities associated with some of the variables as is the case of the blade pitch, angle of attack, and blade chord, furthermore the velocity components also need to be calculated locally as they vary with the inflow (affects U_P, and consequently ϕ).

2.2.2 Prandtl's Tip-Loss Function

Prandtl formalized a solution for the induced effects associated with a finite number of blades which takes into account the number of blades, the radial position of the element to be considered and the local inflow angle, see [9].

The correction factor, F, is expressed as:

$$F = \left(\frac{2}{\pi}\right) cos^{-1}(exp(f)) \tag{2.86}$$

Where $f = f_{root} f_{tip}$ is dependent on the number of blades and radial position:

$$f_{tip} = \frac{N_b}{2}\left(\frac{1-r}{r\phi}\right), \quad \text{and} \quad f_{root} = \frac{N_b}{2}\left(\frac{r}{(1-r)\phi}\right) \tag{2.87}$$

Where $r = y/R$ is the adimensional radial position, and ϕ is in radians.

2.2.3 Compressibility Corrections to Rotor Performance

Over the rotor disk, depending on the flight conditions, high Mach numbers may be reached, this will have a considerable impact on the produced aerodynamic forces so it becomes capital to take into account compressibility corrections. Glauert's rule, see [9], states that:

$$C_{l_\alpha} = \frac{C_{l_\alpha}|_{M=0.1}}{\sqrt{1 - M^2}} \tag{2.88}$$

Where $C_{l_\alpha}|_{M=0.1}$ is the 2D lift-curve-slope at $M = 0.1$ and M is the local Mach number.

2.2.4 Forward flight

When considering that the helicopter is moving forward there are some differences in the local inflow in each blade segment. For example, the transverse component of velocity now needs to account for the flight velocity (V_∞) and the azimuthal position (Ψ) that the blade is in:

$$U_T(y, \Psi) = \Omega y \, cos\beta(\Psi) + V_\infty sin\Psi \tag{2.89}$$

Also now there is significant blade motion other than pure rotation about the rotor shaft (as is the case of flapping), this perturbations have considerable impact on the rotor performance.

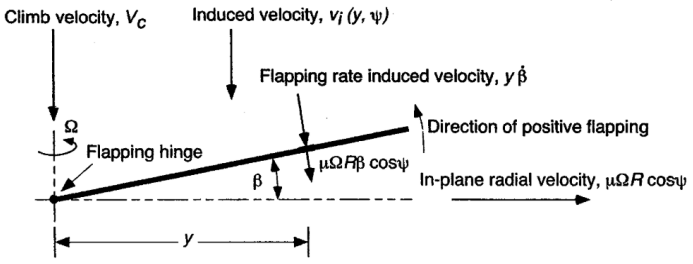

Figure 2.14: Perturbation velocities on the blade ([9], pg. 157)

As can be seen in Figure 2.14 the flapping motion of the blade will change the velocity component that is perpendicular to the rotor plane:

$$U_P(y, \Psi) = V_c + v_i + y\dot{\beta}(\Psi) + V_\infty \, sin\beta(\Psi) \, cos(\Psi) \, cos\beta(\Psi) \tag{2.90}$$

With $\beta(\Psi)$ being the flapping angle and $\dot{\beta}(\Psi)$ the flapping rate which are functions of the azimuthal position.

2.2.5 Linear inflow models

The flight conditions that are considered in this chapter don't allow for the assumption that the flow field around the rotor is axisymmetric. The complexity and nonuniformity of the airflow given the amount of interaction between blades and tip vortices is of an enormous magnitude, nonetheless simple models can be used to estimate the basic effects of the inflow. The simplicity of these models has made them widely used in helicopter rotor aerodynamics problems.

An experiment to measure the time averaged induced velocity over the rotor disk in forward flight was conducted by Brotherhood and Stewart, see [15]. It was concluded that the longitudinal inflow variation was approximately linear for certain speeds. In the range $0 \leq \mu \leq 0.1$ the flow is the most nonuniform, as it is strongly affected by tip vortices that sweep downstream near the rotor, but for $\mu \geq 0.15$ the inflow can be approximated by:

$$\lambda_i = \lambda_0 \left(1 + k_x \frac{x}{R} + k_y \frac{y}{R}\right) = \lambda_0 (1 + k_x r \, cos\Psi + k_y r \, sin\Psi) \tag{2.91}$$

Where k_x and k_y are, respectively, the longitudinal and lateral inflow slopes, and λ_0 is the average induced inflow ratio at the center of the rotor and considering the result from the momentum theory equation 2.56:

$$\lambda_0 = \frac{C_T}{\sqrt{\mu^2 + \lambda_i^2}} \tag{2.92}$$

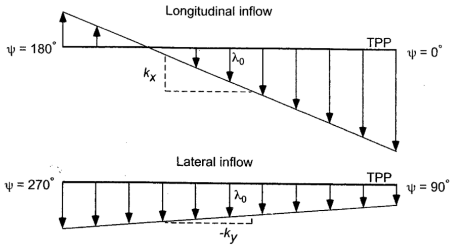

Figure 2.15: Linear inflow model ([9], pg. 159)

For the estimation of the k_x and k_y factors several approximations can be used, one was proposed by Coleman, in [16], in which:

$$k_x = tan\left(\frac{\chi}{2}\right), \quad \text{where} \quad \chi = tan^{-1}\left(\frac{\mu_x}{\mu_z + \lambda_i}\right) \tag{2.93}$$

Where χ is the wake skew angle, μ_x is the longitudinal advance ratio and μ_z is the vertical climb ratio. The wake skew angle increases very rapidly with the advance ratio μ_x and for $\mu_x > 0.2$ the wake is relatively flat.

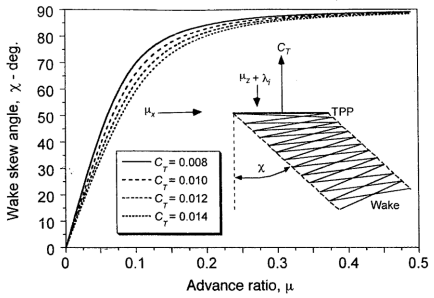

Figure 2.16: Wake skew angle variation with thrust and advance ratio ([9], pg. 160)

Other experiments where conducted and several linear inflow models have been presented as a result:

Authors	k_x	k_y
Coleman et at. (1945), [16]	$tan(\chi/2)$	0
Drees (1949), [17]	$(4/3)(1 - cos\chi - 1.8\mu^2)/sin\chi$	-2μ
Payne (1959), [18]	$(4/3)[\mu/\lambda/(1.2 + \mu/\lambda)]$	0
White & Blake (1979), [19]	$\sqrt{2}sin\chi$	0
Pitt & Peters (1981), [20]	$(15\pi/23)(tan\chi/2)$	0
Howlett (1981), [21]	$sin^2\chi$	0

Table 2.1: Estimated values for the First Harmonic Inflow ([9], pg. 160)

2.3 Rotating blade motion

The motion resulting from the coupling of aerodynamic forces acting on the rotor is paramount to the understanding of the blade motion as to allow for the pilot to successfully control the helicopter. Rotors commonly have articulations near the blade root in the form of flapping and lead-lag hinges. These might be mechanical hinges, semi-rigid or hingeless flexures that allow for the blade to move about a "virtual" hinge location. The blade motion will depend on the geometrical characteristics of the blade itself an on the rotor hub design.

Blades might also have a pitch bearing in their root allowing them to feather, changing their pitch, which can be done collectively (changing the pitch for all the blades at the same time by the same amount), this will control the magnitude of the total rotor produced force, or cyclically (the pitch variation depends

on the azimuthal position of the blade), the latter causes the rotor to tilt, which will change the thrust vector direction and give the pilot control over the helicopter's pitch and roll attitude. As the flow over the rotor looses symmetry these flight controls make it possible for the pilot to maintain a steady and controlled flight.

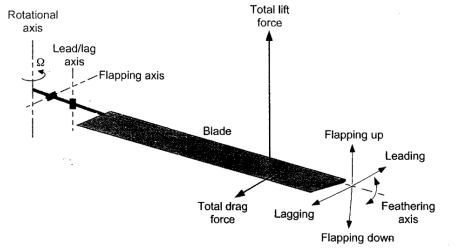

Figure 2.17: Blade motion schematic ([9], pg. 172)

2.3.1 Equation of motion for a Flapping Blade

The equilibrium position of a flapping blade will depend on the relation between aerodynamic and centrifugal forces, typically the coning angles on a helicopter rotor are very small given the much larger nature of centrifugal forces when compared to the aerodynamic ones.

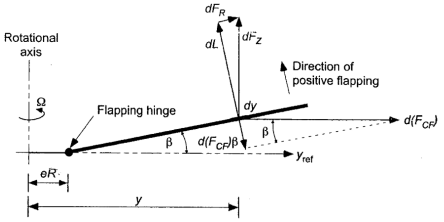

Figure 2.18: Blade forces equilibrium about the flapping hinge, small angle approximation ([9], pg. 175)

The centrifugal force is given by:

$$d(F_{CF}) = my\Omega^2 dy \tag{2.94}$$

Where m is the mass per unit length of the blade.
Integrating:

$$F_{CF} = \int_{eR}^{R} m\Omega^2 y dy \tag{2.95}$$

Where eR is the root cut out section length.
The centrifugal moment:

$$M_{CF} = \int_{eR}^{R} m\Omega^2 y(y - eR) sin\beta dy \tag{2.96}$$

The aerodynamic moment:

$$M_\beta = -\int_{eR}^{R} L(y - eR)dy = -\int_{eR}^{R} \frac{1}{2}\rho U^2 c C_l (y - eR)dy \tag{2.97}$$

So the equilibrium equation for the blade in terms of the flapping motion is simply:

$$M_\beta + M_{CF} = 0 \tag{2.98}$$

The result of equation 2.98 for the hover condition is known as the coning angle β_0 and is constant for all values of Ψ.

Flapping in Forward Flight

In forward flight conditions as a result from the cyclically varying loads the blade flapping motion is periodic is respect to the azimuthal position. So in addition to equations 2.96 and 2.97 the inertial moment needs to be considered:

$$dI_b = my(y - eR)\ddot{\beta}dy \tag{2.99}$$

Where $\ddot{\beta}$ is the flapping acceleration.

The inertial force will be in the opposite direction of the lift produced in that blade section. So the equation of motion in this case is:

$$M_{CF} + M_\beta + I_b = 0 \tag{2.100}$$

With the mass moment of inertia of the blade about the flapping hinge being defined as:

$$I_b = \int_{eR}^{R} m(y - eR)^2 dy \tag{2.101}$$

Integrating:

$$\begin{aligned} &\int_{eR}^{R} m\Omega^2 y(y - eR)sin\beta dy - \int_{eR}^{R} \frac{1}{2}\rho U^2 c C_l (y - eR)dy + \int_{eR}^{R} m(y - eR)^2 \ddot{\beta} dy = 0 \Leftrightarrow \\ &\Leftrightarrow \left(\int_{eR}^{R} m(y - eR)^2 dy\right)\left[\Omega^2 sin\beta\left(1 + \frac{eR\int_{eR}^{R} m(y - eR)dy}{I_b}\right) + \ddot{\beta}\right] = M_\beta \end{aligned} \tag{2.102}$$

And the nondimensional flapping frequency ν_β as:

$$\nu_\beta^2 = 1 + \frac{eR\int_{eR}^{R} m(y - eR)dy}{I_b} \tag{2.103}$$

So equation 2.102 becomes:

$$I_b(\ddot{\beta} + \Omega^2 \nu_\beta^2 \beta) = M_\beta \tag{2.104}$$

Noting that $\Psi = \Omega t$, a manipulation can be made to rewrite equation 2.104, thus:

$$\dot{\beta} = \frac{\partial \beta}{\partial t} = \frac{\partial \beta}{\partial \Psi}\frac{\partial \Psi}{\partial t} = \Omega \frac{\partial \beta}{\partial \Psi} = \Omega \overset{*}{\beta}, \quad \text{and} \quad \ddot{\beta} = \Omega^2 \overset{**}{\beta} \tag{2.105}$$

So finally 2.104 becomes:

$$\overset{**}{\beta} + \nu_\beta^2 \beta = \frac{1}{I_b \Omega^2} M_\beta \tag{2.106}$$

The coning angle β will have a solution based on the pilots inputs for the rotor blade pitch angle (described in section 2.3.2) which have the following expression when an approximation to the first harmonics is made:

$$\theta(\Psi) = \theta_0 + \theta_c cos\Psi + \theta_s sin\Psi \tag{2.107}$$

Where θ_0 is the collective pitch, θ_c the longitudinal cyclic pitch and θ_s the lateral cyclic pitch.

Assuming the solution for the coning angle β can be approximated by the first harmonics we can represented it as:

$$\beta(\Psi) = \beta_0 + \beta_{1_c} cos\Psi + \beta_{1_s} sin\Psi \tag{2.108}$$

In the cases where the flapping hinge is not on the rotor shaft the value for the natural frequency of the rotor is slightly higher than 1/rev, this implies that the phase lag between the forcing and the blade response is less than 90°.

For the hover case the following approximate solutions can be found for the first harmonics, see [9]:

$$\beta_{1_c} = \frac{-\theta_s + (\nu_\beta^2 - 1)\frac{8}{\gamma}\theta_c}{1 + \left[(\nu_\beta^2 - 1)\frac{8}{\gamma}\right]^2} \tag{2.109}$$

$$\beta_{1_s} = \frac{\theta_c + (\nu_\beta^2 - 1)\frac{8}{\gamma}\theta_s}{1 + \left[(\nu_\beta^2 - 1)\frac{8}{\gamma}\right]^2} \tag{2.110}$$

Where γ is the Lock number that can be viewed as the ratio between aerodynamic and inertial forces and is defined as:

$$\gamma = \frac{\rho C_{l_\alpha} c R^4}{I_b} \tag{2.111}$$

Physical description

A more detailed description is presented in the chapters 4.6 and 4.7 of [9].

The coning angle β_0 is the mean part of the flapping motion, it is independent of the blade azimuth, Ψ. It is the angle that results from the moment balance about the flapping hinge.

The longitudinal flapping angle, β_{1_c}, represents the pure cosine flapping motion, i.e. the the fore aft tilt of the rotor tip path plane.

The lateral flapping angle, β_{1_s}, represents the pure sine motion and the lateral tilt of the rotor tip path plane.

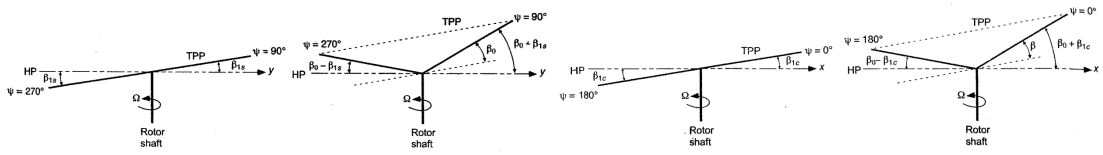

(a) Lateral flapping (b) Longitudinal flapping

Figure 2.19: Flapping motion ([9], pg. 184 and 185)

2.3.2 Helicopter and Rotor trim

To trim the rotor, given certain flight conditions, the pilot needs to guarantee that the rotor is producing enough thrust to overcome the weight of the aircraft, the total drag of the helicopter, and (for the case of the conventional helicopter) the component of the thrust produced by the tail rotor that is not vertical.

The way the pilot controls the main rotor thrust is by changing the blade pitch collectively. The collective pitch θ_0 changes the pitch of all the blades and is used to control the magnitude of the thrust produced. The cyclic pitch, longitudinal θ_c and lateral θ_s, are used to control the tilt of the rotor disk as thus the thrust orientation. The total blade pitch can represented as:

$$\theta(r, \Psi) = \theta_{tw}(r) + \theta_0 + \theta_c cos\Psi + \theta_s sin\Psi \tag{2.112}$$

Where $\theta_{tw}(r)$ is the blade's twist distribution. This equation only considers the first harmonic of the cyclic controls.

The pilot also has the ability to control the tail rotor. The collective pitch θ_{TR} will be changed in order to produce different thrusts as to balance the main rotor torque and control the helicopter yaw motion.

When considering different configurations (coaxial, tandem, or multirotors) the trim conditions are slightly different. The equilibrium condition is that the net torque of all the rotors is zero. Depending on the flight conditions the thrust distribution between all the rotorcraft rotors needs to be adjusted as to achieve this effect.

2.4 Helicopter Performance

The International Standard Atmosphere

The helicopter performance will be greatly influenced by the altitude at which it is flying as density and temperature conditions will affect the aerodynamic loads produced at the blades.
Following chapter 5.2 from [9], the density, ρ in kg/m^3, as a function of altitude, h in meters, is given by:

$$\frac{\rho}{\rho_0} = exp\left(\frac{-0.0296h}{304.8}\right) \tag{2.113}$$

Where $\rho_0 = 1.225\ kg/m^3$ being the density reference value (at sea level).
The temperature, T in Kelvin, is given by;

$$T = 288.15 - 0.001981h \tag{2.114}$$

2.4.1 Forward Flight Performance

In previous chapters, when the forward flight stage was analysed using MT only the induced and profile powers were considered, in this section we intend to include all the components necessary to more accurately predict the total rotor power.

$$P = P_i + P_0 + P_p + P_{other} + P_c \tag{2.115}$$

Where P_i is the induced power, P_0 the profile power required to overcome the viscous losses at the rotor, P_p is the parasitic power associated with the fuselage drag, P_{other} is dependent on the helicopter configuration (for the conventional configuration this component is the tail rotor power), and P_c is the climb power.
The induced power in MT is given by:

$$P_i = kTv_i \tag{2.116}$$

With v_i being given by equation 2.53.
The profile power now is not the same as is the hover case, as it will increase with the advance ratio, a numerical relation introduces the factor K to consider this effect, see [22] and [23]. The assumptions are that $K = 4.5$ when $\mu = 0$ and it will increase linearly until $K = 5$ when $\mu = 0.5$:

$$P_0 = \frac{1}{8}\rho N_b \Omega^3 c C_{d_0} R^4 (1 + K\mu^2) \tag{2.117}$$

The parasitic power depends on the total drag of the helicopter given the flight velocity, altitude, temperature and rotorcraft configuration:

$$P_p = D_f V_\infty = \frac{1}{2}\rho V_\infty^3 S_{ref} C_{D_f} = \frac{1}{2}\rho V_\infty^3 f \tag{2.118}$$

Where D_f is the fuselage drag and, f is the equivalent wetted area defined by:

$$D_f = f\frac{1}{2}\rho V_\infty^2 \Leftrightarrow f = \frac{D_f}{\frac{1}{2}\rho V_\infty^2} \tag{2.119}$$

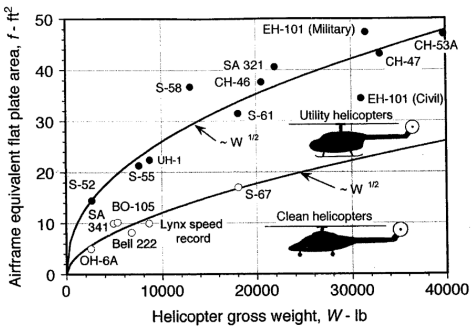

Figure 2.20: Equivalent flat plate area variation with the helicopter gross weight ([9], pg. 307)

The climb power calculates the rate of increase in potential energy of the aircraft. If the climb velocity is V_c and the helicopter weight is W, then:

$$P_c = WV_c \tag{2.120}$$

In the case of a conventional helicopter configuration a tail rotor is needed to counter the torque of the main rotor, and it will require power to function. The power of the tail rotor will need an analogous analysis to the one done on the main rotor in respect to the induced and profile powers:

$$P_{other} = P_{TR} = P_{i_{TR}} + P_{0_{TR}} \tag{2.121}$$

So now having considered all the power components of the helicopter we can see how the forward speed affects each of them. The total power can now be expressed as:

$$\begin{aligned} P &= kTv_i + \frac{1}{8}\rho N_b \Omega^3 c C_{d_0} R^4 (1 + K\mu^2) + \frac{1}{2}\rho V_\infty^3 f + WV_c + P_{TR} \Leftrightarrow \\ \Leftrightarrow C_P &= \frac{kC_T^2}{2\sqrt{\mu^2 + \lambda^2}} + \frac{\sigma C_{d_0}}{8}(1 + K\mu^2) + \frac{1}{2}\frac{f}{A}\mu^3 + \lambda_c C_W + C_{P_{TR}} \end{aligned} \tag{2.122}$$

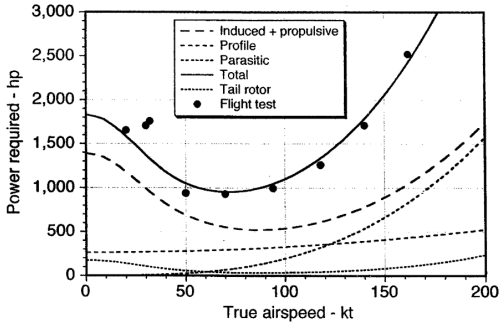

Figure 2.21: Typical power variation with the forward flight speed ([9], pg. 227)

Compressibility Losses and Reverse Flow

A non trivial flow around the rotor occurs when high forward flight speeds are considered. The advancing blade might reach, and exceed, the divergence Mach number of the airfoil leading to greater profile power on the rotor as this effect is not taken into account in the power estimations made through the momentum theory. The region where the Mach number of the flow that is normal to the blade's leading edge exceeds the two dimensional divergence Mach number is defined as:

$$M_{r,\Psi} = M_{\Omega R}(r + \mu sin\Psi) \geq M_{dd} \Leftrightarrow r + \mu sin\Psi \geq \frac{M_{dd}}{M_{\Omega R}} \tag{2.123}$$

Where $M_{\Omega R}$ is the hover tip Mach number, and M_{dd} is the divergence Mach number.

Another phenomenon to consider in this flight conditions is the possibility of a reversed flow region in the retreating blade side. If the flight speed is big enough a reversed flow circular region appears, at $\Psi = 270°$ centered at $r = \mu/2$, and radius μ, and its limit can be defined by:

$$U_T = 0 = \Omega R(r + \mu sin\Psi) \Leftrightarrow r = -\mu sin\Psi \tag{2.124}$$

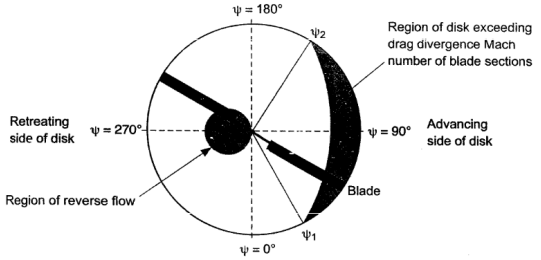

Figure 2.22: Compressibility and reversed flow regions ([9], pg. 221)

In this region the compressibility corrections, explained in section 2.2.3, are necessary to minimize the calculations errors.

Speed for Minimum Power

The previous analysis showed a typical variation in power requirements with the flight speed for a helicopter, see figure 2.21, and it can be easily seen that there is a minimum for a given velocity know as V_{mp}. This velocity is found when the derivative of equation 2.122 in respect to the forward velocity (or advance ratio) is zero:

$$\frac{dC_P}{d\mu} = 0 \tag{2.125}$$

The speed V_{mp} is also the speed at which the helicopter will have the maximum rate of climb (as there will be more available power), and is the optimum speed for autorotation flight which translates to a minimum rate of descent. In addition to these two conditions V_{mp} also gives the speed for the maximum endurance (longest flight time).
The maximum endurance can be estimated for a given specific fuel consumption (SFC):

$$W_F = SFC \times Pt \Leftrightarrow t = \frac{W_F}{SFC \times P} \tag{2.126}$$

Where W_F is the weight of fuel burned in kg, P is the required power in W, and t is the endurance time in seconds.

Maximum Range

Range is defined as the distance the helicopter can cover for a given takeoff weight and amount of fuel, and it can be written as:

$$R = Vt = V\frac{W_F}{SFC \times P} = \frac{W_F}{SFC}\frac{V}{P} \tag{2.127}$$

The range is maximized for a maximum value of V/P, or a minimum P/V which is equivalent to the slope in a power versus airspeed plot.

$$\frac{P}{V} = \frac{k}{V}\sqrt{\frac{T^3}{2\rho A}} + \frac{1}{8V}\rho N_b \Omega^3 c C_{d_0} R^4 (1 + K\mu^2) + \frac{1}{2}\rho V_\infty^2 f + \frac{WV_c}{V} + \frac{P_{TR}}{V} \tag{2.128}$$

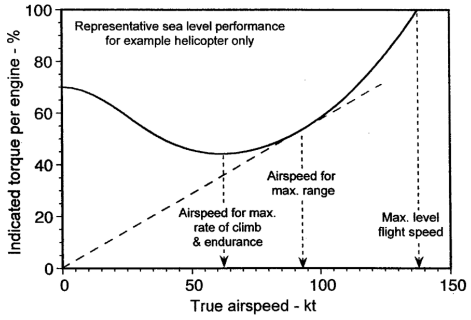

Figure 2.23: Maximum range flight speed graphical representation ([9], pg. 235)

2.4.2 Autorotation Performance

The autorotation maneuver is the self sustained flight condition in which the pilot trades the potential energy of the aircraft (by losing altitude) for power to keep the rotor moving. The airstream will flow upwards through the rotor and provide the required power. This flight condition is essential in the case of an engine or transmission failure as it allows the pilot to land the helicopter in a controlled fashion. A typical autorotation maneuver involves forward speed but lets first consider a purely vertical autorative descent. The inflow angle ϕ must be such that the net in-plane force is null thus the required torque being zero.

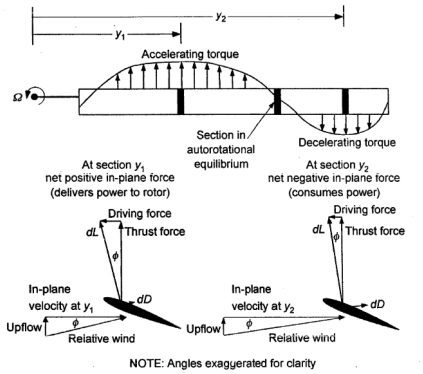

Figure 2.24: Torque distribution along the blade in autorotative flight ([9], pg. 243)

As the inflow angle, and other variables, are not constant along the blade a pure autorotaional equilibrium will only happen in a small region and not on the whole rotor. This region will define the separation between the power consuming and the power providing areas of the rotor. When no forward flight is considered, both of the areas will be circular crowns centered in the rotor shaft (assuming uniform inflow).

Autorotation in Forward Flight

The energy balance is fundamentally the same when comparing forward flight and vertical flight, nonetheless the forward velocity provokes a loss of symmetry in the rotor inflow this changes the power providing and power consuming areas of the rotor.

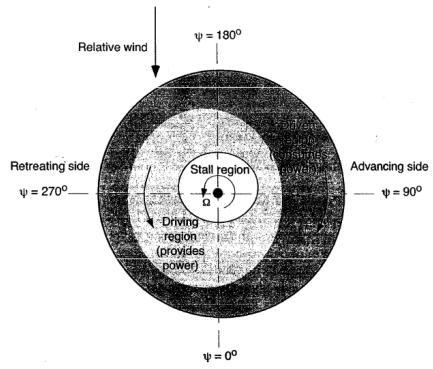

Figure 2.25: Stall, driven, and driving regions of the rotor in autorotation with forward velocity ([9], pg. 247)

An estimation of the rate of autorotative descent given the advance ratio can be made. Considering the results from equation 2.122:

$$C_P = 0 \Leftrightarrow \frac{kC_T^2}{2\sqrt{\lambda^2\mu^2}} + \frac{\sigma C_{d_0}}{8}(1 + K\mu^2) + \frac{1}{2}\frac{f}{A}\mu^3 + \lambda_c C_W + C_{P_{TR}} = 0 \tag{2.129}$$

Neglecting the tail rotor, assuming that $C_T \approx C_W$, and writing in respect to the rate of descent, λ_d, we get:

$$\lambda_d = -\lambda_c \approx \frac{kC_T}{2\sqrt{\lambda^2\mu^2}} + \frac{\sigma C_{d_0}}{8C_T}(1 + K\mu^2) + \frac{1}{2C_T}\frac{f}{A}\mu^3 \tag{2.130}$$

The typical variation of the rate of descent with the forward flight speed is shown in figure 2.26.

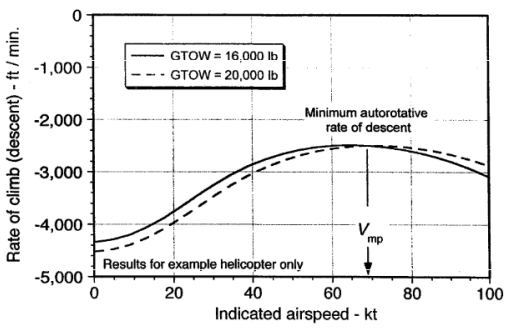

Figure 2.26: Descent velocity for autororation estimation given the advance ratio ([9], pg. 247)

3 Software implementation

The computational tool is intended to allow the user to make the conceptual and preliminary design of a rotary wing aircraft (conventional, co-axial or tandem helicopters) at two different levels of complexity, these will be henceforth called the *basic design* and the *detailed design*. Additionally another tool was developed to the design of small dimensions unmanned rotorcrafts, *drone tool*. One peripheral tool was programmed so that the user could compare airfoil performances when designing the rotor blades *airfoil comparison tool*.

The main idea that dictates the behaviour of the tools is that the user defines the flight conditions (and top level aircraft requirements, in the *detailed tool*) in which the aircraft is to operate and calculations are made in order to assess the feasibility of the design. The user will have the freedom to conduct alterations (namely to the rotor geometry) and compare the performances of the different designs. This comparison is made easier by the clean and simple presentation of the results in the form of plots (three-dimensional plots over the rotor disk, or bi-dimensional plots of the power with varying forward velocity).

3.1 Basic Tool

The information flow and user experience will be exhaustively described in this chapter. First the user will have to choose between three different helicopter configurations, conventional, co-axial or tandem. After this decision the *basic tool* operation will have minimal differences for each configuration in terms of the user experience, only the results will be significantly different.

3.1.1 Structure

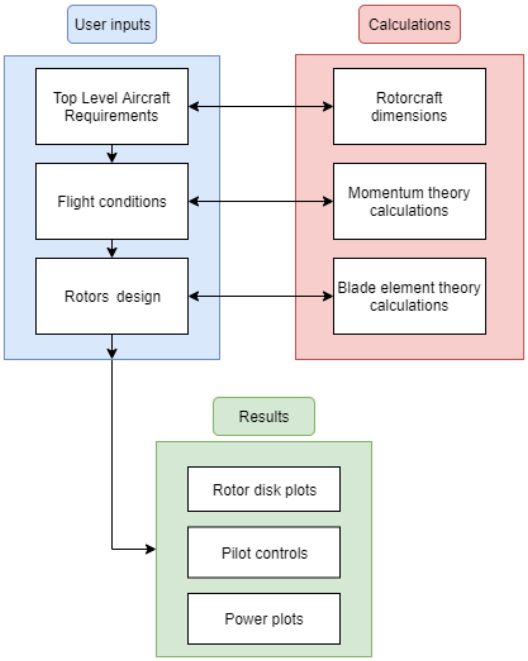

Figure 3.1: Basic tool structure

3.1.2 Information flow and user experience

Note: Throughout this section the *basic tool* for the design of a conventional helicopter will be followed, the differences from the other configurations will be clearly and timely noted.

General Dimensions Tab

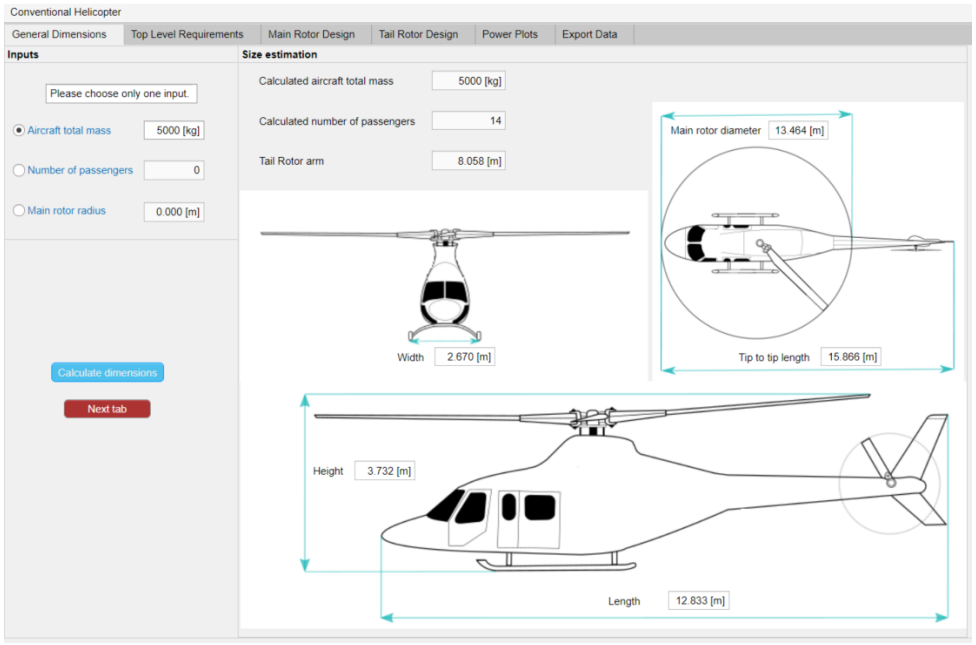

Figure 3.2: Basic tool - General dimensions tab

The user will be asked one single input to start the design of the chosen aircraft this input will be one of the following three (which one to choose is up to the user):

- Aircraft total mass - m in $[kg]$
- Number of passengers - N_{pass}
- Main rotor radius - R in $[m]$

With one of these values the other two can be calculated using the following relations:

$$R = 0.4885 m^{0.308}, \quad \text{see [4]} \tag{3.1}$$

$$m = 1525\, e^{0.0809 \times N_{pass}}, \quad \text{see appendix A.1} \tag{3.2}$$

The number of passengers has to be an integer and cannot be smaller than 1. The rest of the helicopter dimensions (in meters) are estimated based on the rotor radius R using the formulas from [4].

Height:

$$h_{heli} = 0.642 \times (2R)^{0.677} \tag{3.3}$$

Length:

$$l_{heli} = 0.824 \times (2R)^{1.056} \tag{3.4}$$

Tip to tip lenght:

$$ttt_{heli} = 1.09 \times (2R)^{1.03} \tag{3.5}$$

Width:

$$w_{heli} = 0.436 \times (2R)^{0.697} \tag{3.6}$$

Tail rotor arm:

$$a_{heli} = 0.5107 \times (2R)^{1.061} \tag{3.7}$$

The equivalent flat plat area of the helicopter can be estimated based on the aircraft total mass, see figure 2.20, which can be translated to the following:

$$f = (891.45 + \sqrt{794683.1025 - 4412(331.23 - m)})/2206 \tag{3.8}$$

With f in m^2 and m in kg.

Some characteristics of the main and tail rotor can also be calculated using equations from [4].

Main rotor angular velocity $[rad/s]$**:**

$$\Omega = \frac{280}{(2R)^{0.829}} \tag{3.9}$$

Main rotor blade chord $[m]$**:**

$$c = 0.0180\frac{m^{0.539}}{N_b^{0.714}} \tag{3.10}$$

Tail rotor radius $[m]$**:**

$$R_{TR} = 0.0443m^{0.393} \tag{3.11}$$

Tail rotor angular velocity $[rad/s]$**:**

$$\Omega = \frac{364}{(2R_{TR})^{0.828}} \tag{3.12}$$

Tail rotor blade chord $[m]$**:**

$$c_{TR} = 0.0058\frac{m^{0.506}}{N_{b_{TR}}^{0.72}} \tag{3.13}$$

Note: All these values are calculated on the first tab of the tool and are updated in the relevant and adequate input boxes, this means that the user will find that some information will already be present in the further tabs (but will remain editable).

The helicopter dimensions that are calculated when other aircraft configurations are chosen have been slightly altered in order to better fit the empirical data, see appendices B.1 and B.2, (the equations for the rotor sizing remain the same). So for the co-axial configuration the equations are:

Radius:

$$R = 0.555 \times (m)^{0.28} \tag{3.14}$$

Height:

$$h_{heli} = 0.75 \times (2R)^{0.677} \tag{3.15}$$

Length:

$$l_{heli} = 0.824 \times (2R)^{1.01} \tag{3.16}$$

Tip to tip lenght:

$$ttt_{heli} = 1.09 \times (2R)^{1.01} \tag{3.17}$$

Width:

$$w_{heli} = 0.55 \times (2R)^{0.7} \tag{3.18}$$

And for the tandem configuration:

Radius:

$$R = 0.6 \times (m)^{0.28} \tag{3.19}$$

Height:

$$h_{heli} = 0.8 \times (2R)^{0.7} \tag{3.20}$$

Length:

$$l_{heli} = 1.03 \times (2R)^{1.01} \tag{3.21}$$

Tip to tip lenght:

$$ttt_{heli} = 2 \times (2R)^{0.98} \tag{3.22}$$

Width:

$$w_{heli} = 0.6 \times (2R)^{0.7} \tag{3.23}$$

Top Level Requirements Tab

In this tab the user will specify three flight conditions (hover, vertical climb and cruise) in terms of altitude and velocity (when applicable). The calculations will follow the momentum theory described in chapter 2.1. For a better power estimation an induced power factor k is introduced, and it can be different for each flight condition, as well as an estimation for the profile power given the rotor dimensions (equation 3.1) , angular velocity (equation 3.9), solidity (that is calculated using the results from equations 3.1 and 3.10 and assuming a rectangular blade planform) and airfoil profile drag. All of these variables can be changed by the user in this tab. Additionally the user can change the helicopter installed power, which will impact the maximum flight velocity of the aircraft.

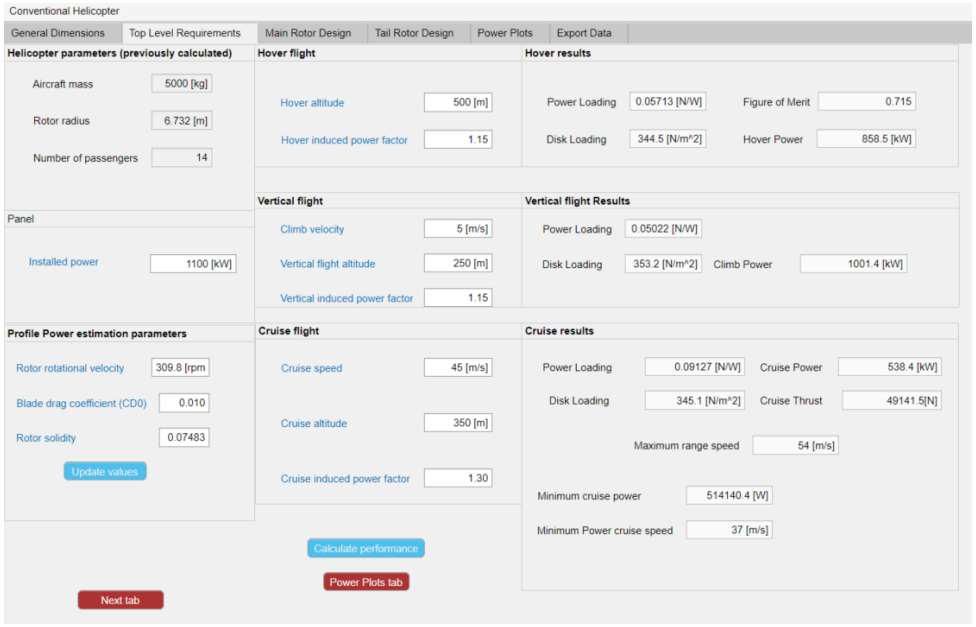

Figure 3.3: Basic tool - Top Level Requirements tab

Note: For the co-axial configuration the induced power factors of the top and bottom rotors can be adjusted individually, and there is the addition of the interference factor between the two rotors. For the tandem configuration the user can specify the distance between the rotors shafts as a percentage of the rotor radius, this value will dictate the interference factor between the two rotors as stated on equation 2.77.

Power and disk loading characteristics are calculated for each flight condition as well as the actual power. For the hover case the figure of merit is also estimated. These are important values in the characterization of the helicopter. For the cruise condition a total thrust force is presented, this takes into account the fuselage drag, and also the minimum power and maximum range speeds are calculated, as is described in section 2.4.1. Additionally to these calculations several plots are generated in which each power component is calculated as a function of the forward speed. A pop-up message is shown when the calculations are finished to inform the user of the availability of these plots.

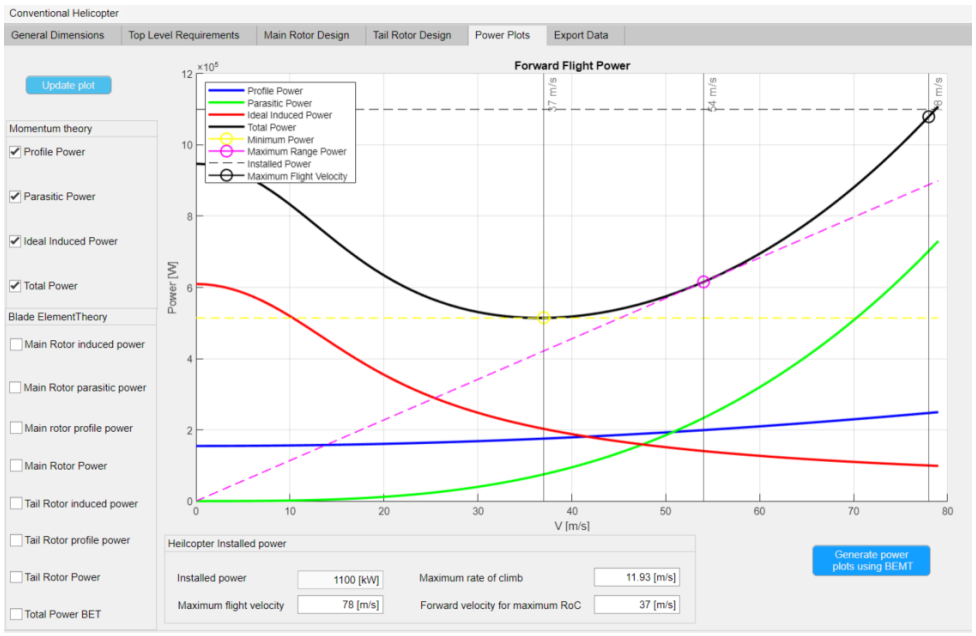

Figure 3.4: Basic tool - Power plots for the Momentum Theory calculations

Any combination of the power components can be plotted, dependent on the user preferences, also the minimum power speed, maximum range speed, maximum flight speed, and maximum rate of climb are clearly shown as to allow a quick an easy interpretation of the results.

Rotor Design Tabs

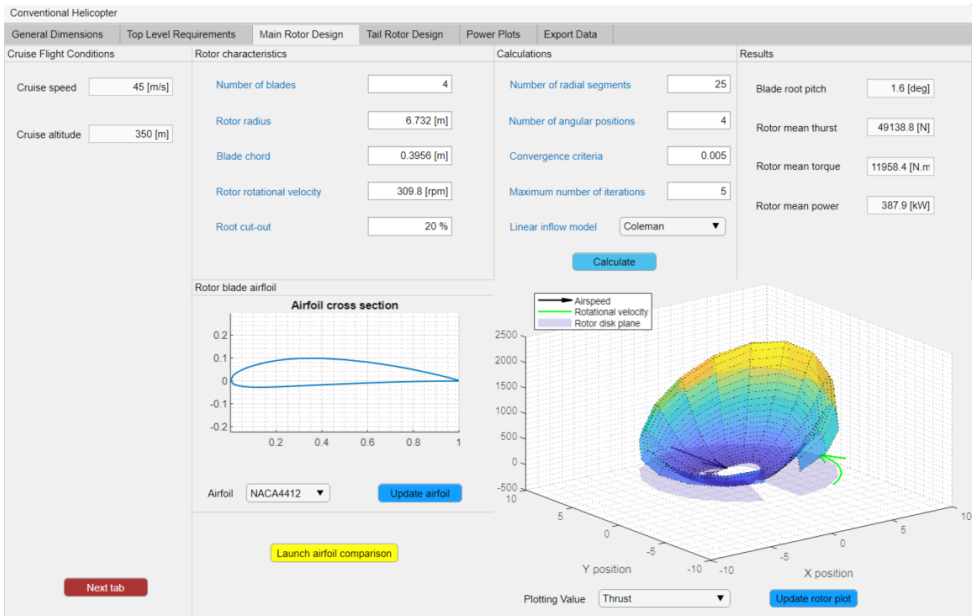

Figure 3.5: Basic tool - Main Rotor Design Tab

After having done the first calculations using the MT the user will now design both the main and tail rotors, the freedom given in this phase is not extremely broad as some assumptions are made in relation to the blade geometry and motion that the user cannot change. These assumptions are that the chord (c) twist (θ_{tw}) and airfoil are constant along the blade and that the blade does not flap nor lag, only pure rotation about the rotor shaft is considered. The flight condition that will be used to make the

calculation is the cruise flight set in the previous tab. The variables that the user will be able to control in terms of the rotor design are:

- Number of blades - N_b
- Rotor radius - R
- Rotor blade chord - c
- Rotor blade airfoil
- Rotor rotational velocity - Ω
- Rotor root-cut-out - r_0

Note: It is very important to consider that any alterations on the above mentioned values would result in different conditions for the MT calculations, for example, if the rotor radius is modified then the rotor area will be different which will have a major impact in the results of the *Top Level Requirements Tab*. So after running the calculations on the *Rotor Design Tabs*, if desired, the user can rerun the *Top Level Requirements Tab* calculations and the rotor geometric characteristics will have been updated.

Rotor Design Tabs - Forces calculations

In this tab the calculations will be made using the BET, the blades will be divided in several different sections and each will be assumed to have constant conditions (flow velocity, angle of attack, and so on), the calculations point will be placed in the middle of the section. All of the aerodynamic forces and moments will be calculated using these approximations, lets take the integration of equation 2.83 along one single blade as an example:

$$L = \int_{r_0}^{R} dL dy = \int_{r_0}^{R} \frac{1}{2}\rho U^2 c C_l dy \tag{3.24}$$

To solve numerically an approximation of the integral by a sum of a finite number of elements is required:

$$L = \int_{r_0}^{R} \frac{1}{2}\rho U^2 c C_l dy \approx \sum_{n=1}^{N} \frac{1}{2}\rho U(n)^2 c C_l(\alpha, n)\Delta y \tag{3.25}$$

Where N is the total number of radial segments, and n the blade element considered at a given moment.

Now applying the compressibility correction and the Prandtl's tip loss function ($F(r, \Psi)$) we get the final result:

$$L \approx \sum_{n=1}^{N} \frac{1}{2}\rho U(n)^2 c \frac{C_l(\alpha, n)}{\sqrt{1 - M(n)^2}} F(n)\Delta y \tag{3.26}$$

This will be done for each force and moment calculation, for each blade in each azimuthal position. The final thrust, torque and power results will be the average value over one complete rotation.

Note: The aerodynamic coefficients considered when making the force calculations are obtained using a very simple 2D analysis at a given Reynolds number for a limited range of angles of attack. No adjustments are made to account for Reynolds number variations and outside of the angles of attack range the lift is considered to be zero and the drag is considered to be the same as the one for a flat plate perpendicular to the flow. These approximations are necessary for the effective functioning of the tool but will result in some errors.

Rotor Design Tabs - Linear inflow calculations

The solving of the inflow equations is a crucial part of the rotor performance calculations, as they will directly impact the velocity, and consequently the inflow angle and the angle of attack distributions. The solution of the inflow for constant flight conditions will depend on the coordinates of the calculation point considered. The calculation process will be explained below:

- First we calculate the value of the inflow for the hover condition assuming an uniform distribution, so following equation 2.19 we can get λ_0.
- Using λ_0 as a starting point for the numerical solution of equation 2.56 we can find the induced inflow (λ_i) in forward flight, still under the uniform distribution assumption.

- Now a system of equations must be solved numerically to find the solutions for the induced inflow $\lambda_i(y, \Psi)$, wake skew angle $\chi(y, \Psi)$, longitudinal $k_x(y, \Psi)$ and lateral $k_y(y, \Psi)$ inflow slopes for each calculation point.
- The induced inflow is given by equation 2.91, the wake skew angle by equation 2.93, and the longitudinal and lateral inflow slopes by the equations on the table 2.1.
- The first calculation will consider the induced inflow (λ_i) in forward flight under the uniform distribution assumption as a starting point (as the calculations start from the blade root), and the following calculation will assumed the last calculated values as a starting point, and so on until the blade tip is reached.

Rotor Design Tabs - Single rotor convergence

The flight condition that we are considering sets the required thrust that the rotor must produce (T_{needed}), as the aircraft weight is known and the drag on the fuselage can be calculated, through equation 2.119. This defines the objective value, now we need to find which flight controls will allow the rotor to operate in such conditions. In this tool the blade motion is purely rotational (the blades do not flap and their rotation happens on the rotor disk plane) and so cyclical controls will not be considered, only the collective pitch (θ_0). We now have one input for our performance analyses (θ_0), and one relevant output to the convergence that is the actual thrust produced by the rotor (T_{actual}).

The convergence process will guarantee that the produced thrust is within a maximum error margin (*convergence criteria*) of the required thrust, and the method used is the Newton-Raphson, see [9] chapter 2.14.3 , as it is widely used in simple convergence problems. In its general form:

$$x_{n+1} = x_n - \frac{f(x_n)}{f'(x_n)} \tag{3.27}$$

Where $f'(x_n)$ is the derivative of f in respect to x is the point x_n. This equation gives us the result x_{n+1} which will approximate the value of $f(x)$ to zero, assuming that the function has real roots.

In our case x is given by the collective pitch, and the function f is represented by the difference between the rotor produced thrust and the rotor required thrust ($T_{actual} - T_{needed}$) that is not analytically defined, so a direct calculation of its derivative is not possible. However a first order estimation can be made in the form of a finite difference (noting that T_{needed} is constant it can be neglect on the derivative calculations):

$$f'(x) \approx \frac{f(x_2) - f(x_1)}{x_2 - x_1} \Leftrightarrow T'_{actual}(\theta_0) \approx \frac{T_{actual}(\theta_{0_2}) - T_{actual}(\theta_{0_1})}{\theta_{0_2} - \theta_{0_1}} \tag{3.28}$$

The first two calculations will be made considering a set of two starting values for the collective pitch that are not the same. This is done as to allow for a derivative to be estimated and thus a new value for the collective pitch is calculated:

$$\theta_{0_{n+1}} = \theta_{0_n} - \frac{T_{actual}(\theta_{0_n}) - T_{needed}}{\frac{T_{actual}(\theta_{0_n}) - T_{actual}(\theta_{0_{n-1}})}{\theta_{0_n} - \theta_{0_{n-1}}}} \tag{3.29}$$

This new value will be used in the next calculation until the convergence criteria is met. So when the non dimensional difference between the rotor produced thrust and the rotor required thrust is smaller than the convergence criteria (ϵ) the calculations will stop.

$$\delta T = \frac{T_{actual} - T_{needed}}{T_{needed}} < \epsilon \tag{3.30}$$

The user has control over some of the calculations parameters:

- Number of radial segments (radial discretization)
- Number of angular positions (azimuthal discretization)
- Convergence criteria
- Maximum number of iterations
- Linear inflow model

Note: The number of angular positions specified by the user is for one single blade of the rotor, so the total number of angular positions will be given by the multiplication of the number of blades by the user specified value.

The number of radial segments and angular positions will defined the number of points on the rotor upon which the calculations will be done, mesh refinement is a delicate subject as the influence on the quality of the results and computational cost is not linear, further analysis on this is made in section 4.2. The maximum number of iterations allows the user to avoid that the tool gets stuck on an unfeasible design that would never converge. The linear inflow will define which model from table 2.1 to use.

Rotor Design Tabs - Wake contraction and translation calculations

If the chosen configuration is not the conventional one then an interaction between the rotors needs to be calculated. Considering the results of section 2.1.13 from equation 2.79, assuming $V_c = 0$ it can be derived:

$$\frac{V_s}{v_i} = 1 + tanh\left(s\frac{k_s}{h}\right) \tag{3.31}$$

So knowing the vertical distance between two rotors s the ratio of the velocity between the top/front rotor disk and the lower/rear rotor disk is given by V_s/v_i. Additionally the contraction of the wake can be found as the radius of the streamtube as a function of s is represented in Figure 2.12 (b). With the new radius that has been calculated the area of influence of the wake on the lower rotor is found.

The radial coordinates of the top/front rotor wake calculations points are updated, as well as the induced velocity values (they are multiplied by the factor V_s/v_i), which means that now they are not coincident with the coordinates of the lower/rear rotor ones. This requires an interpolation between the wake points and the lower/rear rotor points. If the rotors are not co-axial (tandem configuration) the horizontal distance between the two rotor hubs is taken into account on this process as to correctly defined the area influenced by the wake.

Additionally it can be considered a forward velocity, this will imply a horizontal movement of the wake defined by the wake skew angle χ in each calculation point. Given the flight velocity, wake velocity and geometric characteristics of the helicopter configuration the wake movement and its area of influence in the lower/rear rotor is calculated.

There might be some problems associated with the calculations, namely in the wake shedding part of the process where some of the calculations points of the lower/rear rotor might present (erroneously) a value for the wake velocity of zero. This is corrected by a simple smoothing process where the points are identified as being inside the influence area and the values updated to be the average of their vicinity.

After this process the wake velocity is defined with the correct velocity values on the correct calculations points for the performance analysis of the lower/rear rotor.

Rotor Design Tabs - Multi Rotor Convergence

When the chosen configuration is coaxial or tandem the convergence process has an added level of complexity. Considering the convergence method described for the single rotor case we can start our analysis.

The objective for the whole system is to generate enough thrust for the helicopter to operate and that the net torque is zero, the way the thrust is distributed between the two rotors will influence the torque required is each one, so to control the torque the thrust distribution needs to be controlled.

The calculations start by assuming that the thrust is equally distributed between the two rotors. Now the thrust of each rotor is known so the individual rotor analysis can begin, this will be happen exactly as is described for the single rotor case with. First the analysis for the top/front rotor is done, then the wake contraction and translation are calculated and finally the analysis of the lower/rear rotor. After all the analysis the rotor torques are compared, if one rotor has a bigger torque than the other the thrust distribution is adjusted, reducing the thrust produced by the most torque requiring rotor. This process will be repeated until convergence is achieved.

Rotor Design Tabs - Results

The results are presented in four fields with the values for the collective pitch, the produced rotor

thrust, torque and power, and also in the form of a rotor disk plot where the user can visualize the distribution of all the values calculated over the rotor plot. These values are the induced inflow λ_i, the longitudinal k_x and lateral k_y inflow slopes, the wake skew angle χ, the angle of attack α, the inflow angle ϕ, the three velocity components (normal to the blade leading edge, radial, and perpendicular to the rotor plane), the Mach number, the Prandtls' tip loss function F, the aerodynamic lift and drag, the rotor thrust and finally the rotor power. The direction of the rotor rotational velocity and the airspeed given the flight conditions are also plotted. This gives the user a clear and simple way to analyse the results of the design and to easily compare them to previously calculated results.

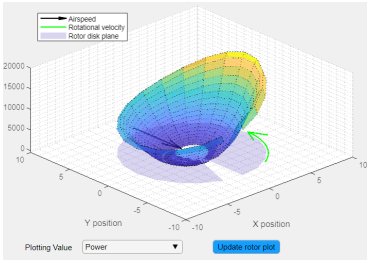

(a) Power

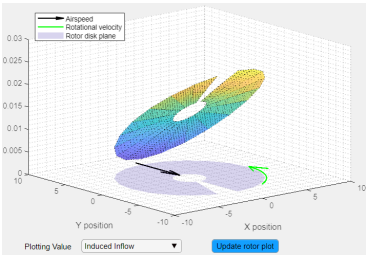

(b) Induced Inflows

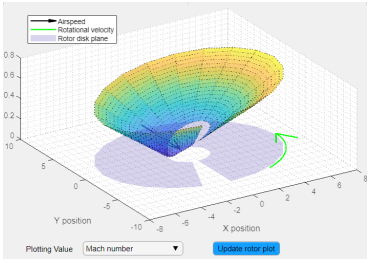

(c) Mach number

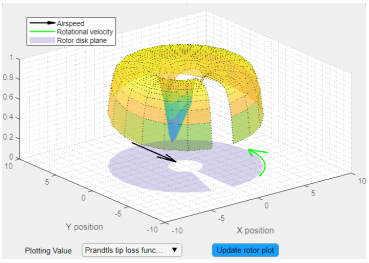

(d) Prandtl's tip loss function

Figure 3.6: Basic tool - Rotor Disk Plots

Rotor Design Tabs - Tail Rotor

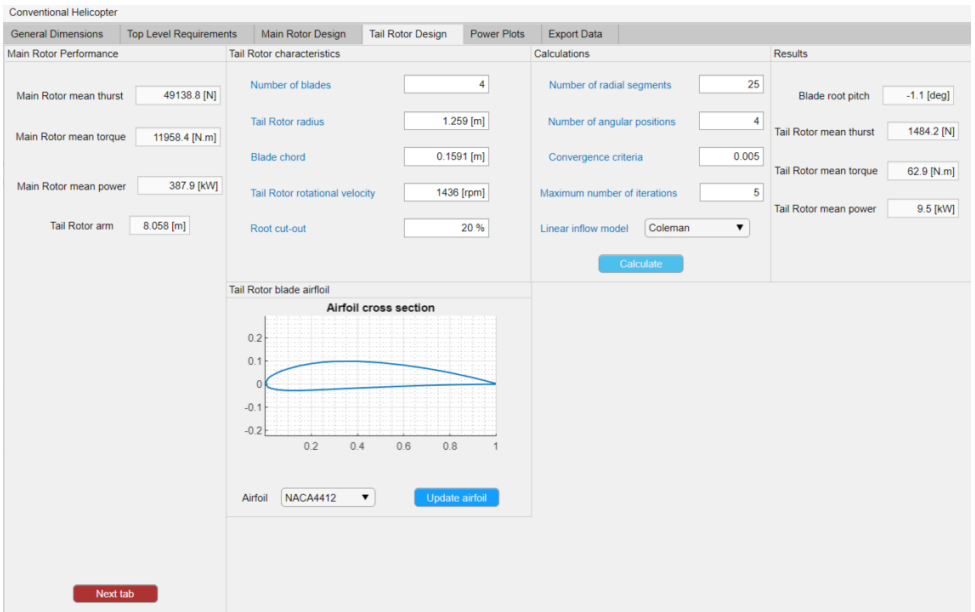

Figure 3.7: Basic tool - Tail Rotor Design Tab

After the calculations on the main rotor are done we can now design the tail rotor, as the main rotor torque has been calculated. The tail rotor design uses exactly the same method as the main rotor design, the only difference being on the definition of the rotor required thrust.

$$T_{TR_{needed}} = \frac{Q_{MR}}{a_{heli}} \tag{3.32}$$

Where Q_{MR} is the main rotor torque and a_{heli} is the tail rotor arm (distance between the tail rotor shaft and the center of gravity of the aircraft, which is assumed to be in the main rotor axis).

Power Plots Tab

After having completely designed the main and tail rotor for the cruise flight condition the user will now have the opportunity to generate additional power plots, based on either MT or BET. This is very useful when trying to adjust for the interference factors used on the *Top Level Requirements Tab*, or simply to compare the values obtained with other designs (generated in this tool or real helicopter designs for validations purposes).

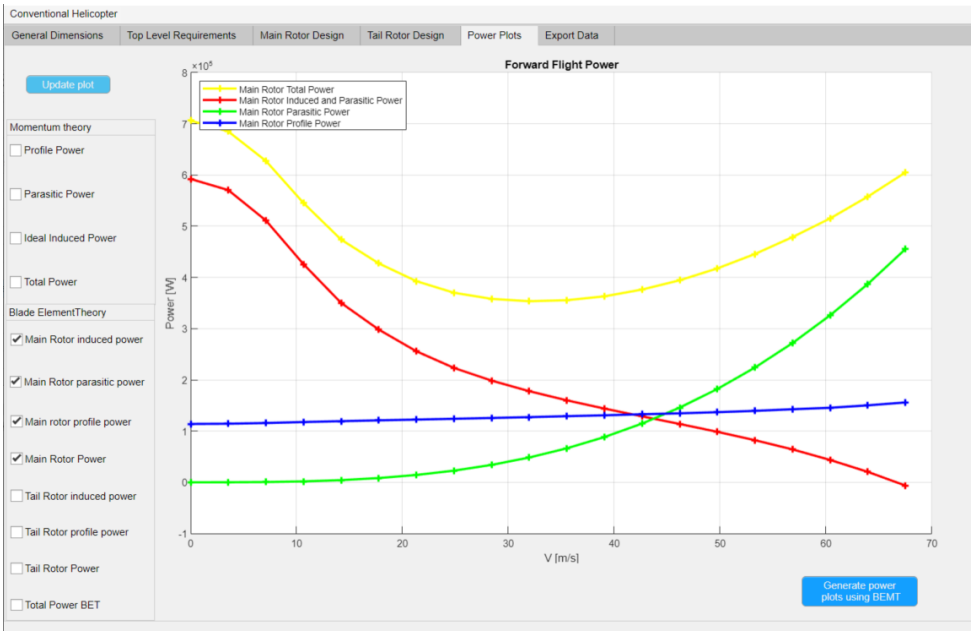

Figure 3.8: Basic tool - Power Plots Tab: Main Rotor Blade Element Theory Power

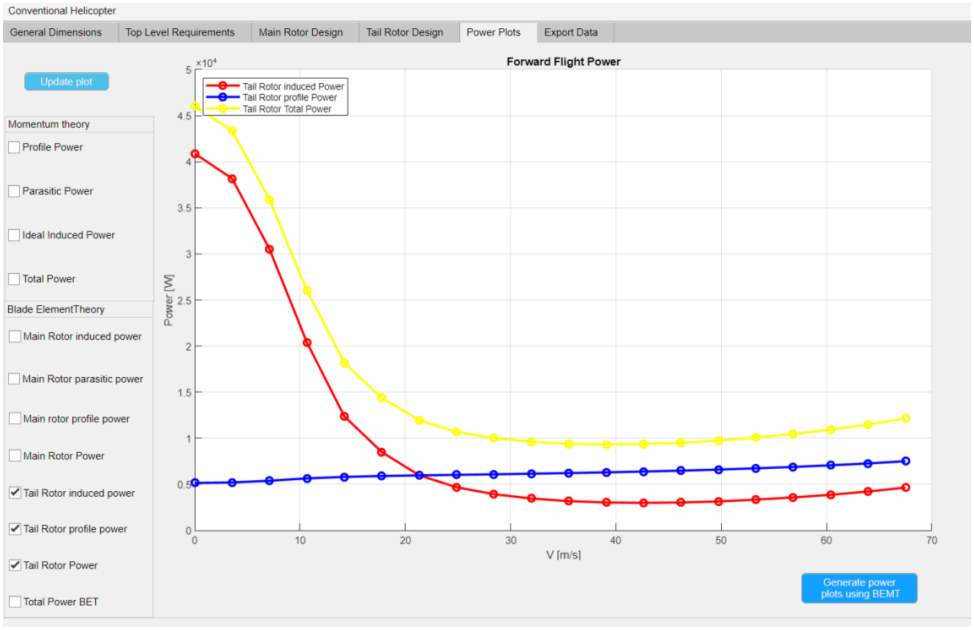

Figure 3.9: Basic tool - Power Plots Tab: Tail Rotor Blade Element Theory Power

In Figure 3.9 it is shown that the tail rotor power starts by decreasing with the flight velocity until it reaches a minimum and starts increasing again.

We can now compare the results for the main rotor power using the two different theories:

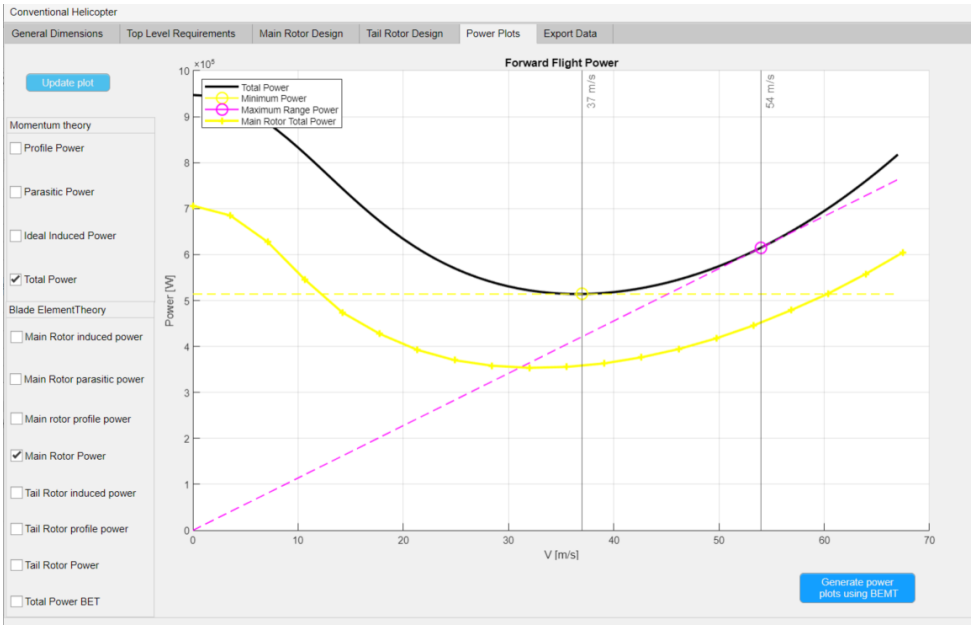

Figure 3.10: Basic tool - Power Plots Tab: Main Rotor Total Power Comparison

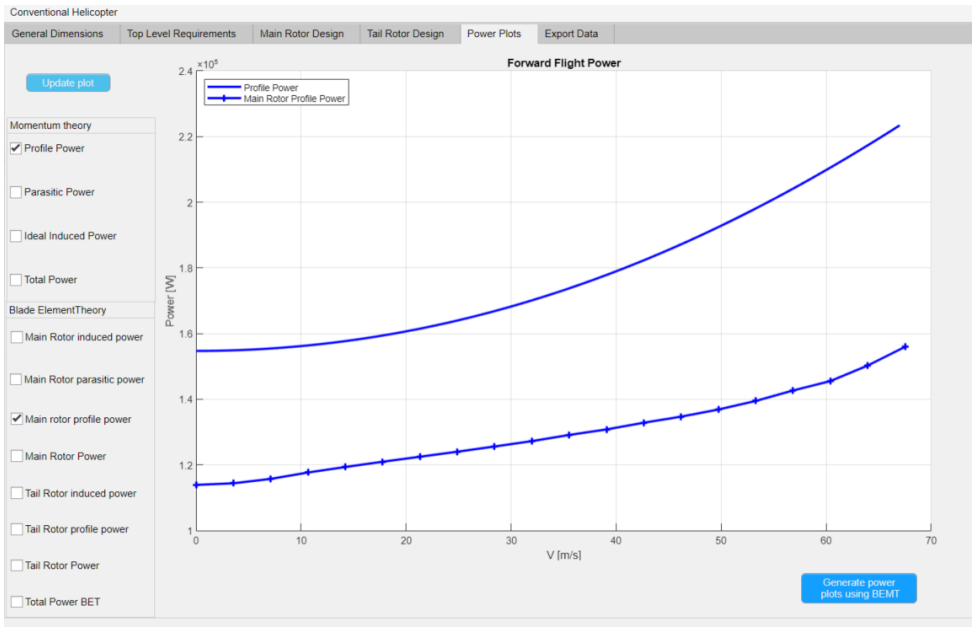

Figure 3.11: Basic tool - Power Plots Tab: Main Rotor Profile Power Comparison

It is easily seen in figure 3.10 that the momentum theory is overestimating the power requirements of the aircraft, this may be corrected by adjusting the induced power factor for the forward flight condition, or by changing the airfoil drag coefficient at zero-lift angle of attack C_{d_0} as this affects the profile power component which also has considerable discrepancies between theories, see figure 3.11.

Adjusting the induced power factor for forward flight from $k = 1.3$ to $k = 1.01$ and the drag coefficient at zero-lift angle of attack from $C_{d_0} = 0.01$ to $C_{d_0} = 0.007$ the plots change significantly.

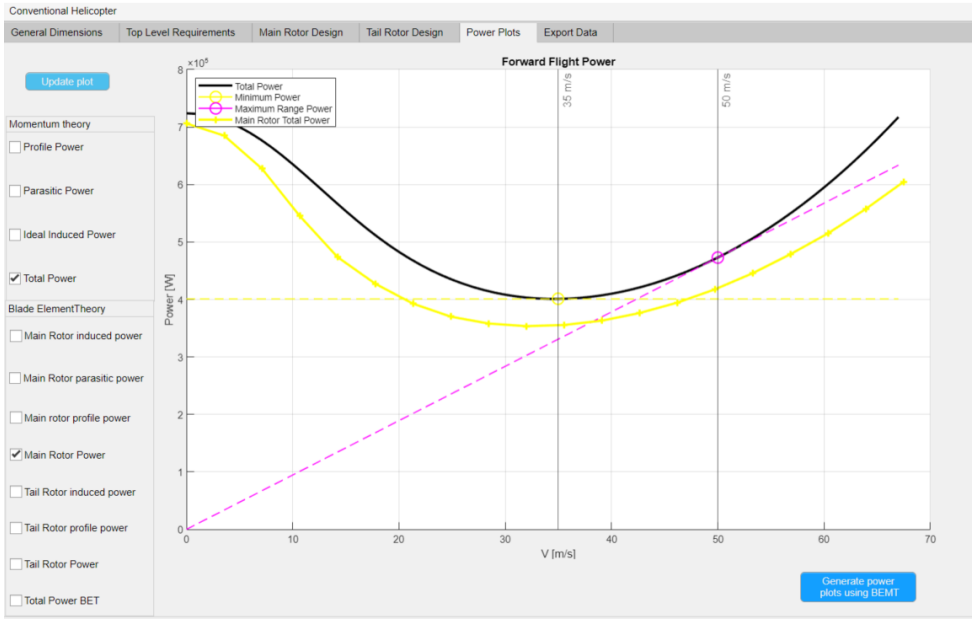

Figure 3.12: Basic tool - Power Plots Tab: Main Rotor Total Power Comparison (after corrections)

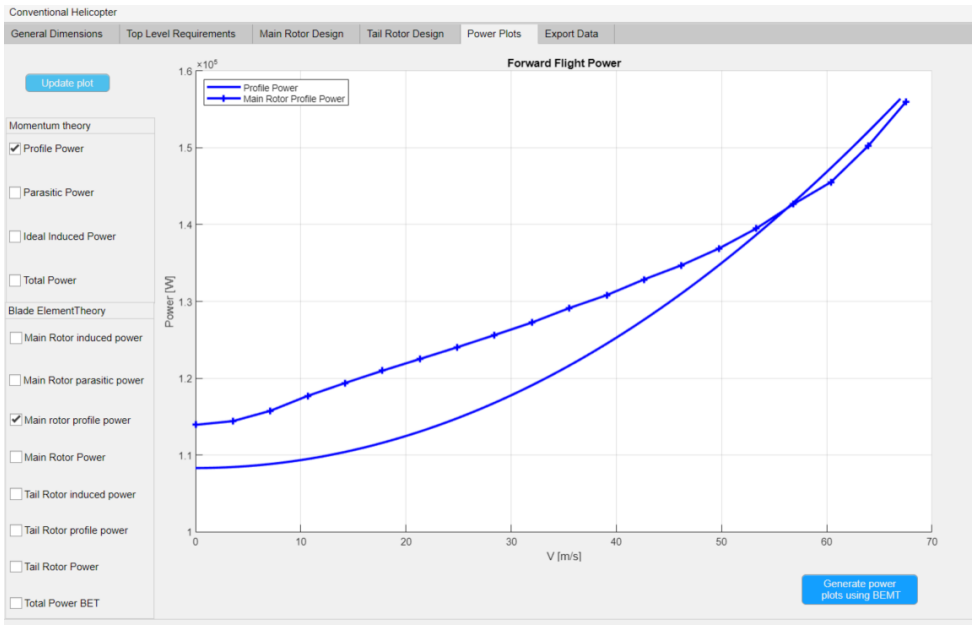

Figure 3.13: Basic tool - Power Plots Tab: Main Rotor Profile Power Comparison (after corrections)

3.2 Detailed Tool

This tool offers a much deeper level of involvement in the helicopter design, more specific top level requirements can be defined, rotor blade geometry is now editable in terms of chord, twist and airfoil distribution along the blade, and a more complete rotor trim is introduced as the blade motion now also considers flapping (the pilot's cyclic controls will be calculated). Once again the user will be able to choose between the three aircraft configurations (conventional, co-axial or tandem), and the example to be followed here will be of the conventional helicopter with the differences from the other configurations being clearly noted along the chapter.

3.2.1 Structure

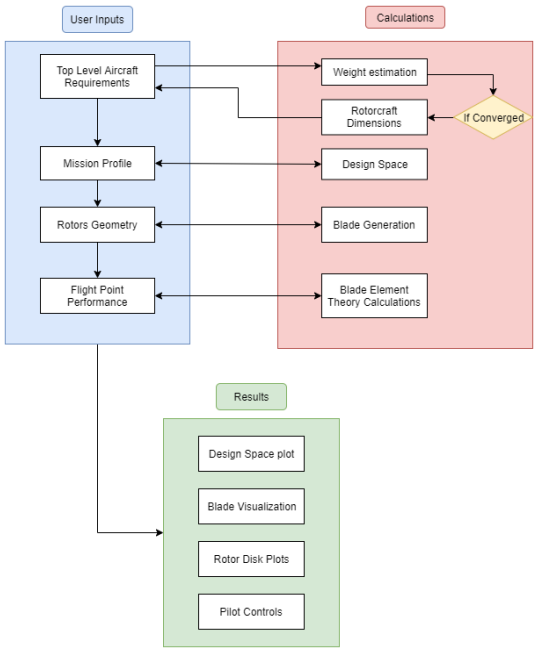

Figure 3.14: Detailed tool structure

3.2.2 Information flow and user experience

Top Level Requirements Tab

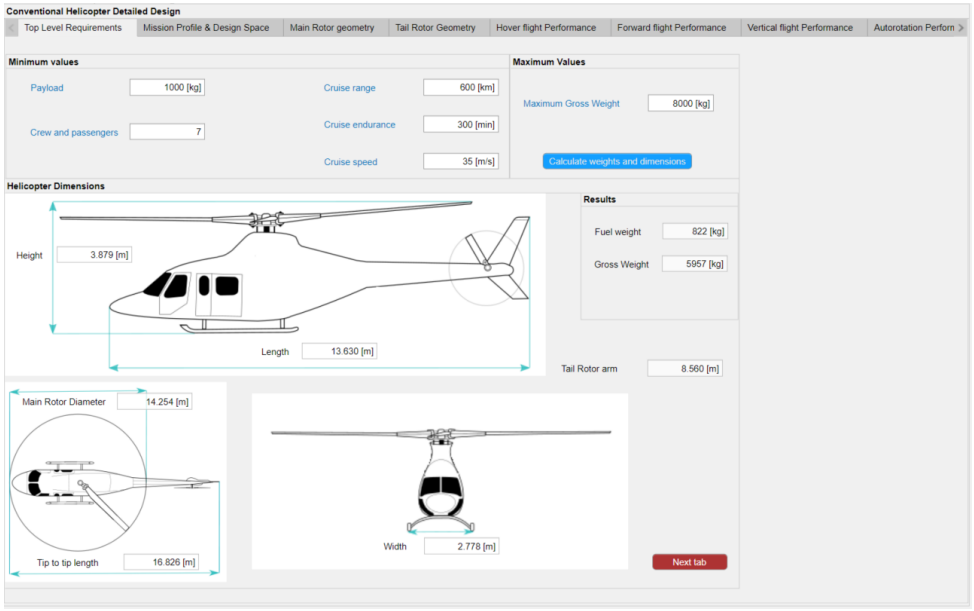

Figure 3.15: Detailed tool - Top Level Requirements Tab

In this tab the user will start the design of the helicopter. Some inputs will be required in regards to the top level aircraft requirements, these being:

- Aircraft payload $[kg]$: $m_{payload}$
- Crew and passengers: N_{pass}
- Cruise minimum range $[km]$: R_{min}
- Cruise endurance $[minutes]$: E
- Cruise speed $[m/s]$: V_{cruise}
- Maximum gross weight $[kg]$: m_{gross}^{max}

After having set all these values a series of calculations follow to assess the feasibility of the design. The first verification is related to the coherence of the cruise conditions (range, endurance, and speed). Using the speed and endurance we calculated an actual cruise range and compare it with the specified minimum range, if the former is smaller than the latter then an error messages shows. The condition that needs to be verified is:

$$R_{min} \leq R_{actual} = V_{cruise} E \times \frac{60}{1000} \tag{3.33}$$

Where the endurance E is given in minutes, and the ranges R_{min} and R_{actual} are given in kilometers.

Two equations need to be introduced now as they are used in the calculations that follow, these equations are for the calculation of the empty weight of the helicopter, m_E see [4], (as a function of the maximum gross weight), of the fuel required, m_F see [4] (as a function of the gross weight and range), crew weight, m_{crew}, and useful weight, m_{useful}, all of these in kilograms:

$$m_E = 0.4854 m_{gross}^{1.015} \tag{3.34}$$

$$m_F = 0.0038 m_{gross}^{0.976} R_{min} \rho_{fuel} \tag{3.35}$$

$$m_{crew} = N_{pass} \times 120 \tag{3.36}$$

Here it is assumed that each crew member/passenger plus their equipment/luggage adds 120 kg to the total aircraft weight.

$$m_{useful} = m_{crew} + m_{payload} + m_F \tag{3.37}$$

Having passed this verification a convergence process is required to find the gross weight of the helicopter given the inputs. The first iteration will have the maximum gross weight as a starting point $m_{gross}^{(n)}$ (where the superscript (n) represents the n^{th} iteration of the calculations), then the convergence process is as follows:

- Crew weight calculation using equation 3.36
- Empty weight calculation using equation 3.34
- Fuel weight calculation using equation 3.35
- Useful weight calculation using equation 3.37
- Calculate a new total aircraft weight: $m_{gross}^{(new)} = m_{useful} + m_E$
- Compare the new total aircraft weight with the value from the start of the iteration $\Delta = m_{gross}^{(n)} - m_{gross}^{(new)}$
- If Δ is smaller than a specified tolerance then the calculations are considered to have converged, if not another iteration will follow using $m_{gross}^{(n+1)} = m_{gross}^{(n)} - \Delta$ as a starting point.
- After the convergence is achieved a final verification is made to check if the result does not exceed m_{gross}^{max}.

Mission Profile and Design Space tab

With the general dimensions and weights calculated the user will now define the flight conditions in which the helicopter is to operate. These conditions are characteristic of a typical helicopter mission profile: take off and climb, hover, cruise flight, and autorotational descent. Furthermore, extreme flight conditions will also be set: maximum velocity forward flight and hover ceiling. This analysis is inspired in the work developed in [6].

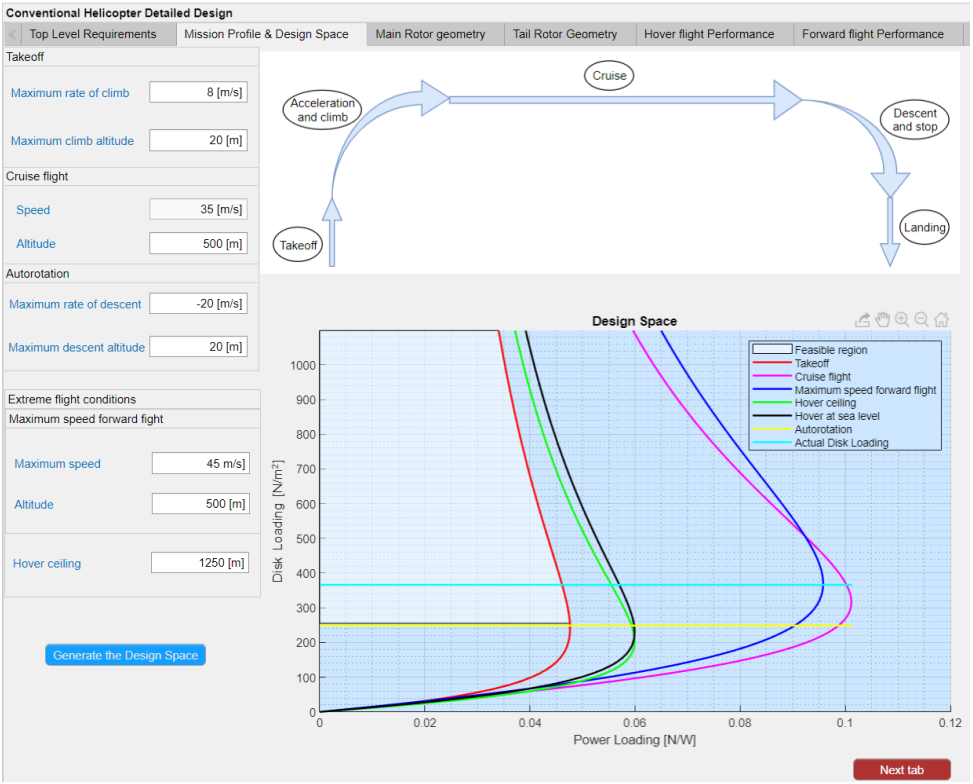

Figure 3.16: Detailed tool - Mission Profile and Design Space Tab

The design space is a plot that shows the power loading variation with different disk loadings for each flight condition. This is a useful tool in the preliminary stages of the design as it is very quickly

generated, allows for the comparison between the power requirements of different flight conditions and can provide an estimation of the total power of the aircraft for a given mission profile.

Hover and Hover Ceiling

The hover power P_h, applying equation 2.26 to the hover condition, is given by:

$$P_h = kP_i + P_0 = k\sqrt{\frac{T^3}{2\rho A}} + \frac{1}{8}\rho N_b \Omega^3 c C_{d_0} R^4 = kT\sqrt{\frac{T}{2\rho A}} + \frac{1}{8}\rho(N_b c R)(\Omega R)^3 C_{d_0} \tag{3.38}$$

Taking into consideration that $N_b c R = \sigma A$, $\Omega R = V_{tip}$ and multiplying and diving the second term by T results in:

$$P_h = kT\sqrt{\frac{1}{2\rho}\left(\frac{T}{A}\right)} + T\frac{1}{8}\rho\sigma V_{tip}^3 C_{d_0}\left(\frac{A}{T}\right) \tag{3.39}$$

Now diving by T, noting that $P_h/T = (PL)^{-1}$ and $T/A = DL$:

$$\frac{P_h}{T} = k\sqrt{\frac{DL}{2\rho}} + \frac{1}{8}\rho\sigma V_{tip}^3 C_{d_0}\left(\frac{1}{DL}\right) \Leftrightarrow (PL)^{-1} = k\sqrt{\frac{DL}{2\rho}} + \frac{1}{8}\rho\sigma V_{tip}^3 C_{d_0}\left(\frac{1}{DL}\right) \tag{3.40}$$

Equation 3.40 gives us the relation between the power loading and the disk loading for the hover condition.

Take off and climb

The climb power P_c is given by:

$$P_c = kP_i + P_0 + P_c = kTv_i + \frac{1}{8}\rho N_b \Omega^3 c C_{d_0} R^4 = kTv_i + T\frac{1}{8}\rho\sigma V_{tip}^3 C_{d_0}\left(\frac{A}{T}\right) + V_c T \tag{3.41}$$

Remembering from equation 2.38 that $v_i = -\left(\frac{V_c}{2}\right) + \sqrt{\left(\frac{V_c}{2}\right)^2 + v_h^2}$ (valid for axial climb) and from equation 2.12 that $v_h^2 = \frac{T}{2\rho A} = \frac{DL}{2\rho}$. Now diving by T

$$\begin{aligned} \frac{P_c}{T} &= kv_i + \frac{1}{8}\rho\sigma V_{tip}^3 C_{d_0}\left(\frac{1}{DL}\right) + V_c \Leftrightarrow \\ \Leftrightarrow (PL)^{-1} &= k\left[-\left(\frac{V_c}{2}\right) + \sqrt{\left(\frac{V_c}{2}\right)^2 + \frac{DL}{2\rho}}\right] + \frac{1}{8}\rho\sigma V_{tip}^3 C_{d_0}\left(\frac{1}{DL}\right) + V_c \end{aligned} \tag{3.42}$$

Equation 3.42 gives us the relation between the power loading and the disk loading for the take off and climb condition.

Cruise and maximum speed forward flight

The level flight power P_{total} is given by:

$$\begin{aligned} P_{total} = kP_i + P_0 + P_p &= kTv_i + \frac{1}{8}\rho N_b \Omega^3 c C_{d_0} R^4 (1 + K\mu^2) + Dv_\infty = \\ &= kTv_i + T\frac{1}{8}\rho\sigma V_{tip}^3 C_{d_0}\left(\frac{A}{T}\right)(1 + K\mu^2) + T\, sin\alpha_{rotor} V_\infty \end{aligned} \tag{3.43}$$

With α_{rotor} being the rotor disk inclination.

From equation 2.53 the following can be derived:

$$v_i^4 + v_i^3(2V_\infty sin\alpha_{rotor}) + v_i^2 V_\infty^2 - v_h^4 = 0 \Leftrightarrow v_i^4 + v_i^3(2V_\infty sin\alpha_{rotor}) + v_i^2 V_\infty^2 - \left(\frac{DL}{2\rho}\right)^2 = 0 \tag{3.44}$$

Which is quartic in v_i and can be solved as a function of DL, thus $v_i(DL)$.

Diving by T the result is:

$$\frac{P_{total}}{T} = kv_i(DL) + \frac{1}{8}\rho\sigma V_{tip}^3 C_{d_0}\left(\frac{1}{DL}\right)(1 + K\mu^2) + sin\alpha_{rotor} V_\infty \tag{3.45}$$

Equation 3.45 gives us the relation between the power loading and the disk loading for the level flight condition.

Autorotation flight

The autorotation condition states that:

$$P = kP_i + P_0 + P_c = kTv_i + \frac{1}{8}\rho N_b \Omega^3 c C_{d_0} R^4 = kTv_i + T\frac{1}{8}\rho\sigma V_{tip}^3 C_{d_0}\left(\frac{A}{T}\right) + V_c T = 0 \tag{3.46}$$

From equation 2.47 the induced velocity v_i is related to the descent velocity V_c, thus $v_i(V_c)$. Now dividing by T and knowing that for a constant velocity descent flight $T = W$.

$$kv_i(V_c) + \frac{1}{8}\rho\sigma V_{tip}^3 C_{d_0}\left(\frac{A}{W}\right) + V_c = 0 \Leftrightarrow v_i(V_c) = -\frac{1}{8}\rho\sigma V_{tip}^3 C_{d_0}\left(\frac{A}{Wk}\right) - \frac{V_c}{k} \tag{3.47}$$

This equation can be solved numerically to find the induced velocity v_i for a given helicopter weight W and autororational descent velocity V_c. Using this result the autorotational disk loading can be calculated:

$$DL = 2\rho v_i^2 \tag{3.48}$$

This result represents the minimum disk loading required for the helicopter to descend at a velocity V_c in autororation.

Rotor Geometry Tabs

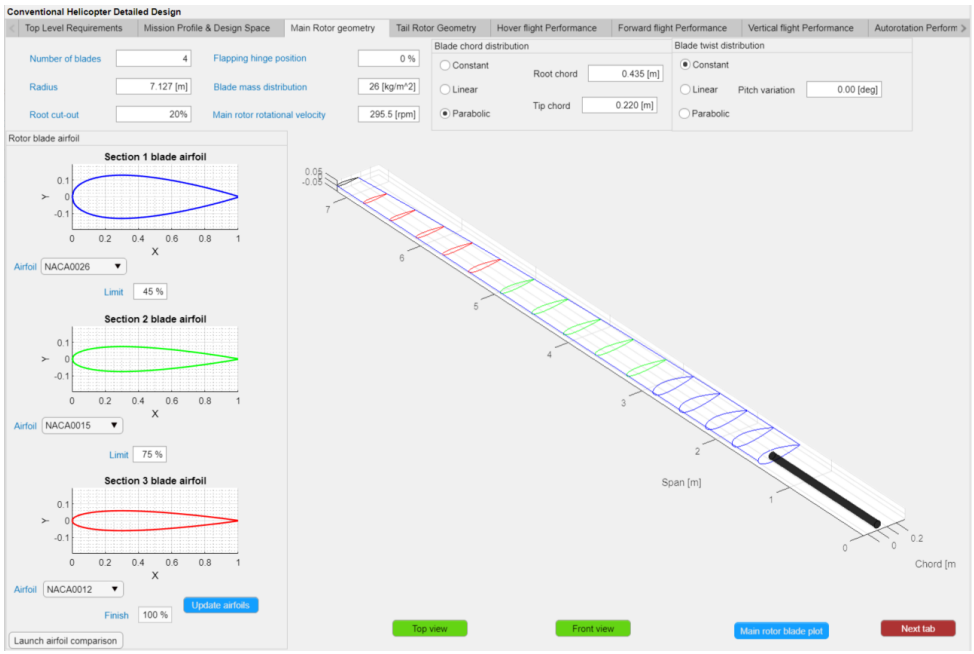

Figure 3.17: Detailed tool - Main Rotor Geometry Tab

In this tab the user will have the possibility to set the geometry of the main rotor blades in detail, the inputs are:

- Number of blades: N_b
- Rotor radius: R in $[m]$
- Root cut-out: r_0 [% of the rotor radius]
- Flapping hinge position eR [% of the rotor radius]
- Blade mass distribution: $[kg/m^2]$
- Rotor rotational velocity: Ω in $[rpm]$
- Chord distribution: $c(y)$ in $[m]$
- Twist distribution: $\theta_{tw}(y)$ in $[°]$
- Airfoil distribution

The chord and twist distributions can be set to be constant, linear or parabolic, the root and tip values need to be defined (for the parabolic variation the slope in respect to the span is assumed to be zero on the blade root).

Note: The chord and twist distributions are continuous variables along the blade span, but the airfoil distribution is done by diving the blade in 3 different sections (the lengths of these are set by the user) in which the airfoil is the same. The aerodynamic environment is not constant on all of the rotor disk, thus justifying the need for a variable geometry along the blade. At the blade tip high velocities are encountered so it becomes necessary to used airfoils with a high divergence Mach number to allow for greater flight velocities, these airfoils, however, might not have high maximum lift coefficients, so the need to use another airfoil in the inner part of the blade for thrust generation purposes arises, this might, in turn, produce higher pitching moments at the blade root, which can be counterbalanced by using yet another different airfoil in the innermost part of the blade. So using three different airfoils with specific characteristics is a design choice that allows for the rotor to be more versatile as was the case for the British Experimental Rotor Program (BERP), see [24]. The flapping hinge position and blade mass distribution will influence the flapping behaviour of the blade as described in section 2.3.1.

Tail Rotor Geometry

The tail rotor geometry is defined is exactly the same ways as the main rotor geometry.

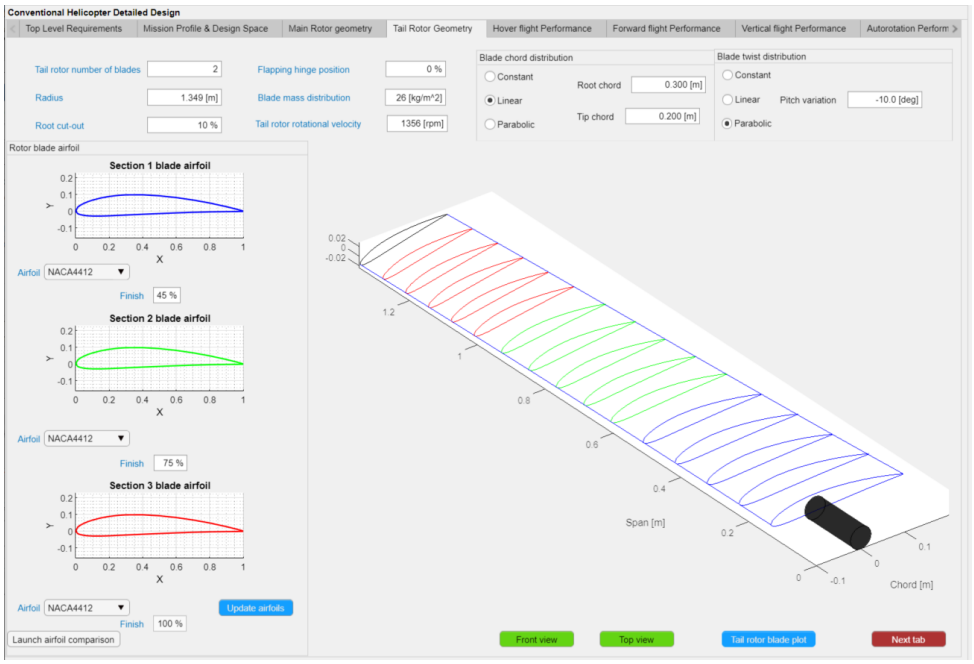

Figure 3.18: Detailed tool - Tail Rotor Geometry Tab

Flight Performance Tabs

Now that the flight conditions and geometries of the rotors have been set the performances analyses can be done. The user will be able to check each of the conditions specified in the *Mission Profile and Design Space tab* individually.

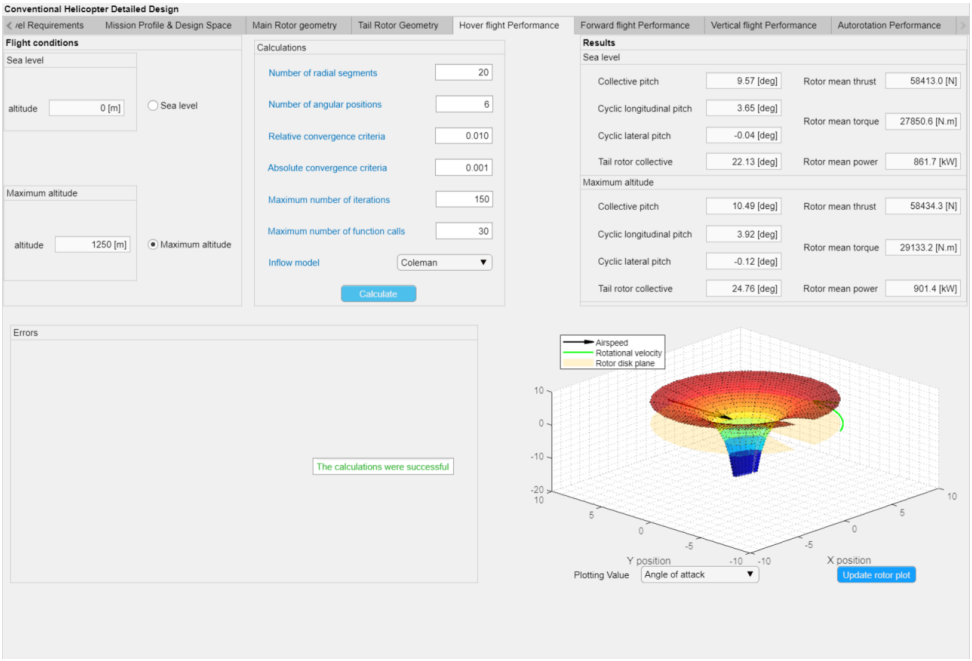

Figure 3.19: Detailed tool - Hover Flight Performance Tab

The user will chosen the flight condition, in Figure 3.19 it is seen that on the *Flight Conditions panel* the user can chosen the *Sea level* or the *Maximum altitude* condition, and can adjust some calculation parameters:

- Number of radial segments
- Number of angular positions
- Relative convergence criteria
- Absolute convergence criteria
- Maximum number of iterations
- Maximum number of function calls
- Linear inflow model

The number of radial segments, angular positions, the relative convergence criteria and the linear inflow models here are exactly the same as they were in section 3.1 for the *Basic Tool*.

The absolute convergence criteria will be used in the convergence process of the rotor inclination. The maximum number of iterations and function calls are specified to prevent the calculations to be stuck in an infinite loop. More detail on these two inputs will be given further in this section.

Flight Performance Tabs - Calculations

In this section the calculations are done using BET and follow the same principles as in the *Basic Tool*. Additionally the flapping motion is considered, this will have an impact on the resultant forces and moments as is described in section 2.3.1.

The flapping behaviour is not know *a priori* so an assumption for the first iteration is done: $\beta_0 = 0$ and β_c and β_s are given be the equations 2.109 and 2.110 respectively. The values for the cyclic pitches are known (as they are pilot inputs) and are constant throughout the iteration. The convergence process of all the pilot inputs will be discussed in the following paragraphs.

The calculations are done on the whole rotor and then, using the results, the blade motion equation 2.106 is solved giving new values for β_0, β_c, and β_s. This process is called a function call. The new results will be used on the next function call and this will continue until all three are converged, it is now clear that one single iteration contains several function calls, this is required for the correct calculation of the blade's flapping motion.

Note: The convergence criteria for the flapping motion is not controllable by the user.

The relative convergence criteria for the flapping angles is given by:

$$rel_{conv} = \left| \frac{\beta^{n+1} - \beta^{n}}{\beta^{n}} \right| \leq 0.01 \tag{3.49}$$

And the absolute convergence criteria for the flapping angles is given by:

$$abs_{conv} = \left| \beta^{n+1} - \beta^{n} \right| \leq 0.001 \tag{3.50}$$

With β representing either one of the three components of the flapping angle and the subscripts the correspondent function call number.

For the iteration to be converged all three components of the flapping motion need to be within the convergence criteria, to be within the convergence criteria either the relative convergence criteria is met or the absolute convergence criteria is met. Having converged the flapping motion the iteration is complete.

Flight Performance Tabs - Single Rotor Convergence

The convergence process in this tab differs from the *Rotor Design Tabs* of the *Basic Tool* because the flapping motion is now taken into account.

We now have three different conditions that need to be verified being: the total thrust T, the forward rotor tilt α_{long}^{TTP} (given by the longitudinal component of the flapping motion β_c, required to overcome the aircraft drag) and the lateral rotor tilt α_{lat}^{TTP} (given by the longitudinal component of the flapping motion β_s, required to compensate the tail rotor thrust).

The total thrust is controlled by the collective pitch θ_0, the longitudinal and lateral inclinations of the rotor will be controlled by the longitudinal θ_c and lateral θ_s cyclic pitches.

Typically the response lag of the pilot controls is of $\Delta\Psi = 90°$, see [9] chapter 4.7, thus directly relating the longitudinal cyclic control with the lateral tilt and the lateral cyclic control with the longitudinal tilt, but alterations to the flapping hinge position (offsetting it from the rotational axis) will result in different lags making each component of the rotor tilt a resultant of the two cyclic inputs.

This could be avoided by changing the azimuthal position of the actuation of the cyclic controls, as is done in some helicopters, but in this tool the cyclic inputs are assumed to always act on $\Psi = 0°$ and $\Psi = 90°$.

For the convergence process will happen as described:

- First two iterations are done only changing the collective pitch, by a fixed step, in order to make a derivative estimation
- Then one iteration is done to try to convergence the total thrust by changing the collective pitch
- Now a fixed step change is done to the lateral cyclic pitch and the results are used to make a derivative estimation
- Then one iteration is done to try to converge the longitudinal rotor tilt by changing the lateral cyclic pitch
- Now a fixed step change is done to the longitudinal cyclic pitch and the results are used to make a derivative estimation
- Then one iteration is done to try to converge the lateral rotor tilt by changing the longitudinal cyclic pitch
- A verification is done to the total thrust, T, and to the rotor tilt, α_{long}^{TTP} and α_{lat}^{TTP}, if the convergence criteria is met the calculations stop

This process allows for the Newton-Raphson method to be used because is each derivative estimation and following calculation only one input is being changed based on a single output. The facts that the three input variable (pilot controls) are iterated one at a time and no two consecutive iterations are done on the convergence of the same input allow for a smoother convergence (as in reality all the inputs influence all the three outputs).

Note: The maximum variation of the pilot inputs diminishes with the number of iterations. This was implement as some calculations got stuck by changing the inputs back and forth between the same values. With this alteration this situation is not allowed to happen.

Flight Performance Tabs - Tail Rotor calculations

The tail rotor calculations are done by the same process as the ones of the main rotor but no cyclic controls are considered, only the collective pitch, even though the blades also have flapping motion.

The thrust that results from the tail rotor analysis takes into account the flapping movement and thus the direction of the force, so only the effective part (perpendicular to the helicopter longitudinal axis) is considered for anti torque purposes.

Flight Performance Tabs - Results

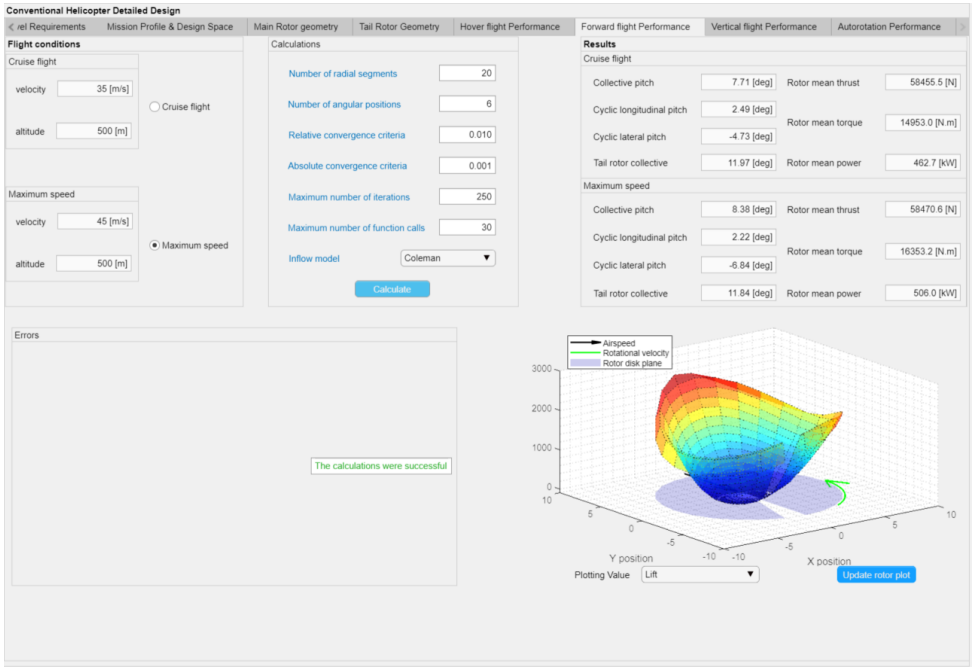

Figure 3.20: Detailed tool - Forward Flight Performance Tab

If all the calculations are successful the results presented for each flight condition are:

- Collective pitch: θ_0 [°]
- Longitudinal cyclic pitch: θ_c [°]
- Lateral cyclic pitch: θ_s [°]
- Tail Rotor collective pitch: θ_{TR} [°]
- Rotor mean thrust $[N]$
- Rotor mean torque $[N.m]$
- Rotor mean power $[kW]$
- Rotor disk plots

If there is any error in the calculation the respective error message will appear, if the calculations occur without any problem a final message representative of that will be displayed, the possible feedback messages are specified on Figure 3.21.

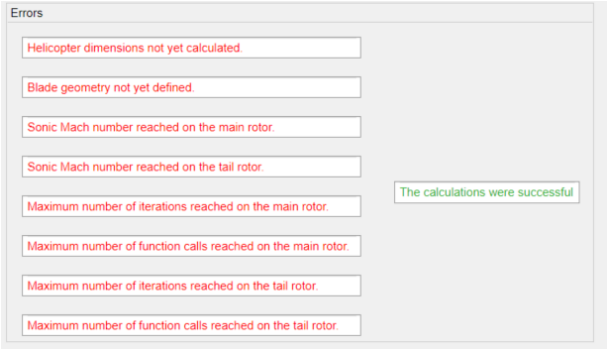

Figure 3.21: Detailed tool - Calculation feedback messages

Note: Figure 3.21 is intended to display all the possible feedback messages that the user will receive, but only one of the messages can be encountered at a time.

If sonic conditions are reached $M = 1$ then the calculations will stop as this tool is not prepared to deal with sonic aerodynamic conditions.

Flight Performance Tabs - Results (Autorotation)

The autorotation tab and calculations are slightly different from the other flight conditions.

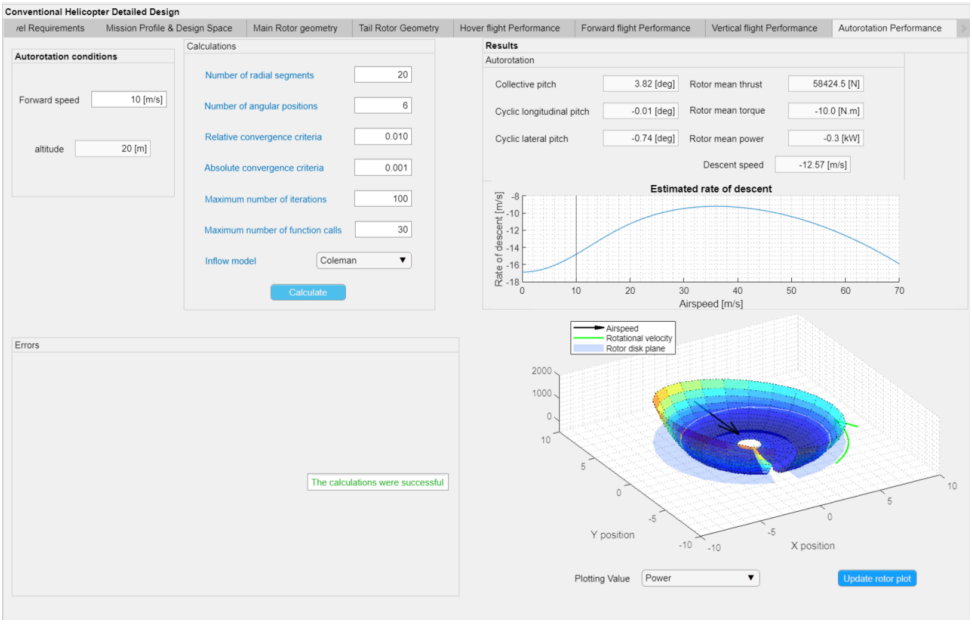

Figure 3.22: Detailed tool - Autorotation Performance Tab

An estimation based on equation 2.26 is plotted, and in the calculations based on BET the inflow assumptions are that the rotor is under a constant inflow (not a linear inflow model), this changes the inflow angle which will have implications in the velocities, angle of attack, tip loss function and overall rotor performance. Additionally, as the characteristic of this flight condition is that the total net power is zero, the tail rotor calculations are neglected, there is no necessity for an anti torque device.

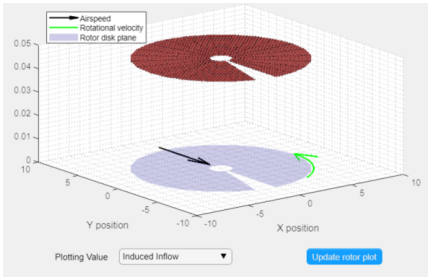

(a) Induced inflow

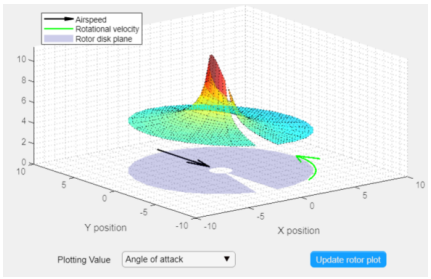

(b) Angle of attack

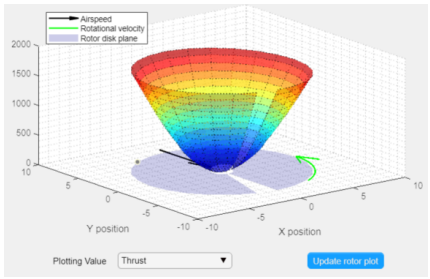

(c) Thrust

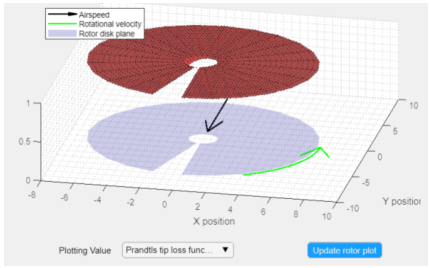

(d) Prandtl's tip loss function

Figure 3.23: Detailed tool - Rotor Disk Plots in Autorotation

3.3 Drone Tool

Through this tool the user will be able to design a multirotor unmanned aircraft of small dimensions. The structure and information flow differs from the *basic* and *detailed tools*, the specifications of which will be explained in the following sections.

3.3.1 Structure

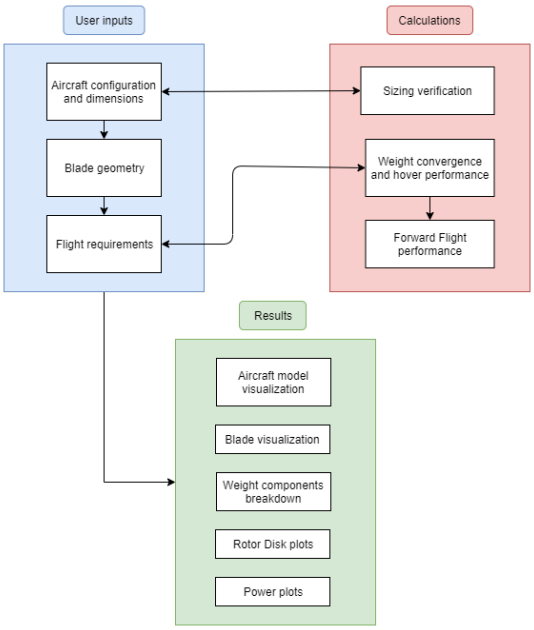

Figure 3.24: Drone tool structure

3.3.2 Information flow and user experience

General Dimensions Tab

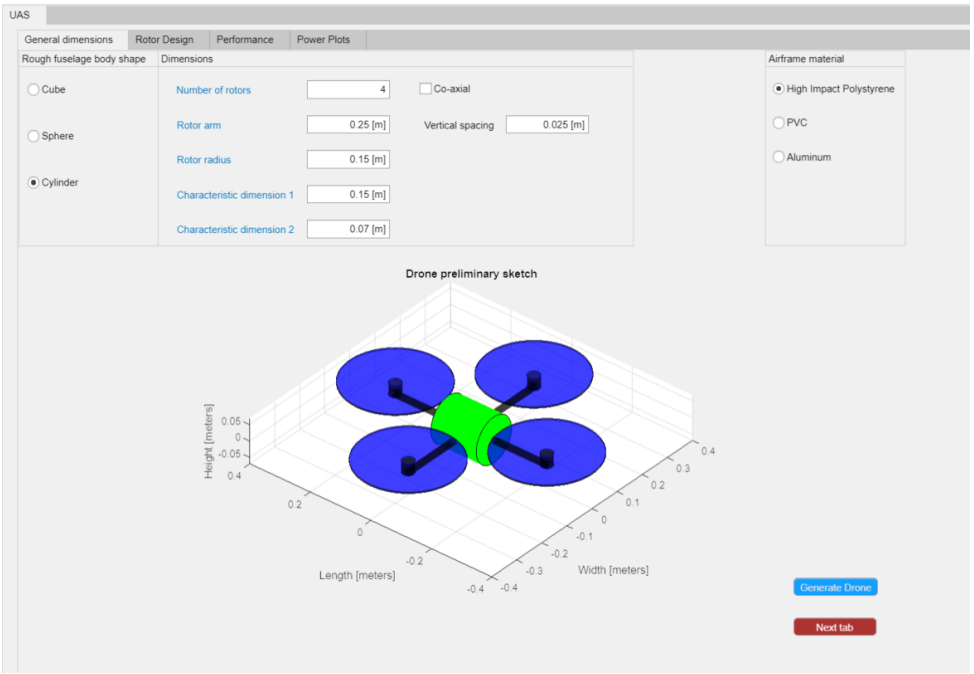

Figure 3.25: Drone tool - General Dimensions Tab

This is the first contact the user will have with the tool and here the general dimensions and aircraft configuration is to be defined.

The inputs required to the user are:

- Fuselage body shape
- Number of rotors
- Coaxial or "single" rotor configuration
- Vertical spacing between coaxial rotors
- Rotor arm
- Rotor radius
- Characteristic dimensions 1 and 2
- Airframe material

The fuselage body shape will influence the fuselage drag coefficient to be used considered in further calculations. For the cube shape $C_D = 1.05$, for the cylinder $C_D = 0.82$ (considering the flow perpendicular to the base of the cylinder), and for the sphere $C_D = 0.45$, see [25] (the shafts that connect the fuselage body to the rotors will also be taken into account on the total drag calculations and are assumed to be cylinders). The vertical spacing defines the distance between the top and bottom rotor disks in the case of a coaxial configuration, the rotor arm is the distance between the fuselage body center and the rotor hub, the characteristic dimensions will define the fuselage size, for the cube the characteristic dimension 1 is the side length, for the sphere the characteristic dimension 1 is the radius, and for the cylinder the characteristic dimension 1 is the height and the characteristic dimension 2 is the base radius. The airframe material will influence the total mass of the aircraft.

Rotor Design Tab

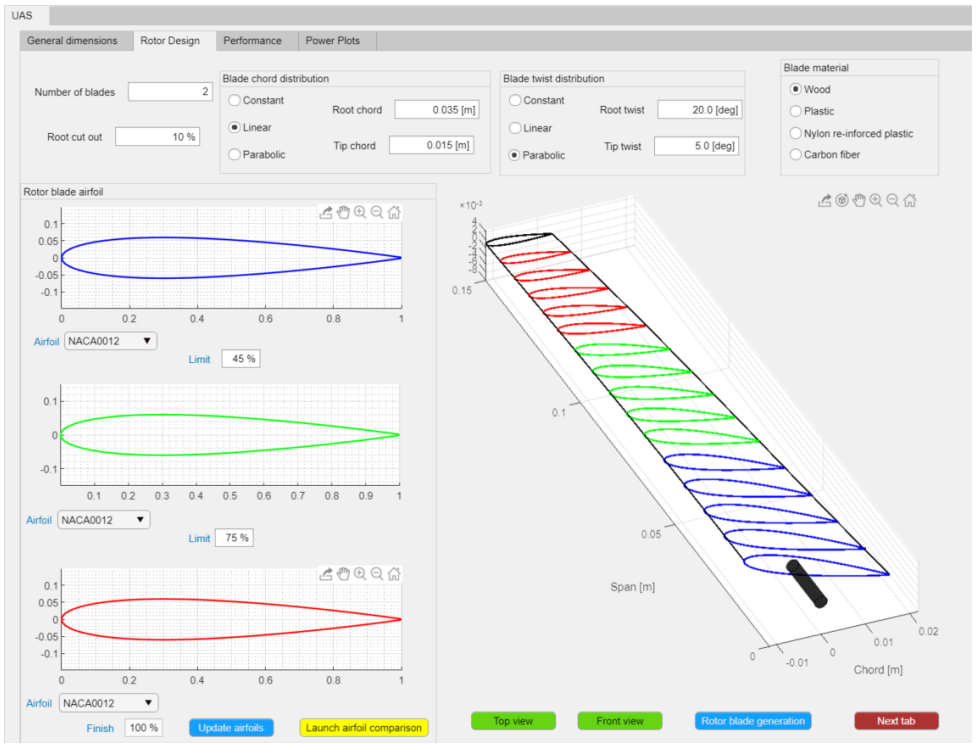

Figure 3.26: Drone tool - Rotor Design Tab

After setting the general dimensions the user can now define a detailed rotor blade geometry in a very similar way as is described in section 3.2.2, the differences being that in here no flapping will be considered and the blade weight is defined by the blade material choice.

Note: The software assumes that all the blades in all the rotors are geometrically identical.

Performance Tab

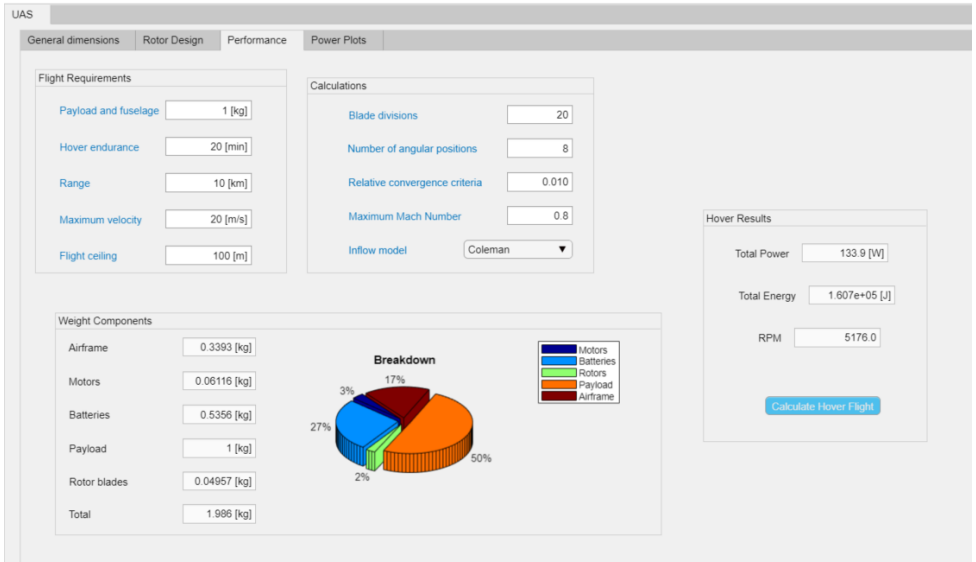

Figure 3.27: Drone tool - Performance Tab

In this section the flight performance requirements are set and weight convergence calculations are done to assess the design feasibility. The user inputs are:

- Payload and fuselage: $m_{payload}$
- Hover Endurance: End_h in minutes
- Range
- Maximum velocity
- Flight ceiling

And also calculation parameters as was the case in the *basic* and *detailed tools*.

Performance Tab - Calculations (Weight Convergence)

The first part of the calculations will be a weight convergence in order to define the mass, in kilograms, of each of the components of the aircraft:

- Airframe: m_f
- Rotor blades: m_r
- Payload and fuselage : $m_{payload}$
- Motors : m_{motors}
- Batteries: $m_{batteries}$
- Total mass: m_{total}

Three of these components will be fixed throughout the calculations, which are the airframe mass m_f, the rotor blades mass m_r, and the payload $m_{payload}$.

The airframe and rotor blades masses are calculated based on the dimensions and materials chosen in the previous tabs. For the airframe the density of the materials, ρ_f is as follows:

- High Impact Polystyrene - $\rho = 1080kg/m^3$
- PVC - $\rho = 1467kg/m^3$
- Aluminum - $\rho = 2768kg/m^3$

The airframe mass, m_f in kilograms, is calculated simply by:

$$m_f = V_f \rho_f \tag{3.51}$$

Where V_f is the airframe volume in m^3, and ρ_f is in kg/m^3.

For the rotor blades of one single rotor the mass is a function of the rotor radius and the material chosen and is given by (see [26]):

$$m_r = p_1(2R)^2 + p_2 2R \tag{3.52}$$

Where m_r is the rotor blades mass in kilograms and the coefficients p_1 and p_2 vary depending on the material considered. For wood $p_1 = 0.00008884$ and $p_2 = 0$. For plastic $p_1 = 0.00005555$ and $p_2 = 0.0002216$. For nylon reinforced plastic $p_1 = 0.0001178$ and $p_2 = -0.0003887$. And for carbon fiber $p_1 = 0.0001207$ and $p_2 = -0.0005122$. The final value for the rotor blades mass is found by multiplying m_r by the total number of rotors.

The motors mass m_{motors} is a function of the rotor torque, an estimation can be made (which includes the speed controler and other necessary components), see [27]:

$$m_{motors} = \left(0.5382Q^{0.8129}\right) \times 0.45359237 \tag{3.53}$$

Where Q is the rotor torque, in $lb.ft$. To get the total motor mass the value m_{motors} needs to be multiplied by the total number of rotors.

The batteries mass $m_{batteries}$ is a function of the total energy defined by the flight requirements. The total energy (in Wh) is given by:

$$E = P_{total} End_h 60 \times 0.000277777778 \tag{3.54}$$

With P_{total} being the total rotors power in W, End_h the endurance time in minutes.

Finally the batteries mass is calculated based on the assumption of a battery energy density $e = 100$ Wh/kg and a battery reserve of an additional 20% capacity.

$$m_{batteries} = Ee \times 1.2 \tag{3.55}$$

The summation of all these components gives the total aircraft mass:

$$m_{total} = m_f + m_r + m_{payload} + m_{batteries} + m_{motors} \tag{3.56}$$

The convergence process can now begin. For the first iteration no information on the batteries and motors exists so an assumption is made, this assumption is that the total mass is given by:

$$m_{total}^{(1)} = (m_f + m_r + m_{payload}) \times 2.5 \tag{3.57}$$

Where the superscript (1) is indicative of the first iteration.
Then the calculations will follow as described:

- Performe the rotor BET analysis for the hover condition using $m_{total}^{(n)}$
- Using the resultant torque from the analysis calculate the motors mass using equation 3.53
- Using the resultant power calculate the batteries mass using equations 3.54 and 3.55
- Calculate a new total mass $m_{total}^{(n+1)}$ using equation 3.56
- Compare the new total mass with the previous value, if the difference is within the converge criteria the process will stop, if not then the new value $m_{total}^{(n+1)}$ will be used in the next iteration.

Performance Tab - Calculations (BET Analysis)

The rotor performance analysis in here is the same as described in section 3.1 the difference being that in the convergence process the variable that is changing is not the collective pitch but rather the angular velocity of the rotor. This is typical for aircrafts of small dimensions.

Performance Tab - Results

The results are presented in the form of a pie chart that breaks down the weight components, and the values for the power of the hover flight condition, the total energy for the required endurance and the rotor rotational velocity in $RPMs$.

Power Plots Tab

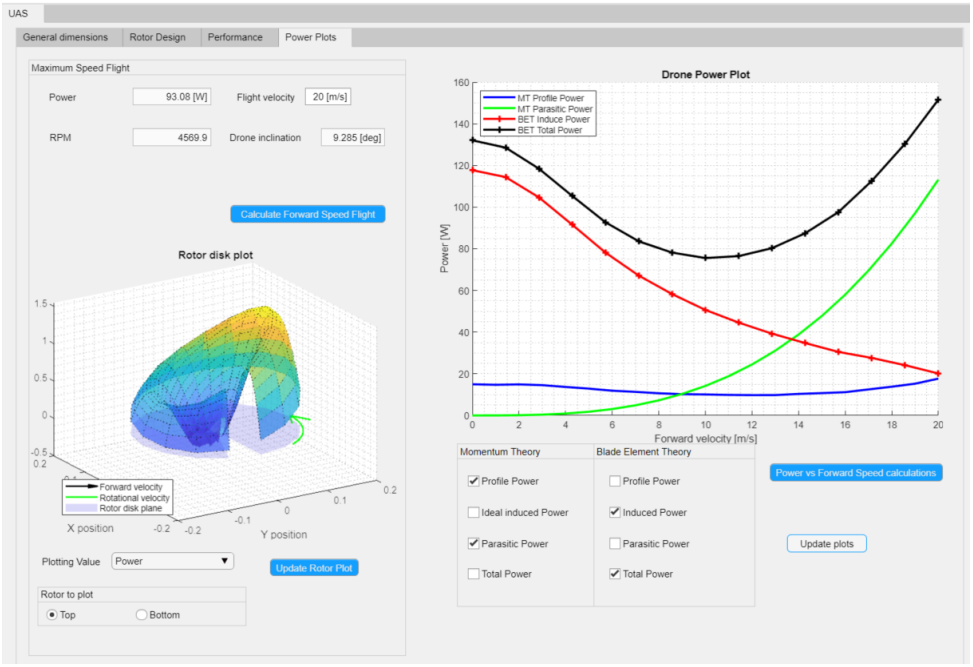

Figure 3.28: Drone tool - Power Plots Tab

In this last tab the user can perform a single point analysis for a specific forward speed (which the user can chose), and visualize the rotor plots for that analysis and also will be able to generate the power curves for different forward speeds (using MT and BET) and compare the results very quickly and easily.

3.4 Airfoil Comparison Tool

This is an extremely simple tool where the user can compare the 2-D aerodynamic performance of the available airfoils in the software database. Two different airfoils can be plotted as well as their C_l and C_d curves when varying the angle of attack. This is useful when the user is designing the blade geometry of the aircraft.

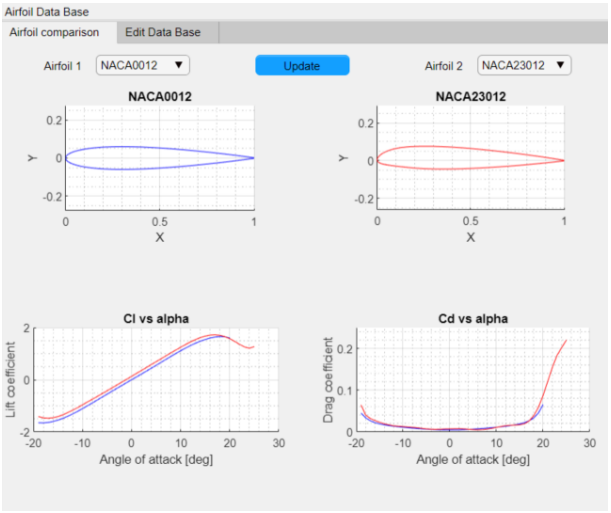

Figure 3.29: Airfoil Comparison Tool

For the tool to successfully read the data file with the airfoil coordinates and the aerodynamic performance data nee to be in specific formats, examples representative of these are shown in appendix C.

4 Validation

The validation process is essential in any sort of design tool to verify how far from reality the results obtained are. In this section the validation of the three tools will be done using an adequate aircraft in each of them. Results from flight tests will be compared with the ones obtained through the software to estimate the error margins of the tool.

4.1 Sizing Validation

The helicopter chosen for the validation process is the Sikorsky UH-60 Black Hawk. The geometric characteristics of the main and tail rotor used are the following, see [28]:

Rotor radius	8.1778 m
Angular velocity	27.0 rad/s
Blade chord	0.5273 m
Blade twist	Nonlinear
Blade airfoil	SC 1095/SC 1094R8
Number of blades	4
Flap hinge offset	0.381 m
Blade mass per unit length	13.92 kg/m
Longitudinal shaft tilt	3 °

Table 4.1: UH-60 Main Rotor characteristics

Rotor radius	1.6764 m
Angular velocity	124.62 rad/s
Blade chord	0.2469 m
Blade twist	-18 °
Blade airfoil	SC 1095
Number of blades	4

Table 4.2: UH-60 Tail Rotor characteristics

4.1.1 Helicopter dimensions

To compare the results of the software for the helicopter dimensions the maximum take off weight (MTOW) in kilograms was used as an input and the calculations were made from that starting point.

	Actual	**Software**	**Error [%]**
MTOW $[kg]$	8329.0	8329.0	0.00
Main rotor radius $[m]$	8.1778	7.878	-3.67
Height $[m]$	3.7592	4.151	+10.42
Length $[m]$	15.4305	15.150	-1.82
Tip to tip length $[m]$	19.7612	18.655	-5.60
Width $[m]$	2.9464	2.979	+1.11
Tail Rotor arm $[m]$	9.8908	9.520	-3.75

Table 4.3: Conventional Helicopter dimensions validation

The results of table 4.3 were calculated using the equations 3.1, 3.3, 3.4, 3.5, 3.6, and 3.7. The result show a good accuracy with the highest error margin being about 10% for the helicopter height.

4.1.2 Main Rotor characteristics

	Actual	**Software**	**Error [%]**
Radius $[m]$	8.1778	7.878	-3.67
Blade chord $[m]$	0.5273	0.5209	-1.21
Angular velocity $[rad/s]$	27.00	28.47	+5.46

Table 4.4: Conventional Helicopter Main Rotor dimensions validation

4.1.3 Tail Rotor characteristics

	Actual	**Software**	**Error [%]**
Radius $[m]$	1.6764	1.539	-8.20
Blade chord $[m]$	0.2469	0.206	-16.57
Angular velocity $[rad/s]$	124.62	127.339	+2.18

Table 4.5: Conventional Helicopter Tail Rotor dimensions validation

4.1.4 Co-axial Helicopter Dimensions

For the co-axial configuration the helicopter chosen for the dimensions comparison was the Kamov Ka-27. In table 4.6 results using both the equations for the conventional and co-axial configurations will be presented to show the necessity of the adaptations made in the beginning of section 3.1.2.

The helicopter dimensions are presented in [29].

	Actual	**Software** $(^*)$	**Error** $(^*)$ **[%]**	**Software**	**Error [%]**
MTOW $[kg]$	12000	12000	0.00	12000	0.00
Radius $[m]$	7.95	8.816	+10.89	7.700	-3.151
Height $[m]$	5.40	4.480	-17.04	4.78	-11.570
Length $[m]$	12.25	17.061	+39.27	13.041	+6.45
Tip to tip length $[m]$	15.90	20.946	+31.73	17.250	+8.49
Width $[m]$	3.80	3.222	-15.21	3.730	-1.86

Table 4.6: Co-axial Helicopter dimensions validation

Note: The superscript $(^*)$ refers to values obtained using the equations from [4] that were generated using data from conventional helicopters, the other results were obtained using the equations presented in appendix B.1.

It is easily observable that the error associated with the equations adapted to the co-axial configuration are lower than the ones associated with the conventional helicopter sizing equations.

4.1.5 Tandem Helicopter Dimensions

For the tandem configuration the helicopter chosen for the dimensions comparison was the Boeing ACH-47A Chinook. In table 4.7 results using both the equations for the conventional and tandem configurations in an analogous way to the one used in table 4.6.

The helicopter dimensions are presented in [30].

	Actual	**Software** (*)	**Error** (*) [%]	**Software**	**Error** [%]
MTOW $[kg]$	14969	14969	0.00	14969	0.00
Radius $[m]$	9.005	9.437	+4.79	8.855	-1.66
Height $[m]$	5.68	4.69	-17.41	5.982	+5.319
Length $[m]$	15.47	18.332	+18.51	18.774	+21.36
Tip to tip length $[m]$	29.90	22.468	-24.86	33.443	+11.85
Width $[m]$	3.78	3.379	-10.61	4.487	+18.693

Table 4.7: Tandem Helicopter dimensions validation

Note: The superscript (*) refers to values obtained using the equations from [4] that were generated using data from conventional helicopters, the other results were obtained using the equations presented in appendix B.1.

In this case the error associated with the adapted equations is not lower for all dimensions. The great diversity in design possibilities and the low quantity of helicopter used to generate the adapted equations might explain these results.

4.2 Mesh Convergence

Before comparing the software calculated results with flight test data a mesh convergence is required. The results of the tool's calculations will depend on the number of calculation points on the rotor disk until a certain amount, this amount needs to be found so that it is known that the results obtained are minimally influenced by the software limitations (physical simplification and numerical errors).

Note: The computer used in the validation process had an Intel i7 quad-core processor and 16 GB of RAM.

The control of the number of calculation points is done by changing the number of radial blade divisions and the number of azimuthal positions (each of these is editable by the user). In this section the number of points will be increased, starting from a small amount, until the results are converged, to check for this convergence a control variable (or variables) is to be chosen and evaluated throughout the process. The rotor thrust cannot be used as a control variable because it is the actual objective of the calculations and it is set independently of the rotor disk discretization. Taking this into account the rotor power and pilot controls (collective, lateral cyclic, and longitudinal cyclic) will be used as they are results of the calculations with a fixed thrust as the objective.

The mesh convergence will be made in two analogous stages as is explained below:

- The number of azimuthal positions will be fixed at a certain value for each blade (which will be multiplied by the number of blades for the total azimuthal positions)
- The number of radial positions will be changed to find the value for the first stage of the mesh convergence
- With the number of radial divisions now found the number of azimuthal positions will be iterated in the same manner
- Now using the new number of azimuthal positions reiterate for the final number of blade divisions
- With the final number of blade divisions the final number of azimuthal positions can be found.

4.2.1 First stage

The flight condition for the mesh convergence was a forward flight at sea level and $V_\infty = 80\ m/s$, as this will result in great asymmetry in the rotor flow increasing the need for a good mesh over the rotor disk. The flight conditions will be constant throughout all the process with the rotor disk inclination (longitudinal and lateral) and rotor total thrust being equal in all calculations, and the starting point for all the convergence processes (initial pilot inputs) is the same.

Radial divisions

Setting the number of azimuthal positions to 16 the number of radial blade divisions was iterated and the results for the rotor power and collective pitch recorded:

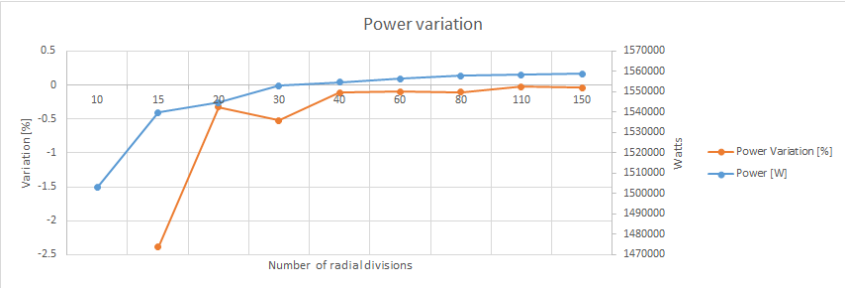

Figure 4.1: Power variation with the number of radial divisions

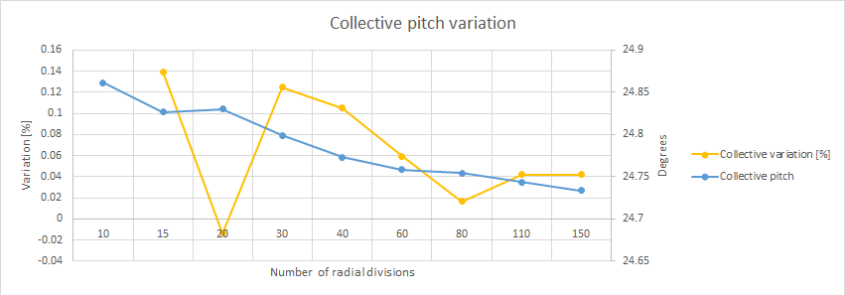

Figure 4.2: Collective pitch variation with the number of radial divisions

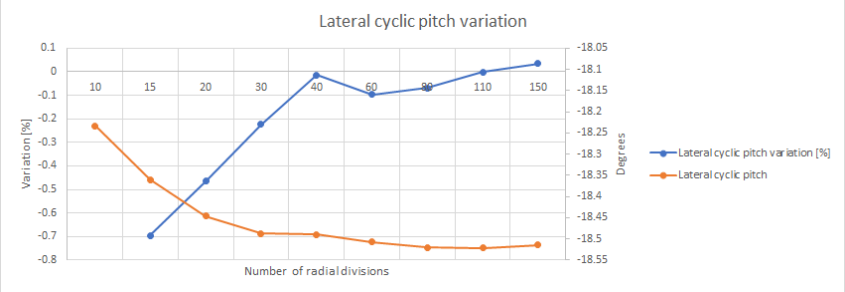

Figure 4.3: Lateral cyclic pitch variation with the number of radial divisions

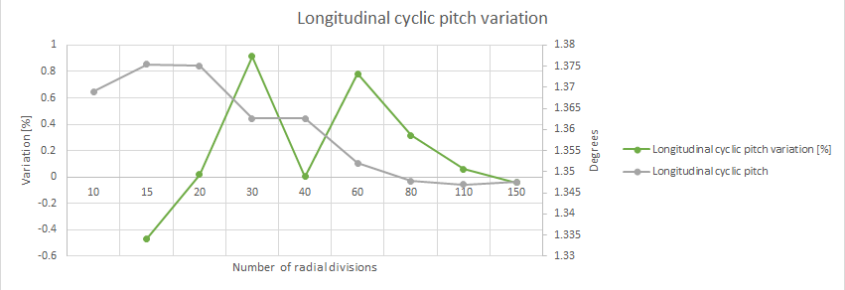

Figure 4.4: Longitudinal cyclic pitch variation with the number of radial divisions

We see that if the number of radial positions is at least 40 the variation in the results will be less than 0.8% in all the control variable which is acceptable for the mesh convergence.

To evaluate if the increase in the number of radial divisions is worth it the computational cost needs to be assessed, this will be made by tracking the time required by each analysis made.

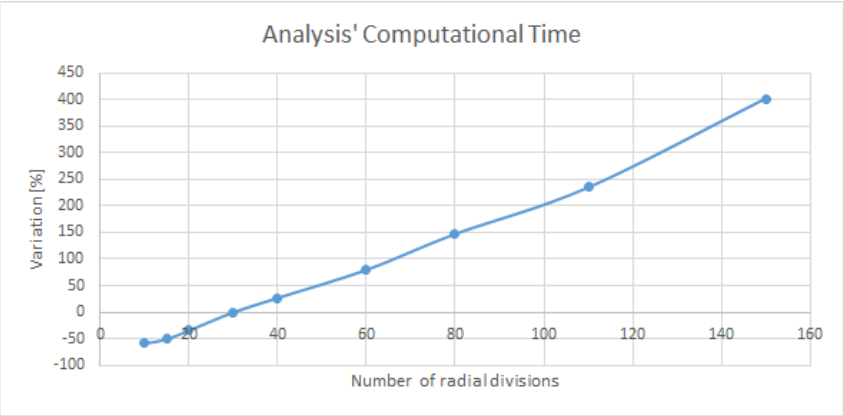

Figure 4.5: Computational time variation with the number of radial divisions

In Figure 4.5 the computational time of the analyses is plotted in terms of variation (in percentage) against the analysis with 30 radial divisions which took 114.585 seconds.

It is seen that the difference in time for an analysis with 20 radial element would be about a 34% decrease but the results would be worse, this time saving doesn't justify the deterioration of the results. When comparing with the 40 blade divisions analysis the time variation would be an increase of around 27% for an improvement of the results (maximum of 0.12% for the power) which is not significant, taking this into account the number of radial divisions for the first stage is set to 30.

Azimuthal positions

Now having the number of radial divisions set at 30 the number of azimuthal positions will be iterated.

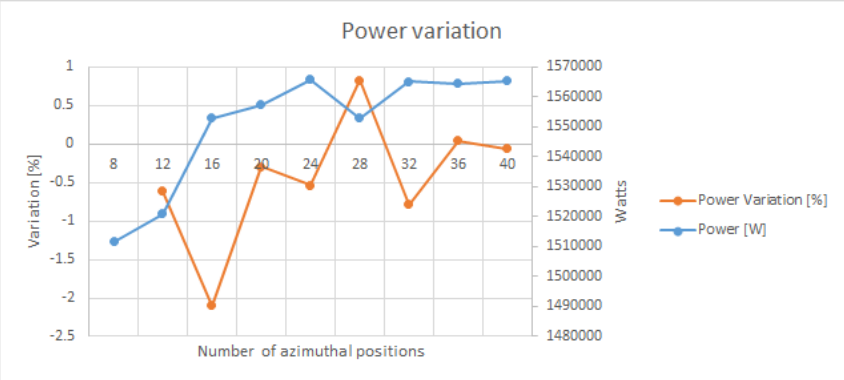

Figure 4.6: Power variation with the number of azimuthal positions

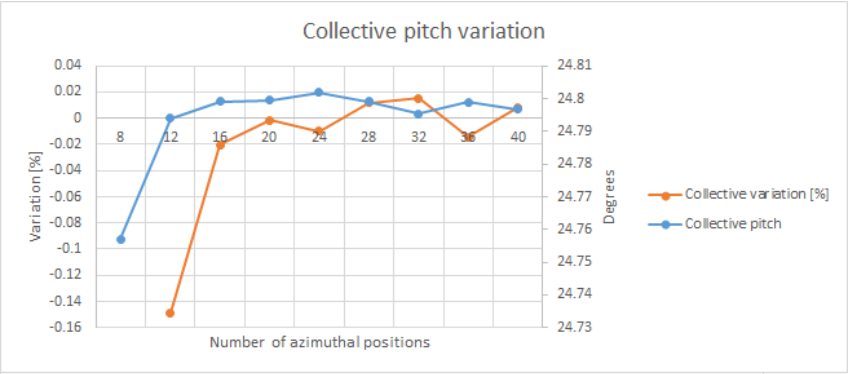

Figure 4.7: Collective pitch variation with the number of azimuthal positions

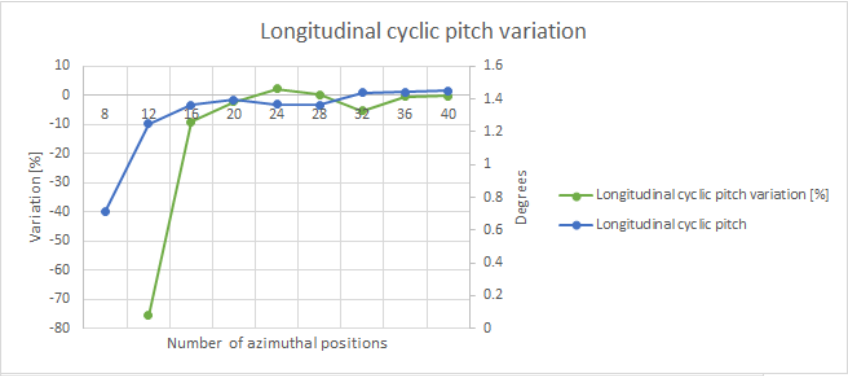

Figure 4.8: Longitudinal cyclic pitch variation with the number of azimuthal positions

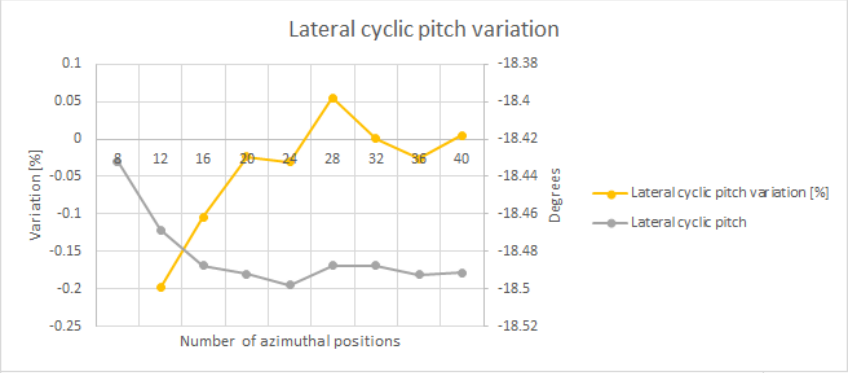

Figure 4.9: Lateral cyclic pitch variation with the number of azimuthal positions

In Figures 4.6, 4.7, 4.8, and 4.9 it can be seen that the variation in the results is small, nonetheless there is a convergence that is achieved for 16 or more total azimuthal positions (when considering all the control variables). Now the computational cost in time needs to be evaluated.

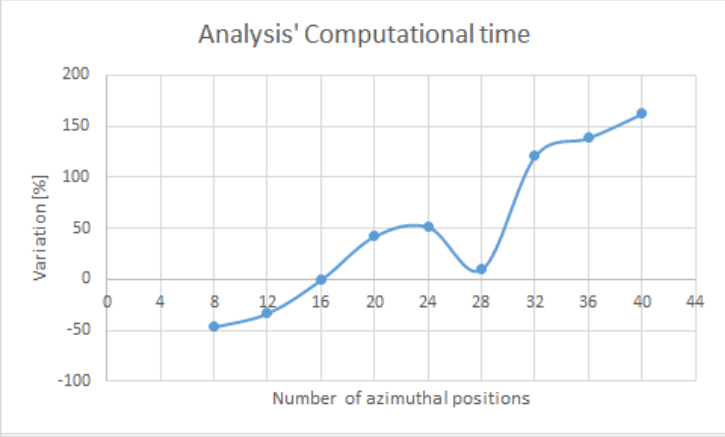

Figure 4.10: Computational time variation with the number of radial divisions

Increasing the number of azimuthal positions beyond 16 is not justified given the non improvement of the results. So the number of azimuthal positions for the first stage will be 16.

Note: 16 is the total number of azimuthal positions on the rotor. For example, for a rotor with 4 blades the value that the user needs to input to achieve 16 positions is 4, if the rotor only has 2 blades the user will need to input 8 azimuthal positions to achieve the same 16 positions.

4.2.2 Second stage

Given the fact that the number of azimuthal positions for the first stage is the same as the one assumed in the beginning of the mesh convergence process a second stage is no longer necessary. Thus the final results for the mesh convergence are the same as for the first stage, 30 blade divisions and 16 azimuthal positions.

4.3 Basic Tool - Main Rotor performance

The rotor performance will be validated comparing the software results with the flight test data from [31]. The rotor geometry used in the software calculations is defined in table 4.1, the airfoil was assumed to be the $SC1095$ along the whole blade and the twist to vary parabolically with the root twist being 16° greater than the tip twist.

The test flight were done considering an weight coefficient $C_W = 0.0065$ which is equivalent to a MTOW of 8329 kilograms at sea level.

$$C_W = \frac{W}{\rho A V_{tip}^2} \tag{4.1}$$

Note: The American convention for the force, power and torque coefficients does not consider the factor of $\frac{1}{2}$ as does the European convention: $C_W = W/\frac{1}{2}\rho A V_{tip}^2$.

Having set the flight conditions and rotor geometry the software results for different advance ratios using different inflow models will be compared with the flight test data.

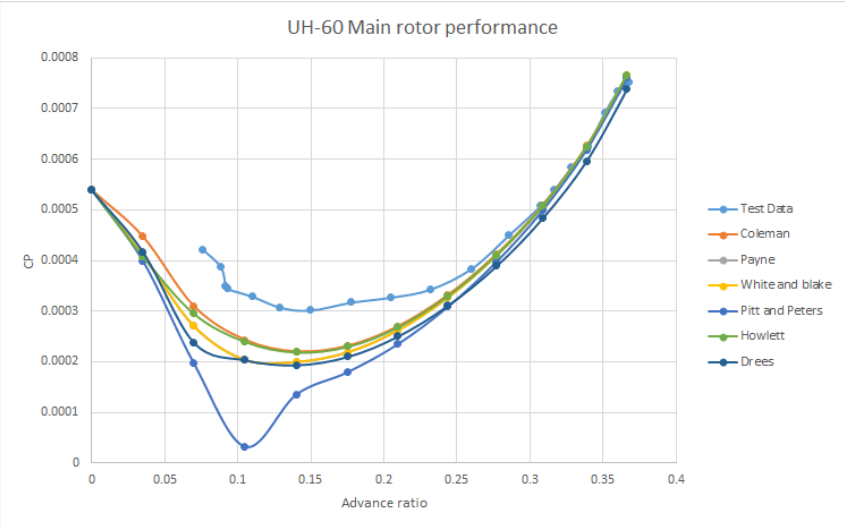

Figure 4.11: Main rotor power coefficient

In Figure 4.11 it is seen that all the inflow models present very similar results with the exception of the Pitt and Peters model [20] for the range $0.07 \leq \mu \leq 0.17$ where the power coefficient presents very low values. This is a result of an error occurring in the solving of the inflow equations, the inflow reaches very negative values (flow going upwards through the rotor) in a large region of the rotor disk resulting in a negative power contribution much greater than what would be expected thus reducing the total power of the rotor.

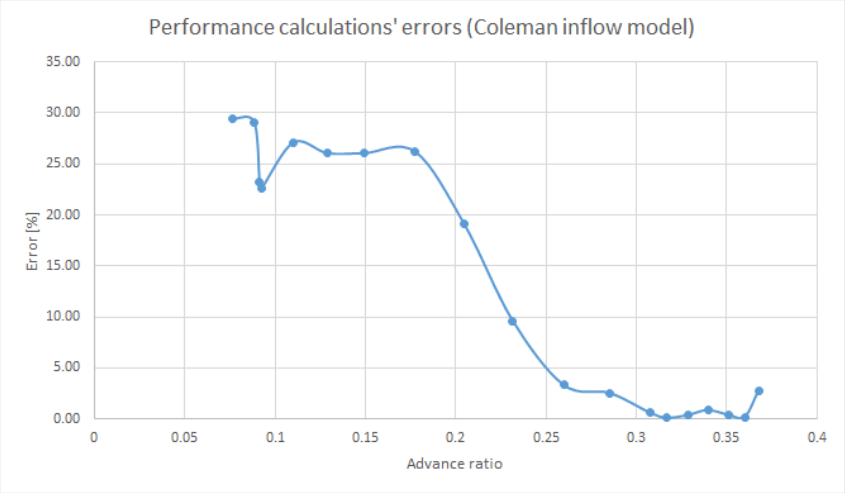

Figure 4.12: Main rotor power coefficient error

Note: The values shown in Figure 4.12 were obtain through interpolation of the results of Figure 4.11 for the Coleman [16] inflow model for the advance ratios of the test data [31]. Given the fact that the results for the different inflows were very similar only one model was used to calculate the associated error.

Remembering that the inflow models are valid for $\mu > 0.15$ it is seen that the results of the software are fairly acceptable given the low level of detail of the *basic tool*, the mean error for the advance ratios considered in Figure 4.12 is of 13.14%, and the time to calculate these results (about 80 seconds to calculate the power requirements from $\mu = 0$ to $\mu = 0.37$ with 12 different single point analyses in total).

4.4 Detailed Tool - Rotor Performance

The same flight test data used in section 4.3 will be used here to validate the values obtained using the *detailed tool*. The results are expected to be closer to the flight test ones given the more complex nature of the tool (the blade geometry is closer to the real one and the flapping motion is now considered).

The geometric characteristics are the same, being defined in 4.1, with the exception of the airfoil distribution which is given by:

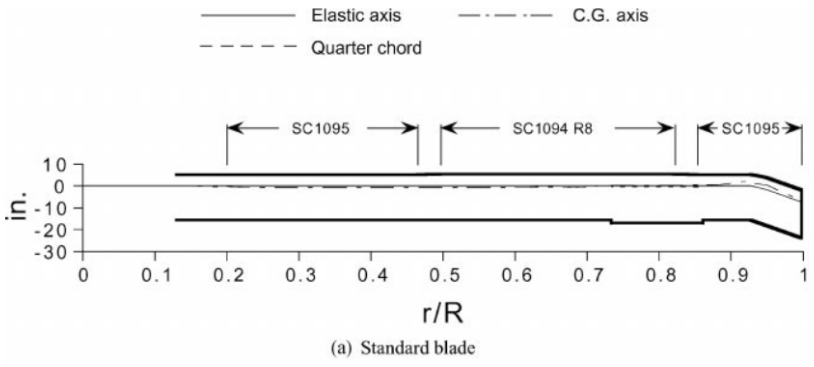

Figure 4.13: UH-60 Main rotor blade airfoils

Now comparing the software obtained results with the flight data:

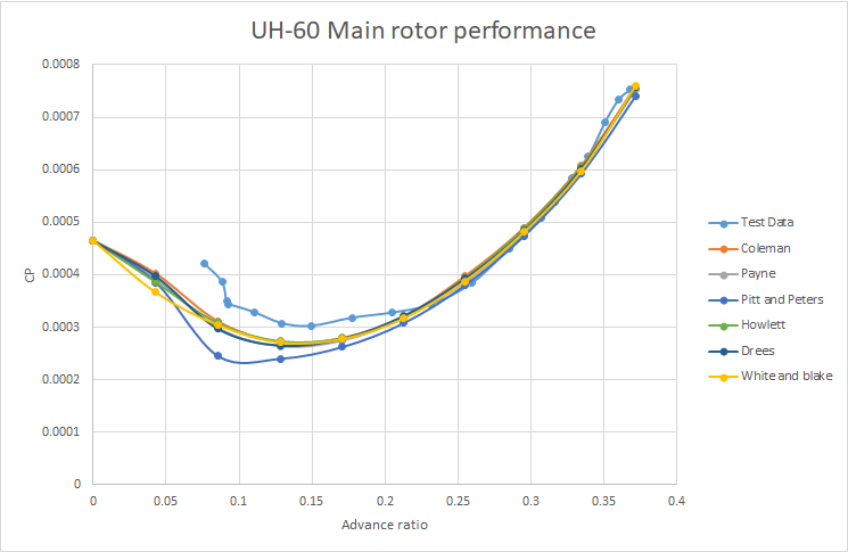

Figure 4.14: Main rotor power coefficient

It can be seen that the results when considering blade flapping (displayed in Figure 4.14) are in better concordance with the flight data when compared to the results in Figure 4.11, this was expected as was stated before. The greatest improvements occur for low advance ratios making the results very close to the actual flight test values throughout the whole velocity range considered.

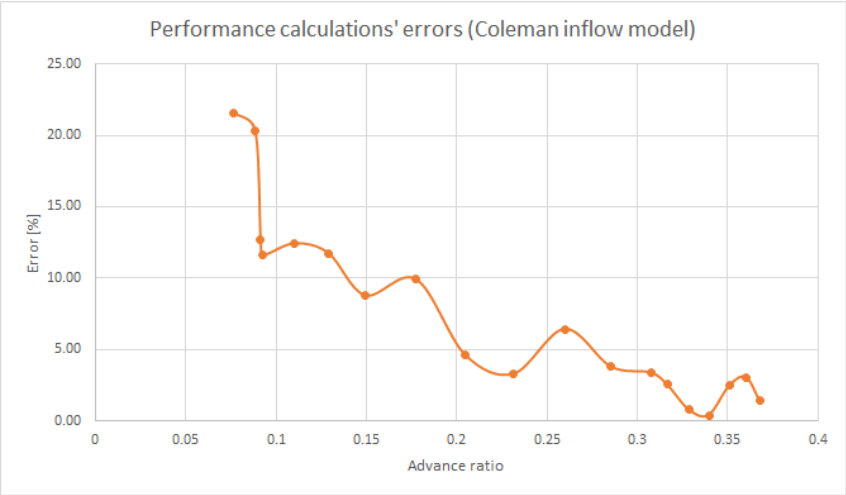

Figure 4.15: Main rotor power coefficient error

Note: The values shown in Figure 4.11 were obtain through interpolation of the results of Figure 4.15 for the Coleman [16] inflow model for the advance ratios of the test data [31]. Given the fact that the results for the different inflows were very similar only one model was used to calculate the associated error.

The mean error for the advance ratios considered in Figure 4.15 is of 7.43% which represents a very significant improvement from the 13.41% when the flapping motion was not considered.

The problem for the inflow model proposed by Pitt and Peters [20] still exists but is much less prominent than it was when the flapping motion was not considered.

The power curves presented in Figure 4.14 are representative of 10 single point calculations between the advance ratios of $\mu \in [0; 0.37]$ and took about one hour each to calculate.

Note: Validation of the pilot controls, blade flapping behaviour and tail rotor power are presented in appendix D.1.

4.5 Co-axial configuration

To validate the analysis of a co-axial system a similar approach will be taken. Values from wind tunnel testing, see [32], will be compared to the software results.

The geometry to be used is described in detail in [33].

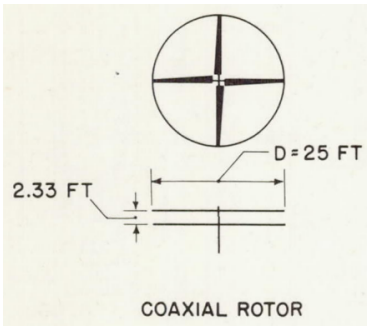

Figure 4.16: Co-axial rotor geometry

Rotor radius	3.81 m
Angular velocity	37.52 rad/s
Blade chord	Linearly tapered
Blade root chord	0.28702 m
Blade tip chord	0.10922 m
Blade twist	Untwisted
Blade airfoil	NACA symmetric 4 series with diminishing thickness
Number of blades	2
Root cut out	0.508 m
Equivalent flat plate area	0.92903 m^2
Rotor Vertical spacing	0.710184 m
Helicopter MTOW	1117.16 kg

Table 4.8: Co-axial Rotor characteristics

The airfoil distribution was approximated by a 3 section blade planform with the *NACA0030* being used from the root cut out until 30% of the span, the *NACA0022* being used from 30% until 77% of the span, and finally the *NACA0018* being used from 77% of the span until the blade tip.

The results from the wind tunnel testing and software analysis are presented in Figure 4.17.

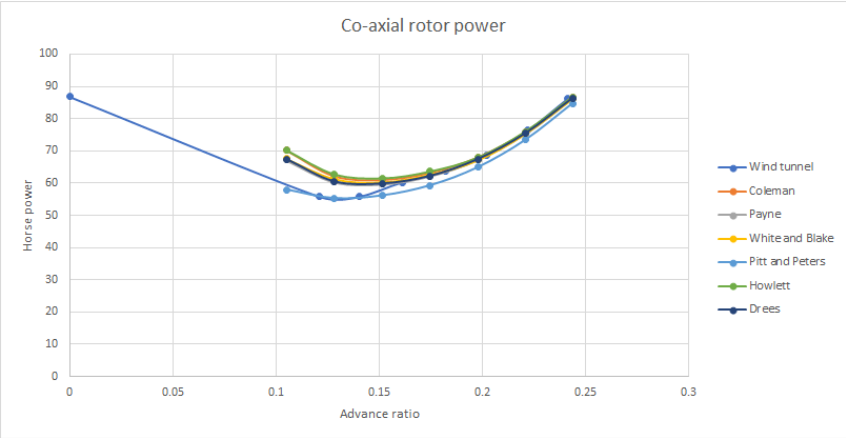

Figure 4.17: Co-axial rotor power

The results for the coaxial configuration show a good agreement between the software values and the wind tunnel test values.

4.6 Tandem configuration

Now performing a same type of analysis to a tandem rotor configuration and using wind tunnel test values from [32] the validation will be done.

The rotor geometry is described in [32].

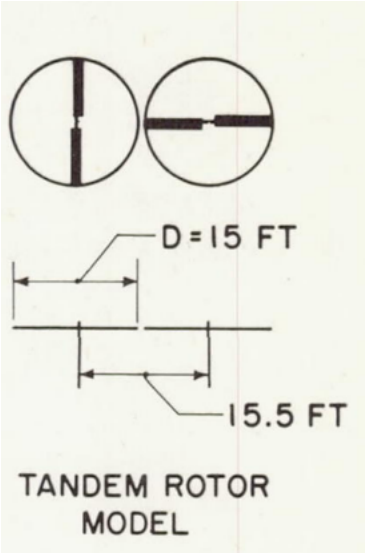

Figure 4.18: Tandem rotor geometry

Rotor radius	2.86 m
Angular velocity	66.66 rad/s
Blade chord	0.21545 m
Blade twist	Untwisted
Blade airfoil	NACA0012
Number of blades	2
Root cut out	0.286 m
Equivalent flat plate area	0.185806 m^2
Rotor shaft spacing	4.7244 m
Helicopter MTOW	323.779 kg

Table 4.9: Tandem Rotor characteristics

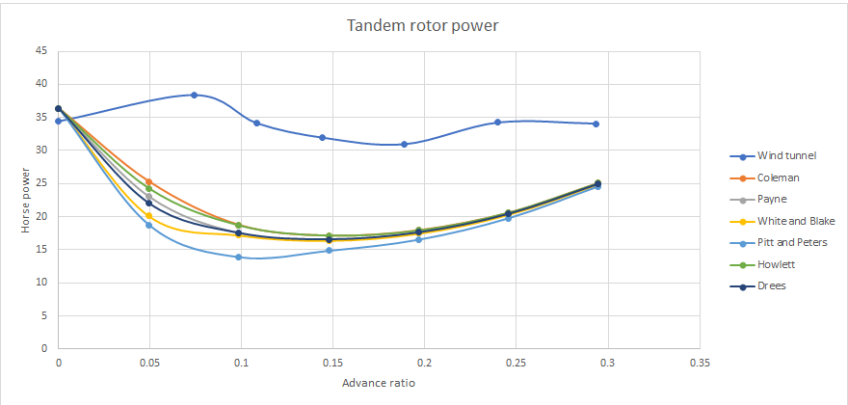

Figure 4.19: Tandem rotor power

The tandem configuration wind tunnel test results are somewhat scattered as is stated in [32], and the software calculated results are not close to the wind tunnel test ones, they follow a similar behaviour as do the results for a single or coaxial rotor.

This difference in the results might due to a low capability of analysing the interaction between the rotor, the presented configuration has no overlap and the two rotors are on the same plane, this means

that in the software calculations no rotor wake will be shedded into the other rotor thus rendering them non interfering with which other.

4.7 Drones

A separate validation process was made for the *drone tool* given the very reduced rotor dimensions taken into account.

Three different propellers from [34] were considered, the detailed geometry of each one is described on appendix D.2.1.

4.7.1 Single rotor validation

APC 8x6E propellers

The first propeller considered is an 8 inch diameter propeller with a 6 inch. Wind tunnel testing was done in [13] and those results will be compared with the software calculated ones. The test procedure was done by evaluating the generated thrust and consumed power for a given rotational velocity. This was done in the same manner for all the propellers considered.

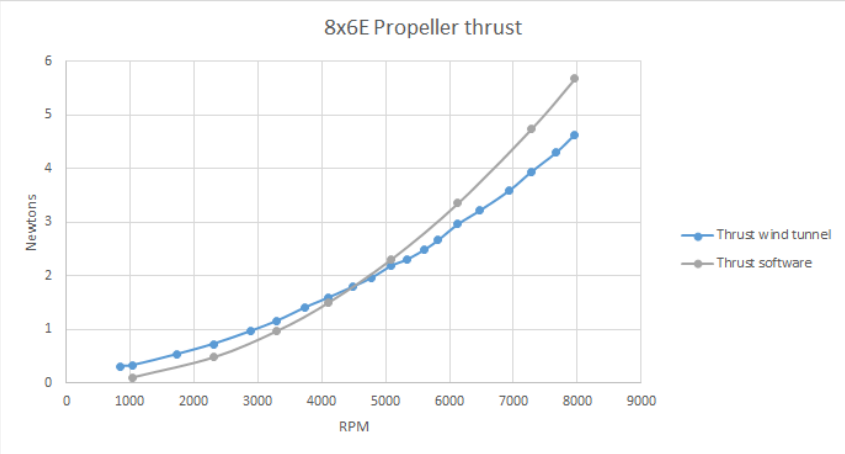

Figure 4.20: Propeller 8x6E thrust validation

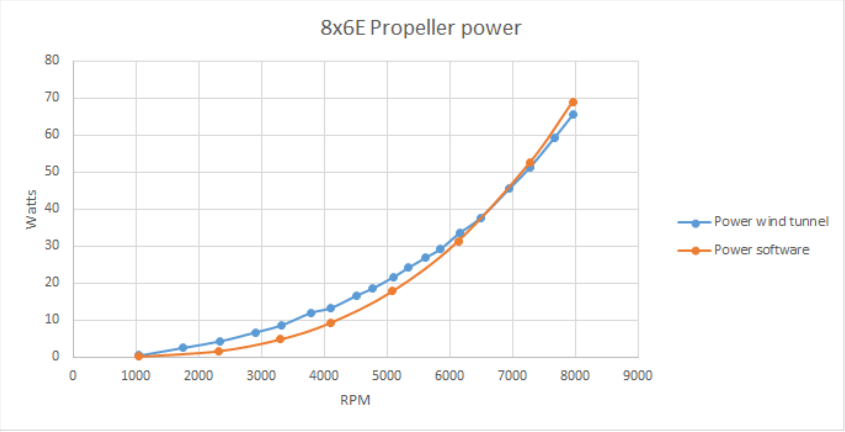

Figure 4.21: Propeller 8x6E power validation

Note: The analysis script requires that an aircraft weight in known *a priori* to set it as the objective value for the rotor thrust. This will influence the induced velocity distribution and can lead to errors if not done correctly. It is necessary that the objective value for the thrust is equal (or at least close enough given certain criteria) to the thrust generated by the rotor.

APC 9x6E propellers

The second propeller considered is an 9 inch diameter propeller with a 6 inch pitch.

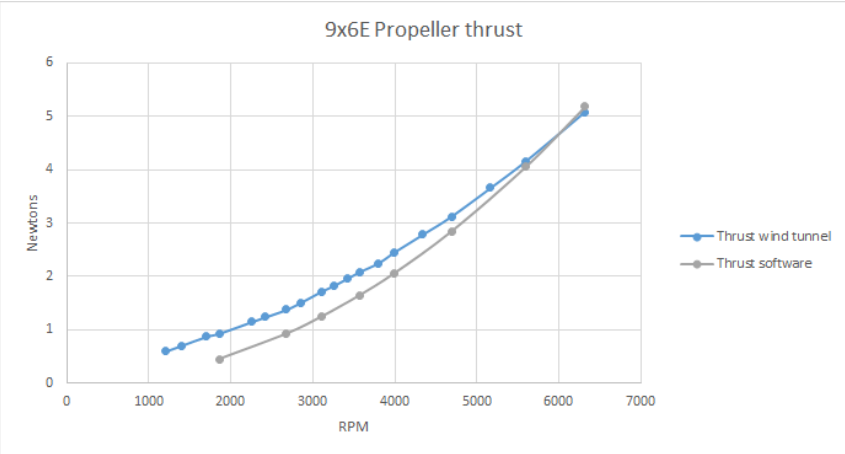

Figure 4.22: Propeller 9x6E thrust validation

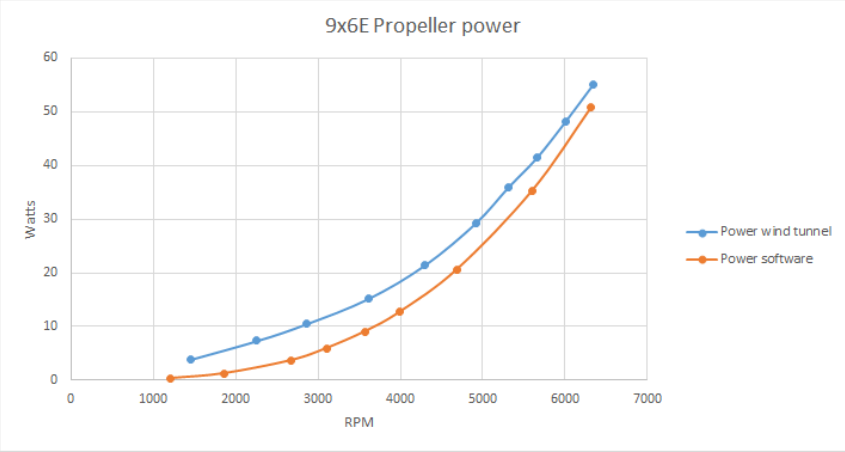

Figure 4.23: Propeller 9x6E power validation

APC 10x6E propellers

The third propeller considered is an 10 inch diameter propeller with a 6 inch pitch.

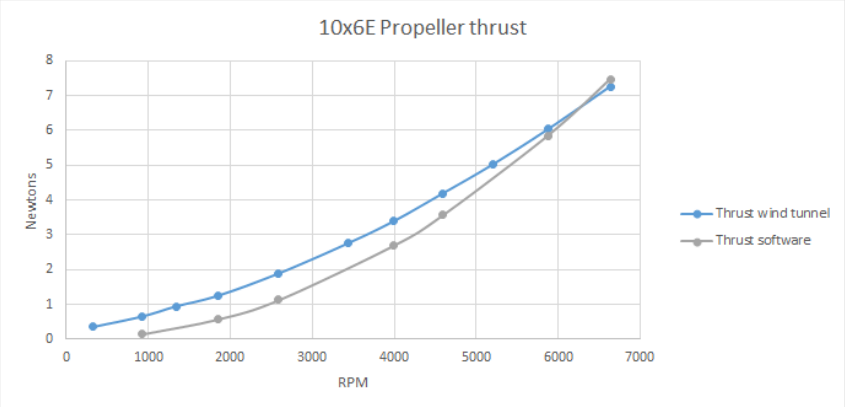

Figure 4.24: Propeller 10x6E thrust validation

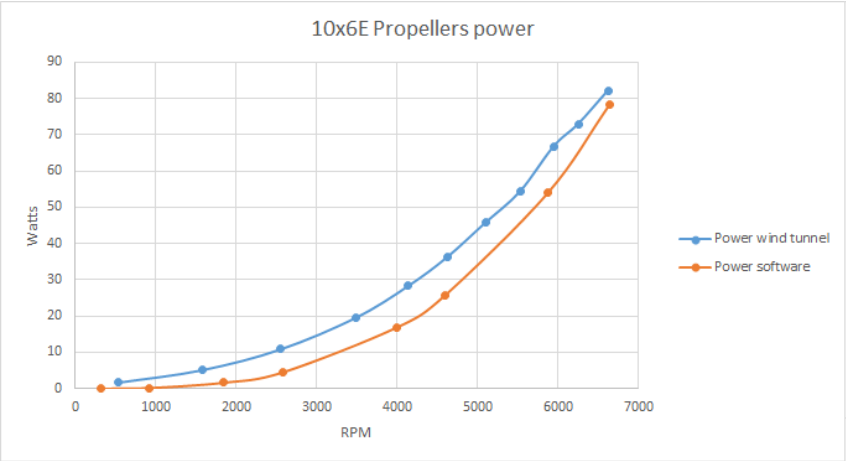

Figure 4.25: Propeller 10x6E power validation

The results are very close for the three propellers considered, for both thrust generated and power consumed.

4.7.2 Co-axial rotors validation

For the validation of the co-axial validation the top rotor was assumed not to be influenced by the presence of the lower rotor as was done in [13]. Both rotors have equal rotational velocities in terms of magnitude but opposite directions. The vertical spacing between the top and bottom rotors was set at 52.2% of the rotor radius.

The propeller considered was the **9x6E**.

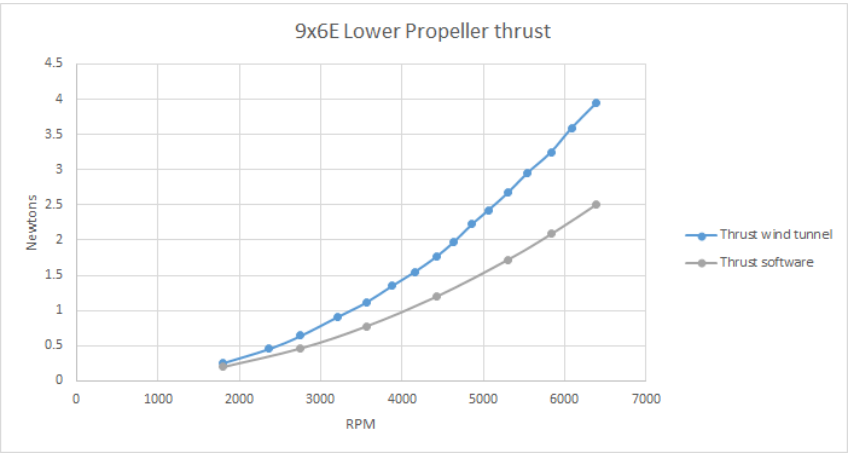

Figure 4.26: Propeller 9x6E thrust validation - Lower rotor

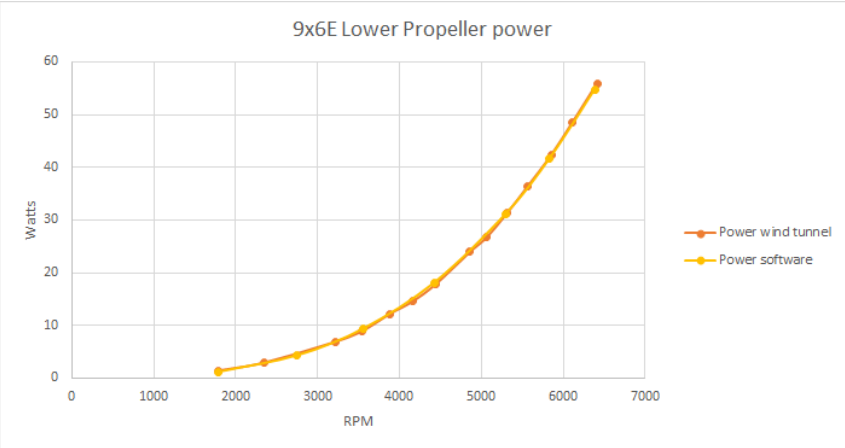

Figure 4.27: Propeller 9x6E power validation - Lower rotor

5 Case Study

In this section a direct software application will be demonstrated. Two different aircrafts (one conventional helicopter and one co-axial) with the same top level requirements will be designed and the performances will be compared in order to choose the more viable solution. The payload was defined to be sufficiently large to justify the use of a multi rotor configuration.

5.1 Top level aircraft requirements

Top level aircraft requirements	
Payload	10000 $[kg]$
Crew and passengers	20
Range	600 $[km]$
Endurance	300 $[minutes]$

Table 5.1: Top level aircraft requirements

For both configurations the initial weight estimation calculations are equal and the results for the total aircraft weight and fuel weight are the following:

Fuel weight	5469 $[kg]$
Total aircraft weight	41500 $[kg]$

Table 5.2: Weight estimation results

5.2 Dimensions

The general aircraft dimensions calculated for both configurations are:

	Conventional	**Co-axial**	**Difference** [%]
Main rotor radius $[m]$	12.96	10.90	-15.9
Height $[m]$	5.82	6.04	+3.9
Length $[m]$	25.63	18.52	-27.7
Tip to tip length $[m]$	31.15	24.50	-21.3
Width $[m]$	4.22	4.76	+12.8
Tail Rotor arm $[m]$	16.14	N/A	N/A
Rotor vertical spacing $[m]$	N/A	1.50	N/A

Table 5.3: Dimensions results for the aircraft (with N/A meaning not applicable)

Note: The difference is calculated in percentage and is in relation to the convention configuration dimension.

The co-axial configuration results in a wider and taller helicopter but it is significantly shorter in length in comparison to the conventional configuration.

The main rotor dimensions are:

	Conventional	**Co-axial**	**Difference** [%]
Main rotor radius $[m]$	12.96	10.90	-15.9
Blade chord $[m]$	1.24	1.24	0.0
Angular velocity $[rad/s]$	18.85	21.76	+15.44
Airfoil	*NACA4412*	*NACA4412*	N/A
Number of blades	4	4	N/A

Table 5.4: Dimensions results for the main rotor

The blades were designed as rectangular, untwisted and with the same airfoil throughout the span. The tail rotor dimensions are:

	Conventional
Tail rotor radius $[m]$	2.89
Blade chord $[m]$	0.77
Angular velocity $[rad/s]$	75.53
Airfoil	*NACA4412*
Number of blades	2

Table 5.5: Dimensions results for the tail rotor

5.3 Flight conditions

Both aircrafts will be required to flight under the same set of conditions, which are:

- **Sea level hover**
  - Velocity: 0 m/s
  - Altitude: 0 m
- **Maximum altitude hover**
  - Velocity: 0 m/s
  - Altitude: 1250 m
- **Vertical climb**
  - Velocity: 8 m/s
  - Altitude: 20 m
- **Cruise flight**
  - Velocity: 35 m/s
  - Altitude: 500 m
- **Maximum velocity flight**
  - Velocity: 45 m/s
  - Altitude: 500 m
- **Autorotational flight**
  - Forward velocity: 10 m/s
  - Altitude: 20 m

5.3.1 Design space

Given the these flight conditions and the helicopters' dimensions a design space was generated for both aircrafts.

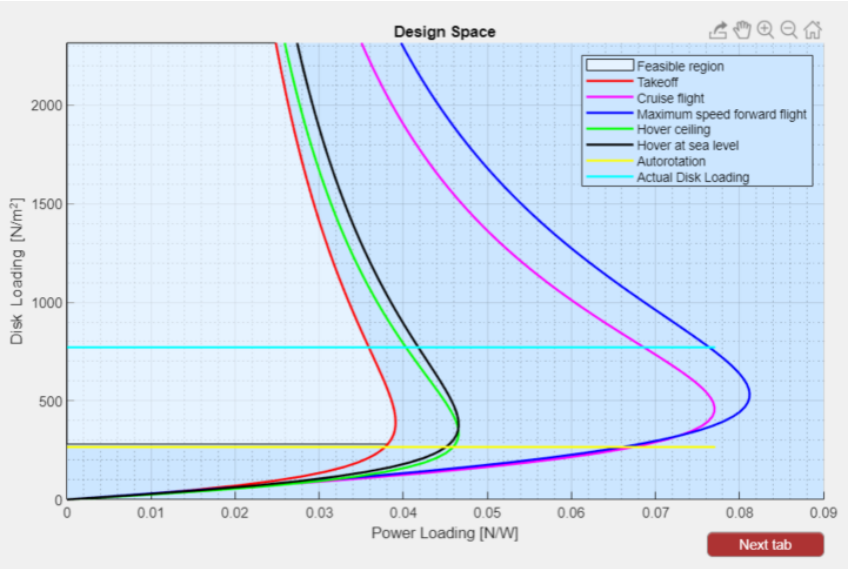

Figure 5.1: Conventional helicopter configuration - Design space

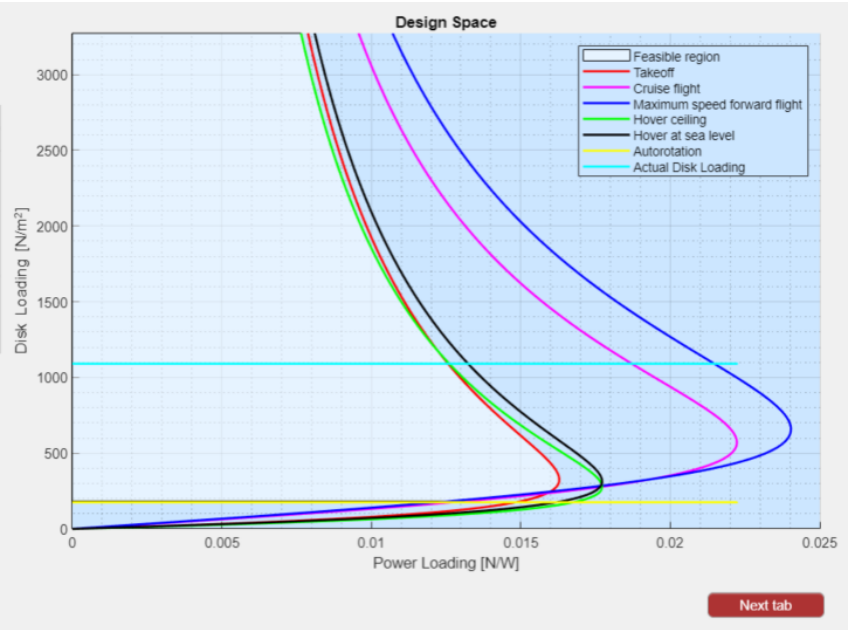

Figure 5.2: Co-axial helicopter configuration - Design space

As can be seen by comparing Figures 5.1 and 5.2 the co-axial configuration has smaller values for the power loading which means that for the same weight the aircraft requires more power (which was expected as co-axial configurations are typically less efficient than conventional configurations in terms of rotor performance).

5.3.2 Performance comparison

Now both configurations will be analysed, using BET and considering the flapping motion, for each of the flight conditions presented in 5.3 and their performances will be compared.

	Conventional power $[kW]$	**Co-axial power** $[kW]$	**Difference** [%]
Sea level hover	9652.7	10756.5	+11.4
Maximum altitude hover	10062.4	11087.6	+10.2
Vertical climb	14623.0	14749.1	+0.9
Cruise flight	5098.8	4767.2	-6.5
Maximum velocity flight	4616.1	4237.3	-8.2

Table 5.6: Flight performance comparison (calculated using BET)

For the autorotational flight the power is null (by definition of the flight condition) so the result to be looked at is the descent velocity that allows for the helicopter to operate in autorotation. For the conventional case this result was a descent velocity of 19.24 m/s and for the co-axial case is was of 25.32 m/s, which represents a difference of 31.6 %.

It is noted hat the co-axial configuration is less efficient when looking at axial flight conditions, but for these specific cases (geometry, dimensions, and flight characteristics) the co-axial helicopter requires less power for the level flight operations (cruise and maximum velocity).

It can also be seen that the power required for the maximum velocity flight is lower than the power for the cruise flight (for both configurations) which means that that velocity value is on the descendent part of the power curve and the minimum power flight conditions is yet to be found. More on this in section 5.3.3.

5.3.3 Power plots

Now comparing the power requirements variation with the forward flight velocity at an altitude of 500 meters and an installed power value of 15000 kW for both helicopters.

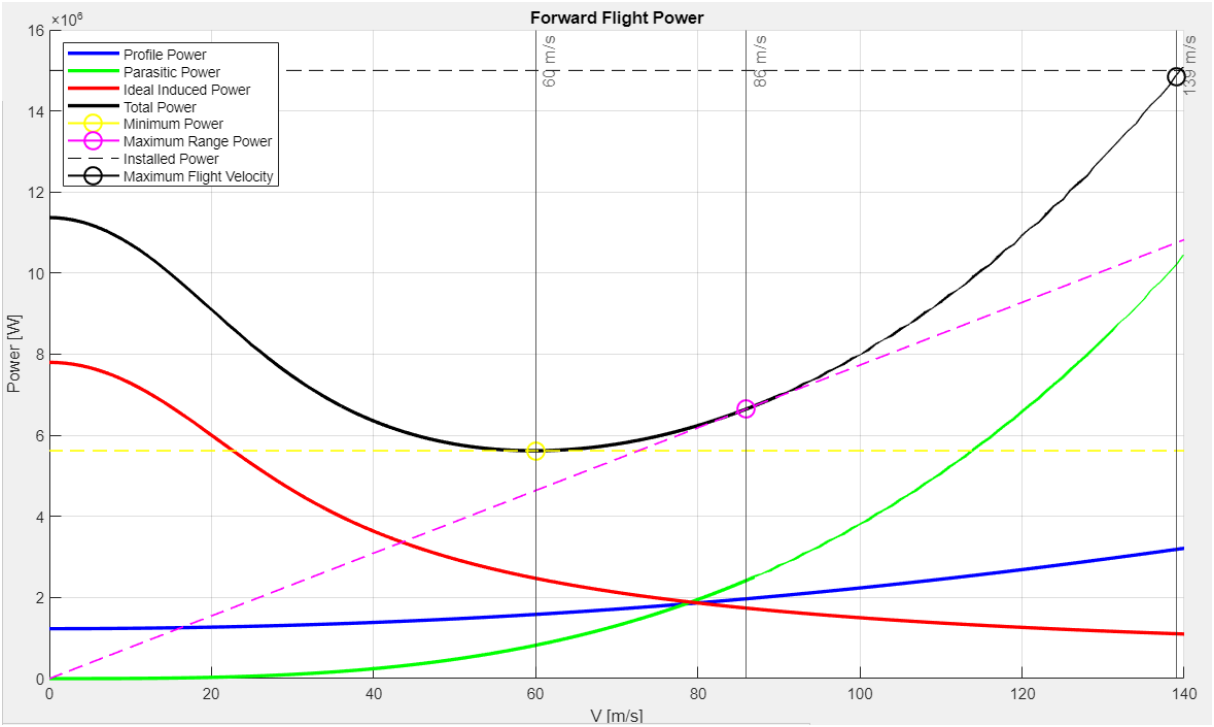

Figure 5.3: Conventional helicopter configuration - Power curve

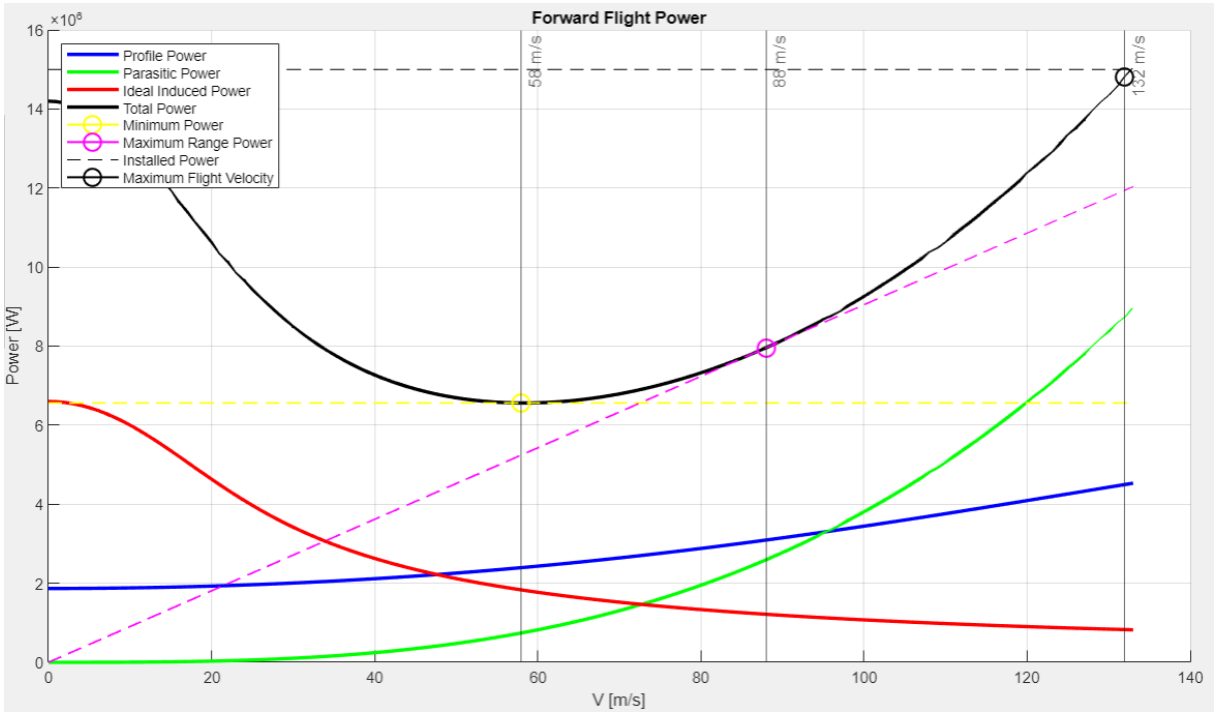

Figure 5.4: Co-axial helicopter configuration - Power curve

	Conventional	**Co-axial**	**Difference** [%]
Minimum power velocity $[m/s]$	60	58	-3.3
Minimum power for level flight $[kW]$	5619.4	6560.7	+16.8
Maximum range velocity $[m/s]$	86	88	+2.3
Maximum forward velocity $[m/s]$	139	132	-5.0

Table 5.7: Performance results using MT for both configurations

The two configurations show similar results for the minimum power flight velocity, maximum range velocity and maximum forward velocity. The major difference is in terms of the power for maximum range where a difference of almost 17 % with the co-axial configuration consuming more power.

The velocity values calculated for the minimum power flight are both higher than the velocity for the maximum velocity flight conditions specified in section 5.3, as was predicted in section 5.3.2.

Note: These power plots were obtained using MT so there will be a difference in the results when comparing with the BET calculations.

6 Conclusions

6.1 Achievements

This work set out to provide a free, open source, user friendly computational tool for the design of rotary wing aircrafts of different configurations. The developments made here represent a significant change in the complexity of the analysis when compared with the previous work done in [1], [2], and [3] with the introduction of the blade flapping motion, the addition of the *drone tool*, and some feature inside the helicopter design tools (such as the design space generation).

The results presented in section 4 are the proof that the software is capable of providing quality results very quickly and of presenting them in a clear manner so that the user can evaluate the design impacts of the aircraft performance.

The results obtained for the UH-60 were extremely good, as is shown in Figure 4.14, for all inflow models available in the tool, with the Pitt and Peters [20] model having some minor issues for a small velocities range (explained is section 4.3), and there was a significant improvement when comparing with the results where no flapping was considered, see Figure 4.11. This shows the major impact that the blades' flapping motion has on the rotor performance and that it was well modelled and calculated in the tool presented.

For the co-axial configuration both helicopter rotors and small drones' rotors were considered both showing good results as is demonstrated in Figure 4.17 for the helicopter case, and throughout section 4.7.2 for the drone case.

The versatility of the tool is clearly demonstrated in section 5 where two different designs are obtained using the same requirements as starting points. This is the perfect example of the applicability of this software as the user can easily and quickly design different helicopters, compared the results (dimensions and performance) and from that point chose what is most suitable for their specific case.

The work developed here is shown to be a very viable and useful tool and its open source nature makes it all the more attractive for the people interested.

6.2 Further work

The modular nature of the tool makes it possible for other analysis to be added to the software without compromising the work already developed and increasing the depth of the aircraft design. Features like blade structural and aeroelastic analysis can be introduced based on the force and moments distributions already calculated through the tool. A gas turbine module can be used to assess for the power plant efficiency and performance, as well as as for emissions calculations. Noise and vibrations analysis is another component that was not addressed in this work and can be useful given the regulation limitations for certain aircrafts. Fuselage parameterization in terms of passenger distribution and general outer shape might be of some interest. The generation of a flight envelope (*V-n diagram* plotting the Load factor against the airspeed) is another feature that could be studied.

In terms of the blade motion and aerodynamic performance developments can easily be introduced. More complex blade motions like lead-lag and feathering can be applied. Wake swirl considerations for a more comprehensive rotor interaction. Dynamic stall which can have major impacts on helicopter blades' performance can be introduced (this would required a more complete aerodynamic performance analysis of the airfoils used). A trim function taking into account the aerodynamic forces and moments of the fuselage (the aircraft attitude can then be calculated), this would allow for more complex maneuvers to be examined (turn maneuvers).

When considering multi rotor aircrafts (helicopters or drones) the rotor geometry is assumed to be identical throughout this work, the possibility for different rotor geometries in a single aircraft might be of some used, for example in a co-axial configuration, given the different airflow conditions of the top and bottom rotor, it might be more efficient to have different designs for the different rotors.

Compound aircrafts have been developed to expand the range of operations and might be added to the tool in further versions. Also rotor performance optimization is something to be considered, as a helicopter has very different flight conditions and cannot be optimally design for all with a single design it could be interesting to do some work in this regard (knowing all the mission profile and the flight

conditions trying to optimize the rotor for fewest fuel consumption or emission, or for least amount of time to perform the mission). Even blade morphing could be introduced to adapt the rotor geometry to the flight condition that it is in.

7 References

[1] Roman Vasyliovych Rutskyy. *Desenvolvimento duma ferramenta computacional para projecto preliminar do helicóptero de configuração convencional*, Masters' Thesis, Instituto Superior Técnico, Lisboa, 2014.

[2] Anatol Conjocari. *Preliminary design tool of conventional/coaxial/tandem helicopters*, Masters' Thesis, Instituto Superior Técnico, Lisboa, 2016.

[3] Miguel Ponte. *Development of a Preliminary Design Tool for Conventional Co-axial and Tandem Helicopter Configurarion*, Masters' Thesis, Instituto Superior Técnico, Lisboa, 2016.

[4] Rand Omri, Khromov Vladimir, *Helicopter Sizing by Statistics*, Faculty of Aerospace Engineering, Technion - Israel Institute of Technology, Haifa, 2002.

[5] Wayne Johnson. *CAMRAD/JA - A Comprehensive Analytical Model of Rotorcraft Aerodynamics and Dynamics*. Johnson Aeronautics, Palo Alto, California, 1988.

[6] Kushagra Vidyarthi, Mathijs Beuker, Mark Voskuijl, Marilena Pavel. *HOPLITE - A conceptual design environment for helicopters incorporating morphing rotor technology*. Faculty of Aerospace Engineering, Delft University of Technology, Delft, The Netherlands, 2018.

[7] Max Lier, Alex Krenik, Philipp Kunze, Dieter Kohlgrüber, Marius Lützenburger, Dominik Schwinn. *A Toolbox for Rotorcraft Preliminary Design* German Aerospace Center (DLR), Braunschweig, Germany, 2015.

[8] Benoit, B., Dequin, A.-M., Kampa, K., von Grünhagen, W., Basset, P.-M., Gimonet, B. *HOST: A general helicopter simulation tool for Germany and France* American Helicopter Society 56^{th} Annual Forum, Virginia Beach, USA, 2000.

[9] J. Gordon Leishman. *Principles of Helicopter Aerodynamics*, Cambridge Aerospace Series, 2006.

[10] Gessow, A. and Meyers, G. C., Jr. *Aerodynamics of the Helicopter*, Macmillan Co. (republished by Frederick Ungar Publishing, New York, 1967), 1952.

[11] Sissingh, G. *Contribution to the Aerodynamic of Rotating-Wing Aircraft*, NACA TM 921, 1939.

[12] Seddon, J. and Newman, S. *Basic Helicopter Aerodynamics*. John Wiley & Sons, Ltd, 2011.

[13] Amado, I. S. *Experimental Comparison of Planar and Coaxial Rotor Configurations in Multi-rotors* Masters' Thesis, Instituto Superior Técnico, Lisboa, 2017.

[14] Jones R. T. and Cohen D. *Aerodynamic Components of Aircraft at High Speeds* - Chapter 1, Princeton University Press, Princeton, 1957.

[15] Brotherhood P., Stewart W. *An Experimental Investigation of a Flow through a Helicopter Rotor in Forward Flight*. ARC R & M 2734, 1949.

[16] Coleman R. P, Feingold M. A, and Stempin C. W. *Evaluation of the Induced Velocity Fields of an Idealized Helicopter Rotor*. NACA ARR L5E10, 1945.

[17] Drees J. M. *A Theory of Airflow Through Rotors and Its Application to some Helicopter Problems*. Journal of the Helicopter Association of Great Britain, July-September, 1949.

[18] Payne P. R. *Helicopter Dynamics and Aerodynamics*. Pitman & Sons, London, 1959.

[19] White F. and Blake B. B. *Improved Method of Predicting Helicopter Control Response and Gust Sensitivity*. 35^{th} Annual Forum of the American Helicopter Society, Washington DC, May, 1979.

[20] Pitt D. M. and Peters D. A. *Theoretical Predications of Dynamic Inflow Derivatives*. Vertica, 1981.

[21] Howlett J. J. *UH-60 Blackhawk Engineering Simulation Program: Vol. 1 - Mathematical Model.* NASA CR-66309, 1981.

[22] Glauert, H. *On the Horizontal Flight of a Helicopter*, ARC R & M 1730, 1926.

[23] Bennett, J. A. J. *Rotary Wing Aircraft*, Aircraft Engineering, 12 Jan-Aug, 1940.

[24] F. Perry, J. Wilby, P. Jones, G. Jones. *The BERP Rotor - How Does it Work and What Has it Been Doing Lately?* Vertiflite, 44(2):44–48, 1998.

[25] El-Sayed Aziz, Constantin Chassapis, Sven Esche, Sumei Dai, Shanjun Xu, Ruiqing Jia. *AC 2008-613: Online Wind Tunnel Laboratory* American Society for Engineering Education, 2008.

[26] Stephen Haviland, Dmitry Bershadsky. *Electric Multirotor Propulsion System Sizing for Performance Prediction and Design Optimization* Georgia Institute of Technology, Aerospace Engineering. 57th AIAA/ASCE/AHS/ASC Structures, Structural Dynamics, and Materials Conference, January 2016.

[27] Wayne Johnson, Christopher Silva, Eduardo Solis. *Concept Vehicles for VTOL Air Taxi Operations.* AHS Technical Conference on Aeromechanics Design for Transformative Vertical Flight, San Francisco, CA, January 16-19, 2018.

[28] Dong Han, Vasileios Pastrikakis, George N. Barakos. *Helicopter performance improvement by variable rotor speed and variable blade twist.* Elsevier Masson SAS, 2016.

[29] Vertipedia. Kamov Ka-27. URL: `https://vertipedia.vtol.org/aircraft/getAircraft/aircraftID/154` Retrieved: 07/2020.

[30] Vertipedia. Boeing ACH-47A Chinook. URL: `https://vertipedia.vtol.org/aircraft/getAircraft/aircraftID/807` Retrieved: 07/2020.

[31] Wayne Johnson, William G. Bousman, Hyeonsoo Yeo. *Performance Analysis of a Utility Helicopter with Standard and Advanced Rotors* American Helicopter Society Aerodynamics, Acoustics, and Test and Evaluation Technical Specialist Meeting, San Francisco, CA, January 23–25, 2002.

[32] Richard C. Dingeldein. *Wind-Tunnel Studies of the Performance of Multirotor Configurations* Langley Aeronautical Laboratory, Langley Field, VA, August, 1954.

[33] Robert D. Harrington. *Full-Scale-Tunnel Investigation of the Static-Thrust Performance of a Coaxial Helicopter Rotor* Langley Aeronautical Laboratory, Langley Field, VA, August, 1951.

[34] APC Propellers. URL `https://www.apcprop.com/`. Retrieved: 04/2020.

A Conventional Helicopter Equations

A.1 Number of passengers

Data from 23 different conventional helicopters was collect to generate a simple relation between the number of passengers and crew members with the maximum take off weight (MTOW) in kilograms, the resulting relation is:

$$MTOW = 1525\, e^{0.0809 \times N_{pass}} \tag{A.1}$$

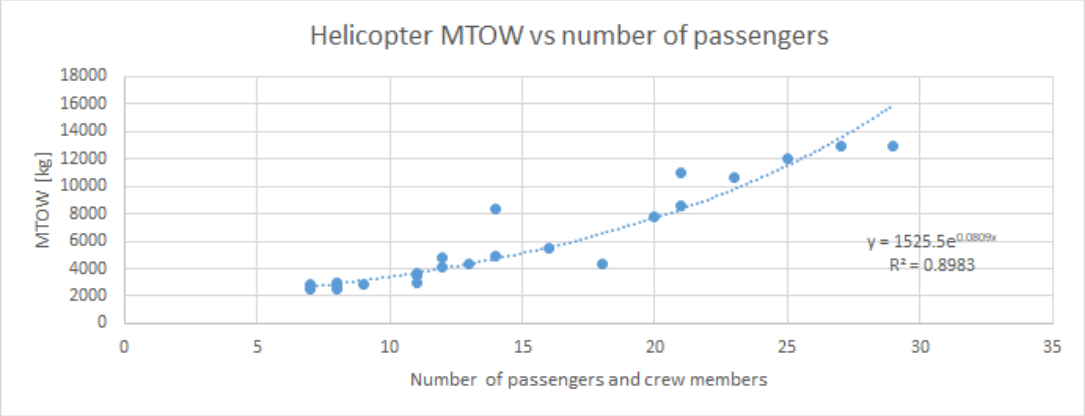

Figure A.1: Number of passengers and crew members variation with the Helicopter MTOW

B Different Helicopter Configurations Equations

Equations 3.3, 3.4, 3.5, 3.6, and 3.7 present a relationship between the characteristic dimensions of a conventional helicopter with it's main rotor radius, no relations of this sort were found for other helicopter configurations so based on the mentioned equations and on data collected from co-axial helicopters some relations were developed and used on the software tool.

B.1 Co-axial Helicopters

Data from 18 co-axial helicopters was collected, this data set is somewhat incomplete inasmuch as some of the characteristic dimensions in question are not known in all the aircrafts, nevertheless it was possible to reach some coherent relations.

The first equation generated was the one that relates the rotor diameter with the helicopter MTOW and the result is:

$$R = 0.555 \times (MTOW)^{0.28} \tag{B.1}$$

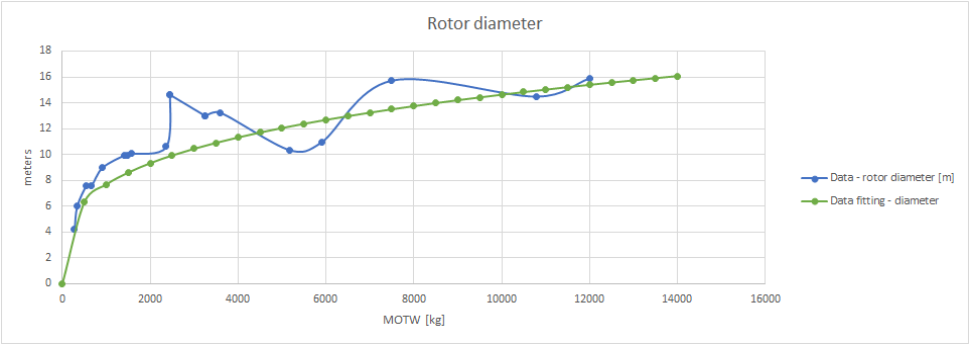

Figure B.1: Rotor diameter variation with the helicopter MTOW in kilograms

The equations for the different dimensions as functions of the rotor radius are as follows:

Note: The plots show the variation of the dimensions with the helicopter MTOW. First the rotor diameter is calculated based on the MTOW value and then the specific dimension is calculated.

Height:

$$h_{heli} = 0.75 \times (2R)^{0.677} \tag{B.2}$$

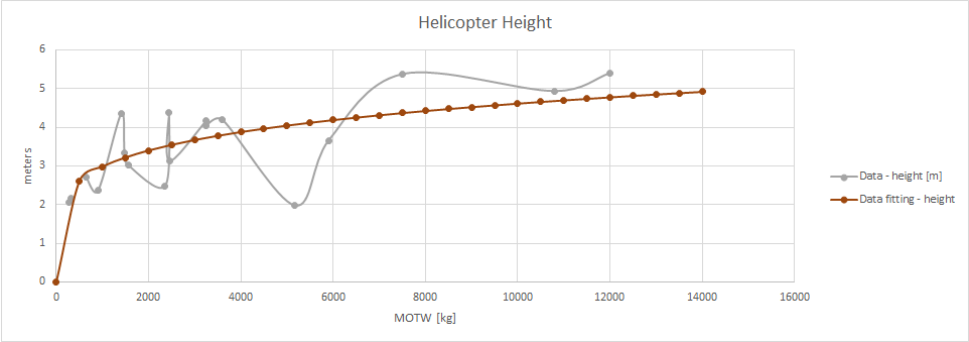

Figure B.2: Helicoper height variation with the helicopter MTOW in kilograms

Length:

$$l_{heli} = 0.824 \times (2R)^{1.01} \tag{B.3}$$

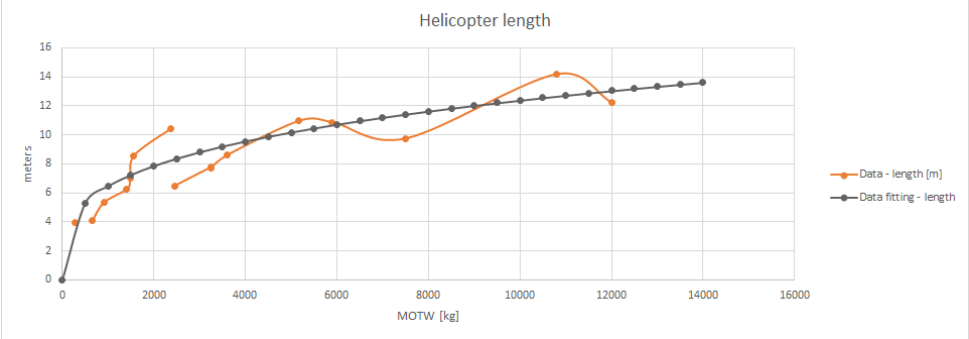

Figure B.3: Helicoper length variation with the helicopter MTOW in kilograms

Tip to tip lenght:

$$ttt_{heli} = 1.09 \times (2R)^{1.01} \tag{B.4}$$

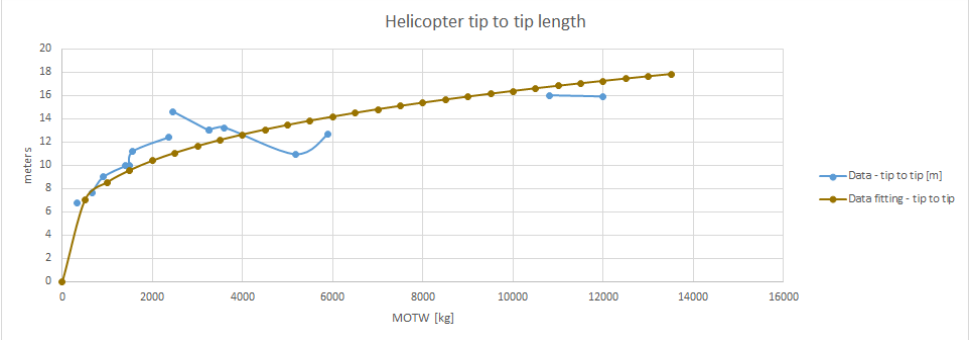

Figure B.4: Helicoper tip to tip length variation with the helicopter MTOW in kilograms

Width:

$$w_{heli} = 0.55 \times (2R)^{0.7} \tag{B.5}$$

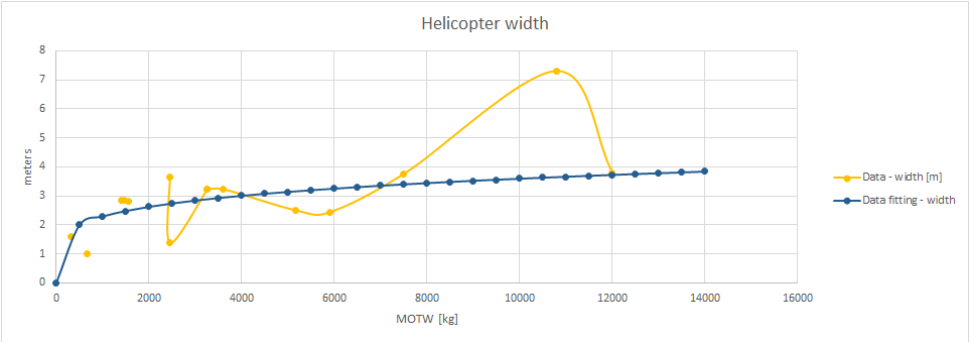

Figure B.5: Helicoper width variation with the helicopter MTOW in kilograms

B.2 Tandem Helicopters

For the tandem configuration the same was done from a data set of 18 helicopters and the results are:

Radius:

$$R = 0.6 \times (m)^{0.28} \tag{B.6}$$

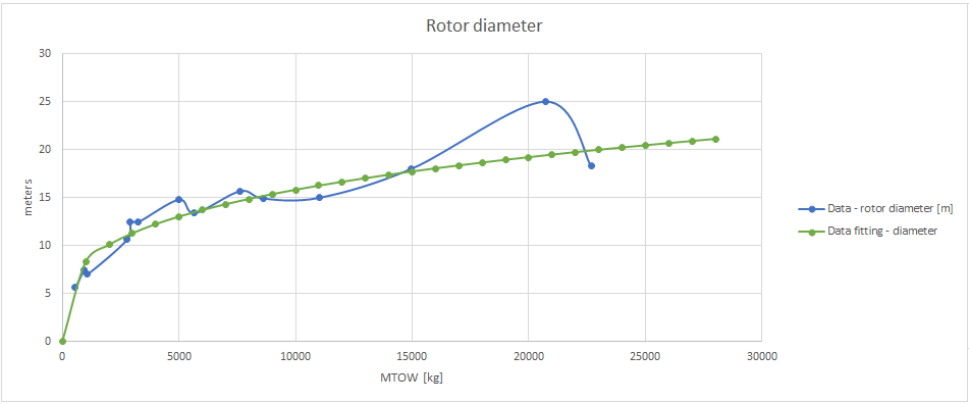

Figure B.6: Rotor diameter variation with the helicopter MTOW in kilograms

Height:

$$h_{heli} = 0.8 \times (2R)^{0.7} \tag{B.7}$$

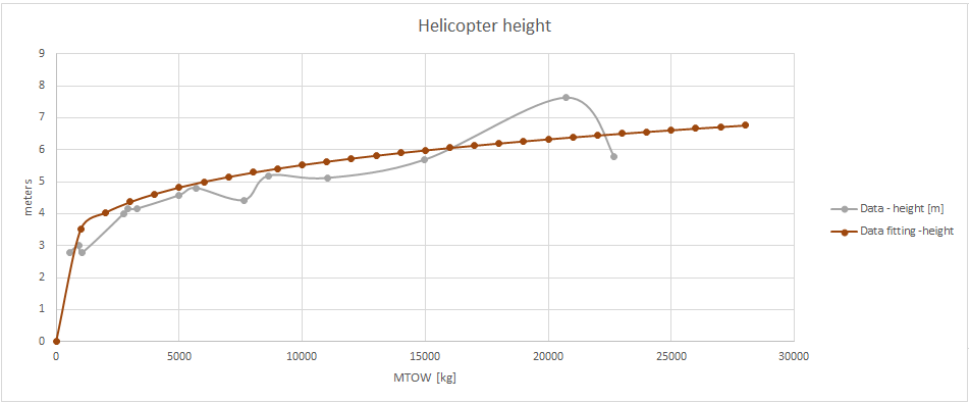

Figure B.7: Helicoper height variation with the helicopter MTOW in kilograms

Length:

$$l_{heli} = 1.03 \times (2R)^{1.01} \tag{B.8}$$

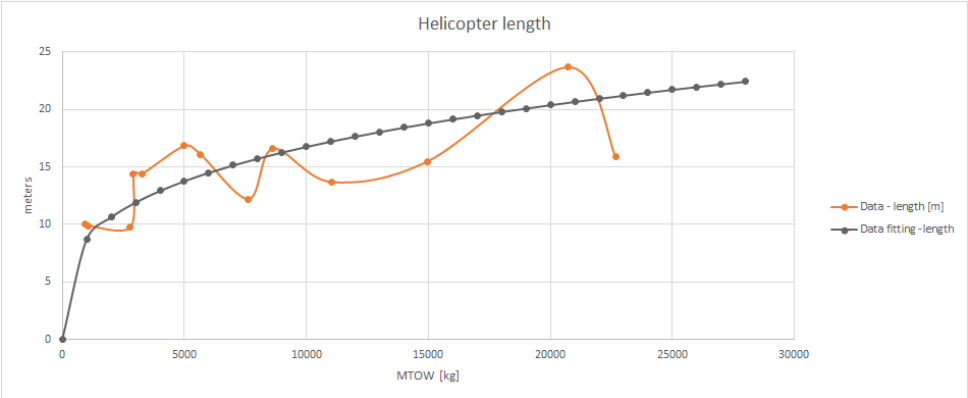

Figure B.8: Helicoper length variation with the helicopter MTOW in kilograms

Tip to tip lenght:

$$ttt_{heli} = 2 \times (2R)^{0.98} \tag{B.9}$$

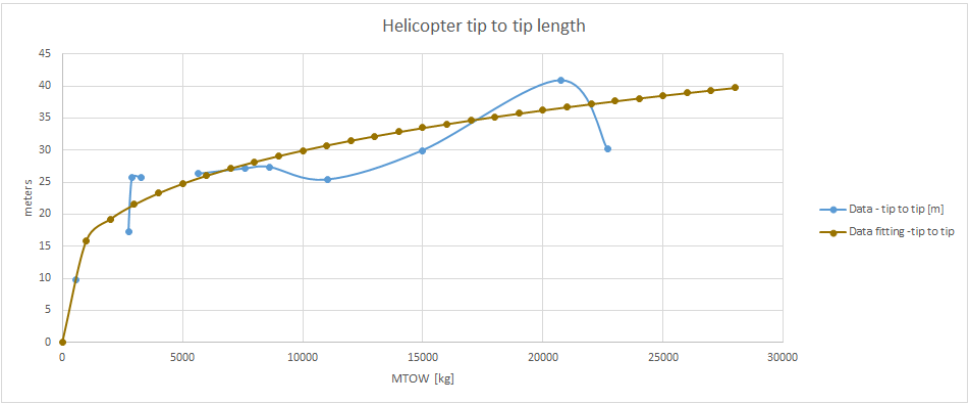

Figure B.9: Helicoper tip to tip length variation with the helicopter MTOW in kilograms

Width:

$$w_{heli} = 0.6 \times (2R)^{0.7} \tag{B.10}$$

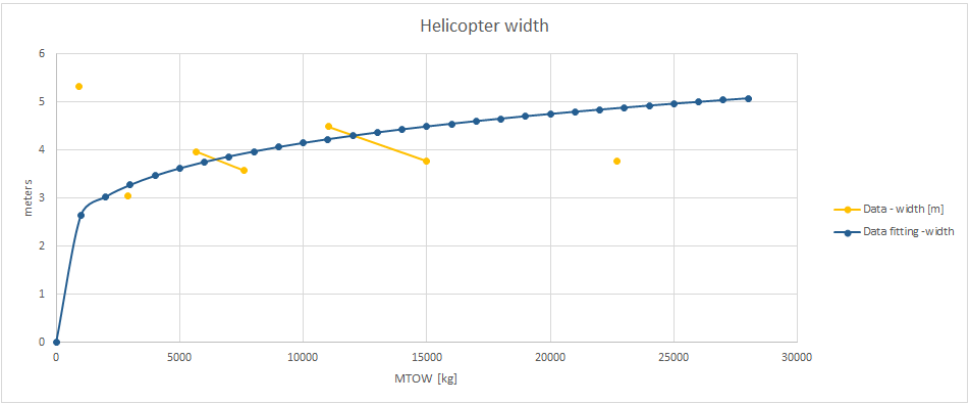

Figure B.10: Helicoper width variation with the helicopter MTOW in kilograms

C Airfoil data format

The airfoil coordinates need to be saved as a *DAT* file, the x coordinate is to be on the first column and the values need to start at the trailing edge and go through the airfoil in a anticlockwise direction

finishing in the trailing edge once again (but not on the starting point).

```
NACA 0012

 1.000000  0.001260
 0.975528  0.004642
 0.904508  0.013914
 0.793893  0.026905
 0.654508  0.040917
 0.500000  0.052940
 0.345492  0.059575
 0.206107  0.057714
 0.095492  0.046049
 0.024472  0.025893
 0.000000  0.000000
 0.024472 -0.025893
 0.095492 -0.046049
 0.206107 -0.057714
 0.345492 -0.059575
 0.500000 -0.052940
 0.654508 -0.040917
 0.793893 -0.026905
 0.904508 -0.013914
 0.975528 -0.004642
 1.000000 -0.001260
```

Figure C.1: Airfoil coordinates file format

Note: The number of points in the airfoil in this example is very reduced and is only meant to be taken as a representation of the files actually used on the software.

The airfoil performance data is stored in a *.txt* file and its format is the one directly exported by the *XFoil* software (used to perform the 2-D simulations of the airfoils of the software).

To perform an *Xfoil* simulation the following steps need to be taken:

- Get the *.dat* file in a format the can be read by the program, then save the file
- Open *Xfoil*
- To load the airfoil coordinates file write: **load 'filename'.dat**
- To clean up airfoil paneling write: **pane**
- To open the "Direct Operating Points" menu write: **oper**
- To turn on viscous mode and set the Reynolds number wirte: **visc 'Reynolds number'**
- Toggle what graph is displayed: **seqp**
- Toggle polar point accumulation: **pacc**
- Enter the name of the file to be saved: **'filename'**
- Enter the name of the dump file: **'dumpfilename'**
- Set the sequence on angles of attack to run (starting at α_0 degrees up to α_f degrees with a step of $\Delta\alpha$ degree): **aseq** α_0 α_f $\Delta\alpha$

After all these steps the file will be ready to be read by the *airfoilDataAquisition* function.

```
      XFOIL         Version 6.99

Calculated polar for: NACA 0012

1 1 Reynolds number fixed          Mach number fixed

xtrf =   1.000 (top)        1.000 (bottom)
Mach =   0.000     Re =     3.000 e 6     Ncrit =   9.000

   alpha    CL        CD       CDp       CM     Top_Xtr  Bot_Xtr
  ------ -------- --------- --------- -------- -------- --------
 -19.000  -1.6487   0.04535   0.04170  -0.0298   1.0000   0.0084
 -18.000  -1.6524   0.03374   0.02976  -0.0322   1.0000   0.0086
 -17.000  -1.6283   0.02701   0.02277  -0.0300   1.0000   0.0088
 -16.000  -1.6015   0.02200   0.01750  -0.0235   1.0000   0.0096
 -15.000  -1.5519   0.01925   0.01460  -0.0160   1.0000   0.0104
 -14.000  -1.4759   0.01727   0.01250  -0.0117   1.0000   0.0110
 -13.000  -1.3930   0.01529   0.01041  -0.0081   1.0000   0.0125
 -12.000  -1.3008   0.01385   0.00890  -0.0056   1.0000   0.0137
 -11.000  -1.2082   0.01240   0.00741  -0.0027   1.0000   0.0159
 -10.000  -1.1178   0.01126   0.00624   0.0010   1.0000   0.0186
  -8.000  -0.8955   0.00924   0.00427   0.0000   0.9956   0.0282
  -7.000  -0.7698   0.00831   0.00343  -0.0034   0.9889   0.0390
  -6.000  -0.6559   0.00750   0.00273  -0.0039   0.9686   0.0579
  -5.000  -0.5504   0.00680   0.00213  -0.0024   0.9288   0.0904
  -4.000  -0.4428   0.00619   0.00161  -0.0013   0.8706   0.1474
  -3.000  -0.3337   0.00571   0.00121  -0.0006   0.7925   0.2271
  -2.000  -0.2234   0.00535   0.00093  -0.0002   0.7026   0.3219
  -1.000  -0.1120   0.00516   0.00078  -0.0001   0.6077   0.4178
   0.000   0.0000   0.00510   0.00073  -0.0000   0.5132   0.5133
   1.000   0.1120   0.00517   0.00078   0.0001   0.4174   0.6077
   2.000   0.2234   0.00536   0.00093   0.0002   0.3213   0.7023
   3.000   0.3337   0.00571   0.00121   0.0006   0.2270   0.7922
   4.000   0.4428   0.00619   0.00161   0.0013   0.1474   0.8707
   5.000   0.5503   0.00680   0.00213   0.0024   0.0904   0.9288
   6.000   0.6559   0.00750   0.00273   0.0039   0.0579   0.9686
   7.000   0.7699   0.00831   0.00343   0.0034   0.0389   0.9889
   8.000   0.8956   0.00924   0.00427  -0.0000   0.0282   0.9956
   9.000   1.0225   0.01024   0.00522  -0.0039   0.0222   0.9994
  10.000   1.1177   0.01126   0.00624  -0.0010   0.0186   1.0000
  11.000   1.2082   0.01240   0.00741   0.0027   0.0159   1.0000
  12.000   1.3009   0.01385   0.00890   0.0055   0.0137   1.0000
  13.000   1.3931   0.01529   0.01041   0.0081   0.0125   1.0000
  14.000   1.4762   0.01727   0.01249   0.0116   0.0110   1.0000
  15.000   1.5524   0.01925   0.01460   0.0159   0.0104   1.0000
  16.000   1.6022   0.02200   0.01750   0.0234   0.0096   1.0000
  17.000   1.6298   0.02697   0.02273   0.0298   0.0088   1.0000
  18.000   1.6543   0.03367   0.02969   0.0320   0.0086   1.0000
  19.000   1.6514   0.04520   0.04155   0.0296   0.0084   1.0000
  20.000   1.5978   0.06559   0.06237   0.0207   0.0082   1.0000
```

Figure C.2: Airfoil performance file format

D Software Validation

D.1 Conventional Helicopter

Detailed tool validation for the pilot controls of the main rotor:

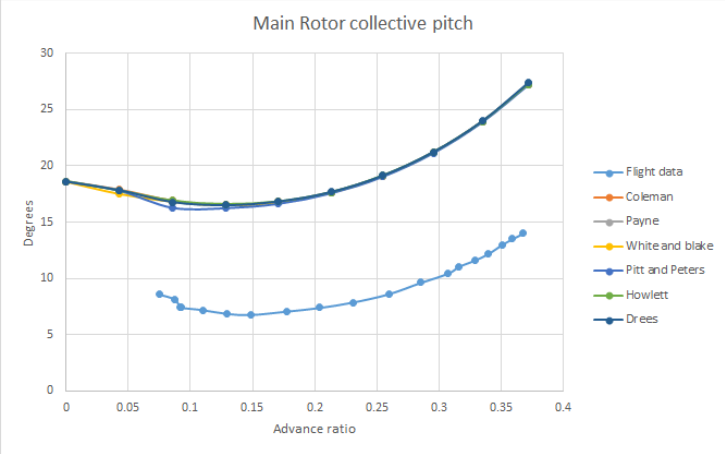

Figure D.1: Detailed Tool Collective pitch validation

The results show good coherence in terms of variation with the advance ratio but have an offset, this might be because the root pitch is assumed to be zero when the collective pitch is zero and this might not be the case for the actual helicopter geometry.

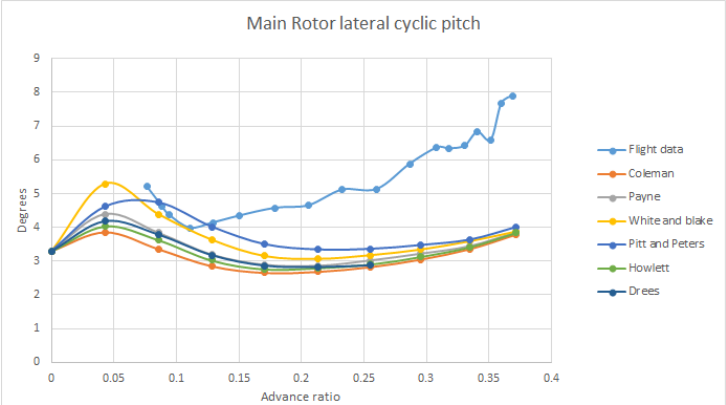

Figure D.2: Detailed Tool Lateral cyclic pitch validation

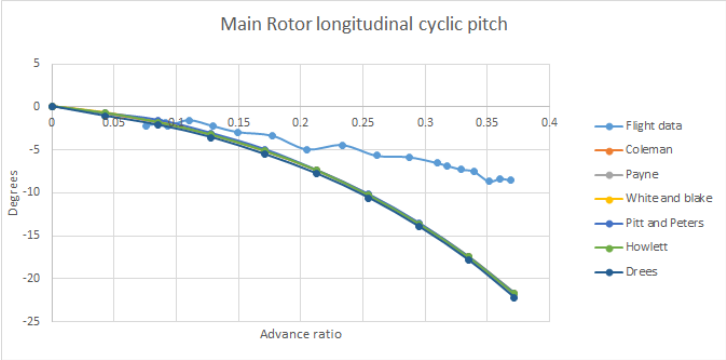

Figure D.3: Detailed Tool Longitudinal cyclic pitch validation

Now the results for the flapping motion of the main rotor blades:

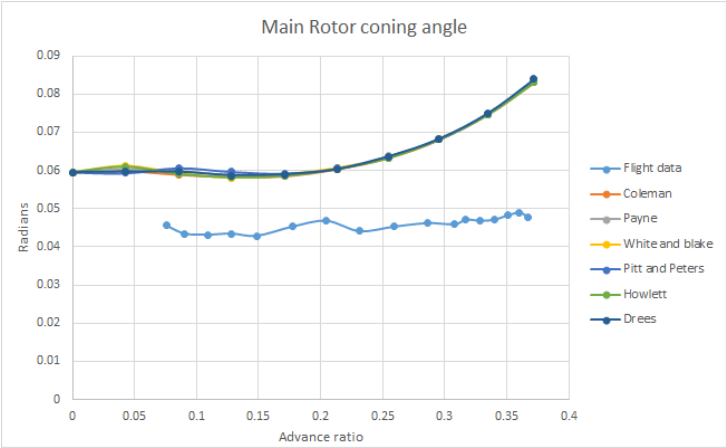

Figure D.4: Detailed Tool Main Rotor coning angle validation

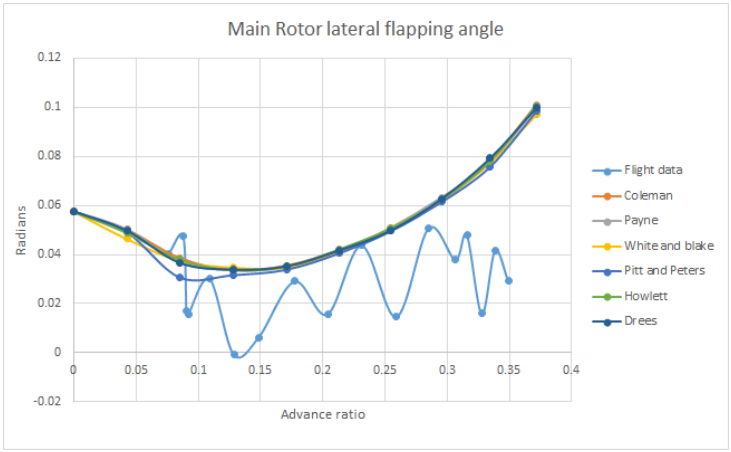

Figure D.5: Detailed Tool Main Rotor lateral flapping angle validation

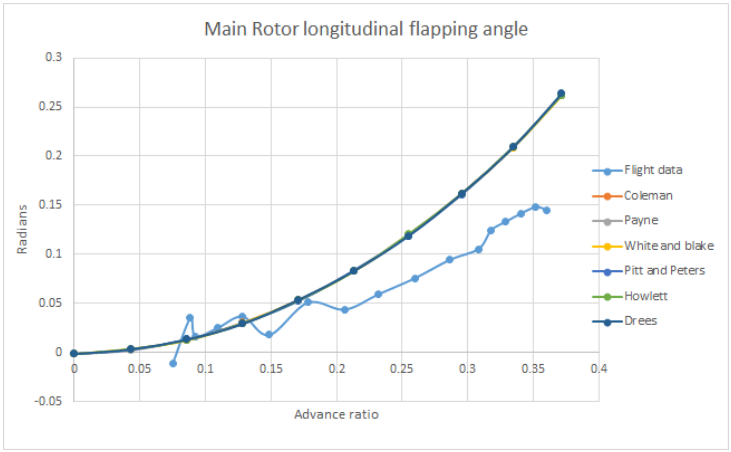

Figure D.6: Detailed Tool Main Rotor longitudinal flapping angle validation

Both cyclic pitches have offsets between the flight test and software values, this might be due to the fact that aircraft pitching and rolling behaviour is not considered (the rotor inclination is only achieved by blade flapping in the software), in reality the helicopter attitude will change for different flight conditions which will influence the rotor inclination required and consequently the flapping behaviour.

And finally the results for the tail rotor power coefficient:

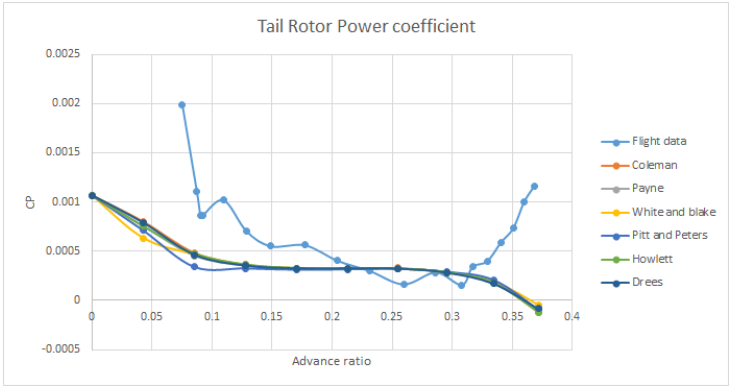

Figure D.7: Detailed Tool Tail Rotor power coefficient validation

The tail rotor power is greatly influence by the complex flow resultant from the main rotor and fuselage wake and these phenomena are not considered in this software, this might be one explanation

for the difference between the flight data and the software results.

D.2 Drone

D.2.1 Propeller Geometry

APC Propellers - 8x6E:

STATION (IN)	CHORD (IN)	PITCH (QUOTED)	PITCH (LE-TE)	PITCH (PRATHER)	SWEEP (IN)	THICKNESS RATIO	TWIST (DEG)
0.9536	0.6922	6.0000	6.0000	5.3044	0.3978	0.1795	45.0400
1.0038	0.7241	6.0000	6.0000	5.3478	0.4039	0.1727	43.5699
1.0541	0.7535	6.0000	6.0000	5.3871	0.4094	0.1663	42.1750
1.1043	0.7806	6.0000	6.0000	5.4231	0.4146	0.1602	40.8512
1.1545	0.8053	6.0000	6.0000	5.4564	0.4193	0.1546	39.5946
1.2048	0.8277	6.0000	6.0000	5.4873	0.4235	0.1495	38.4013
1.2602	0.8498	6.0000	6.0000	5.5189	0.4277	0.1442	37.1543
1.3547	0.8816	6.0000	6.0000	5.5676	0.4337	0.1365	35.1793
1.4544	0.9074	6.0000	6.0000	5.6119	0.4384	0.1299	33.2877
1.5541	0.9255	6.0000	6.0000	5.6486	0.4417	0.1250	31.5684
1.6538	0.9366	6.0000	6.0000	5.6745	0.4434	0.1217	30.0021
1.7536	0.9412	6.0000	6.0000	5.6862	0.4437	0.1200	28.5712
1.8533	0.9396	6.0000	6.0000	5.6904	0.4426	0.1191	27.2606
1.9530	0.9323	6.0000	6.0000	5.6934	0.4402	0.1182	26.0568
2.0527	0.9199	6.0000	6.0000	5.6957	0.4366	0.1174	24.9482
2.1524	0.9028	6.0000	6.0000	5.6997	0.4317	0.1165	23.9248
2.2521	0.8814	6.0000	6.0000	5.7050	0.4258	0.1156	22.9776
2.3518	0.8564	6.0000	6.0000	5.7107	0.4187	0.1147	22.0990
2.4515	0.8280	6.0000	6.0000	5.7160	0.4106	0.1138	21.2820
2.5512	0.7969	6.0000	6.0000	5.7203	0.4015	0.1129	20.5208
2.6510	0.7634	6.0000	6.0000	5.7201	0.3915	0.1120	19.8100
2.7507	0.7282	6.0000	6.0000	5.7199	0.3807	0.1111	19.1451
2.8504	0.6915	6.0000	6.0000	5.7203	0.3691	0.1103	18.5218
2.9501	0.6540	6.0000	6.0000	5.7218	0.3567	0.1094	17.9365
3.0498	0.6160	6.0000	6.0000	5.7247	0.3436	0.1085	17.3859
3.1495	0.5781	6.0000	6.0000	5.7289	0.3299	0.1076	16.8672
3.2492	0.5408	6.0000	6.0000	5.7348	0.3156	0.1067	16.3778
3.3489	0.5044	6.0000	6.0000	5.7380	0.3009	0.1058	15.9152
3.4487	0.4696	6.0000	6.0000	5.7340	0.2856	0.1049	15.4774
3.5484	0.4367	6.0000	6.0000	5.7215	0.2700	0.1041	15.0625
3.6481	0.4063	6.0000	6.0000	5.7004	0.2540	0.1032	14.6688
3.7478	0.3788	6.0000	6.0000	5.6622	0.2377	0.1023	14.2947
3.8466	0.3325	6.0000	6.0000	5.4973	0.1997	0.1014	13.9422
3.9404	0.2226	6.0000	6.0000	5.4748	0.0959	0.1006	13.6227

Figure D.8: Propeller 8x6E from [34]

APC Propellers - 9x6E:

STATION (IN)	CHORD (IN)	PITCH (QUOTED)	PITCH (LE-TE)	PITCH (PRATHER)	SWEEP (IN)	THICKNESS RATIO	TWIST (DEG)
1.0000	0.8667	6.0000	5.9969	5.4074	0.4034	0.1589	43.6646
1.0500	0.8902	6.0000	6.0000	5.4465	0.4090	0.1538	42.2852
1.1000	0.9105	6.0000	6.0000	5.4782	0.4141	0.1492	40.9618
1.1500	0.9278	6.0000	6.0000	5.5068	0.4188	0.1448	39.7053
1.2000	0.9435	6.0000	6.0000	5.5323	0.4231	0.1408	38.5119
1.2500	0.9577	6.0000	6.0000	5.5551	0.4270	0.1372	37.3778
1.3000	0.9706	6.0000	6.0000	5.5756	0.4304	0.1339	36.2996
1.3551	0.9833	6.0000	6.0000	5.5953	0.4337	0.1307	35.1715
1.4492	1.0014	6.0000	6.0000	5.6232	0.4382	0.1261	33.3824
1.5483	1.0157	6.0000	6.0000	5.6448	0.4415	0.1226	31.6641
1.6475	1.0254	6.0000	6.0000	5.6582	0.4433	0.1205	30.0976
1.7467	1.0306	6.0000	6.0000	5.6634	0.4437	0.1196	28.6661
1.8458	1.0317	6.0000	6.0000	5.6659	0.4427	0.1189	27.3545
1.9450	1.0289	6.0000	6.0000	5.6669	0.4405	0.1182	26.1495
2.0442	1.0223	6.0000	6.0000	5.6670	0.4369	0.1175	25.0396
2.1433	1.0123	6.0000	6.0000	5.6683	0.4322	0.1168	24.0146
2.2425	0.9991	6.0000	6.0000	5.6708	0.4264	0.1161	23.0659
2.3417	0.9829	6.0000	6.0000	5.6741	0.4195	0.1154	22.1856
2.4408	0.9639	6.0000	6.0000	5.6774	0.4115	0.1147	21.3670
2.5400	0.9424	6.0000	6.0000	5.6800	0.4026	0.1140	20.6041
2.6392	0.9185	6.0000	6.0000	5.6814	0.3928	0.1132	19.8916
2.7383	0.8927	6.0000	6.0000	5.6779	0.3821	0.1125	19.2250
2.8375	0.8649	6.0000	6.0000	5.6740	0.3706	0.1118	18.6001
2.9367	0.8356	6.0000	6.0000	5.6703	0.3584	0.1111	18.0132
3.0358	0.8050	6.0000	6.0000	5.6665	0.3455	0.1104	17.4611
3.1350	0.7732	6.0000	6.0000	5.6631	0.3319	0.1097	16.9409
3.2342	0.7405	6.0000	6.0000	5.6597	0.3178	0.1090	16.4499
3.3333	0.7072	6.0000	6.0000	5.6564	0.3032	0.1083	15.9859
3.4325	0.6734	6.0000	6.0000	5.6533	0.2881	0.1076	15.5467
3.5317	0.6395	6.0000	6.0000	5.6507	0.2726	0.1069	15.1304
3.6308	0.6056	6.0000	6.0000	5.6485	0.2568	0.1062	14.7354
3.7300	0.5720	6.0000	6.0000	5.6470	0.2407	0.1055	14.3601
3.8292	0.5388	6.0000	6.0000	5.6458	0.2243	0.1047	14.0030
3.9283	0.5065	6.0000	6.0000	5.6453	0.2077	0.1040	13.6629
4.0275	0.4751	6.0000	6.0000	5.6441	0.1911	0.1033	13.3386
4.1267	0.4449	6.0000	6.0000	5.6244	0.1743	0.1026	13.0292
4.2258	0.4162	6.0000	6.0000	5.5712	0.1576	0.1019	12.7335
4.3235	0.3712	6.0000	6.0000	5.3432	0.1232	0.1012	12.4549
4.4105	0.2850	6.0000	6.0000	4.9788	0.0460	0.1006	12.2167
4.5000	0.0088	6.0000	6.0240	6.0241	-0.2185	0.1000	12.0274

Figure D.9: Propeller 9x6E from [34]

APC Propellers - 10x6E:

STATION (IN)	CHORD (IN)	PITCH (QUOTED)	PITCH (LE-TE)	PITCH (PRATHER)	SWEEP (IN)	THICKNESS RATIO	TWIST (DEG)
1.1400	0.8958	6.0000	6.0000	5.4512	0.4126	0.1613	39.9515
1.2000	0.9193	6.0000	6.0000	5.4909	0.4184	0.1550	38.5119
1.2600	0.9384	6.0000	6.0000	5.5282	0.4236	0.1493	37.1578
1.3200	0.9554	6.0000	6.0000	5.5629	0.4283	0.1441	35.8832
1.3800	0.9708	6.0000	6.0000	5.5952	0.4324	0.1393	34.6824
1.4400	0.9845	6.0000	6.0000	5.6240	0.4361	0.1350	33.5502
1.5121	0.9989	6.0000	6.0000	5.6547	0.4398	0.1305	32.2742
1.6298	1.0175	6.0000	6.0000	5.6961	0.4444	0.1243	30.3669
1.7496	1.0307	6.0000	6.0000	5.7276	0.4473	0.1193	28.6255
1.8694	1.0382	6.0000	6.0000	5.7494	0.4483	0.1156	27.0586
1.9892	1.0405	6.0000	6.0000	5.7627	0.4477	0.1129	25.6431
2.1091	1.0379	6.0000	6.0000	5.7686	0.4454	0.1110	24.3598
2.2289	1.0307	6.0000	6.0000	5.7689	0.4416	0.1098	23.1919
2.3487	1.0192	6.0000	6.0000	5.7682	0.4363	0.1086	22.1255
2.4685	1.0037	6.0000	6.0000	5.7665	0.4296	0.1076	21.1486
2.5883	0.9845	6.0000	6.0000	5.7609	0.4215	0.1066	20.2508
2.7082	0.9621	6.0000	6.0000	5.7533	0.4122	0.1057	19.4232
2.8280	0.9366	6.0000	6.0000	5.7444	0.4018	0.1048	18.6584
2.9478	0.9084	6.0000	6.0000	5.7347	0.3903	0.1040	17.9495
3.0676	0.8779	6.0000	6.0000	5.7250	0.3777	0.1033	17.2910
3.1874	0.8453	6.0000	6.0000	5.7158	0.3643	0.1026	16.6778
3.3073	0.8110	6.0000	6.0000	5.7070	0.3499	0.1020	16.1054
3.4271	0.7753	6.0000	6.0000	5.6992	0.3348	0.1015	15.5701
3.5469	0.7386	6.0000	6.0000	5.6921	0.3190	0.1010	15.0684
3.6667	0.7010	6.0000	6.0000	5.6857	0.3026	0.1006	14.5974
3.7865	0.6630	6.0000	6.0000	5.6800	0.2856	0.1002	14.1543
3.9064	0.6249	6.0000	6.0000	5.6748	0.2681	0.0999	13.7369
4.0262	0.5871	6.0000	6.0000	5.6699	0.2503	0.0997	13.3429
4.1460	0.5497	6.0000	6.0000	5.6656	0.2321	0.0995	12.9705
4.2658	0.5132	6.0000	6.0000	5.6618	0.2137	0.0994	12.6180
4.3856	0.4778	6.0000	6.0000	5.6503	0.1952	0.0993	12.2839
4.5055	0.4439	6.0000	6.0000	5.6254	0.1765	0.0993	11.9667
4.6253	0.4119	6.0000	6.0000	5.5845	0.1579	0.0994	11.6653
4.7451	0.3819	6.0000	6.0000	5.5227	0.1393	0.0995	11.3786
4.8620	0.3229	6.0000	6.0000	5.2530	0.0897	0.0997	11.1119
4.9800	0.0930	6.0000	6.0000	5.7765	-0.1300	0.1000	10.8549

Figure D.10: Propeller 10x6E from [34]